CHALMERS

Reverberation Chamber Performance and Methods for Estimating the Rician K-factor

Evaluation of Reverberation Chamber Measurements at the National Institute of Standards and Technology in Boulder, Colorado, USA and Comparison of Methods for Estimating the Rician K-factor in Wireless Channels

Master of Science Thesis

CHRISTIAN S. LÖTBÄCK PATANÉ

Department of Signals and Systems
CHALMERS UNIVERSITY OF TECHNOLOGY
Gothenburg, Sweden, 2010

Reverberation Chamber Performance and Methods for Estimating the Rician K-factor

Evaluation of Reverberation Chamber Measurements at the National Institute of Standards and Technology in Boulder, Colorado, USA and Comparison of Methods for Estimating the Rician K-factor in Wireless Channels

CHRISTIAN S. LÖTBÄCK PATANÉ

Department of Signals and Systems
CHALMERS UNIVERSITY OF TECHNOLOGY
Gothenburg, Sweden 2010

Reverberation Chamber Performance and Methods for Estimating the Rician K-factor
Evaluation of Reverberation Chamber Measurements at the National Institute of Standards and Technology in Boulder, Colorado, USA and Comparison of Methods for Estimating the Rician K-factor in Wireless Channels
CHRISTIAN S. LÖTBÄCK PATANÉ

Examiner: Professor Per-Simon Kildal

Department of Signals and Systems
Chalmers University of Technology
SE-412 96 Göteborg
Sweden
Telephone + 46 (0)31-772 1000

Gothenburg, Sweden 2010

Preface

This is a Master of Science thesis which awards the author a Master of Science degree in Engineering Physics. The author is a student at Chalmers University of Technology in Gothenburg, Sweden. In the year 2010 I spent six months as a guest researcher at the National Institute of Standards and Technology (NIST) in Boulder, Colorado, USA. This thesis presents the outcome of my work conducted at NIST, in close collaboration with the Antenna Group at Chalmers. The examiner and tutor at Chalmers has been Professor Per-Simon Kildal at the Antenna Group and the Department of Signals and Systems. The supervisors at NIST were Professor Christopher L. Holloway and Doctor Kate A. Remley.

Acknowledgements

The author wants to thank Professor Per-Simon Kildal, Professor Christopher L. Holloway and Doctor Kate A. Remley for their invaluable help and guidance. I want to further acknowledge all the people who have made the completion of this thesis possible. A special thanks to Ryan J. Pirkl at NIST who has been a great support whenever my programming skills or my knowledge in statistics were insufficient. Also, thanks to Chih-Ming Wang at NIST for his input regarding statistical properties, Jason B. Coder and John M. Ladbury at NIST and Chen Xiaoming at Chalmers for their expertise on practical matters concerning the reverberation chamber and my fellow student Haider Ali Shah for his inputs on wireless communication issues.

Finally, I want to thank my family and friends for all their support. A special thanks to my mother who has been a great encouragement throughout my studies at Chalmers and always believed in me.

Your support made this thesis possible.

Christian
Boulder, July 2010

Reverberation Chamber Performance and Methods for Estimating the Rician K-factor

Evaluation of Reverberation Chamber Measurements at the National Institute of Standards and Technology in Boulder, Colorado, USA and Comparison of Methods for Estimating the Rician K-factor in Wireless Channels

CHRISTIAN S. LÖTBÄCK PATANÉ

Department of Signals and Systems

Chalmers University of Technology

Abstract

The aim of this Master's thesis is to evaluate the performance of two reverberation chambers with different stirring capabilities at the National Institute of Standards and Technology (NIST) in Boulder, Colorado, USA, in terms of the field uniformity and the number of independent samples. The field uniformity is estimated by employing a system validation procedure proposed in the literature. It is seen that the standard deviation of the mean field in different positions in the chambers is smaller in one of the chambers and close to an ideal value, thus having better measurement accuracy. This is an effect of a more efficient stirring, which gives more independent samples. The field uniformity is determined by means of a standard procedure proposed in the literature. Furthermore, improved stirring sequences are developed, which are shown to increase the number of independent samples significantly. The new stirring sequences can be applied to other chambers as well, with some minor modifications. Theoretical formulas for the number of independent samples and the standard deviation in the chamber are also compared to measured data. A detailed derivation of Professor P.-S. Kildal's new physical model for the standard deviation in a reverberation chamber is proposed. This equation is shown to give good agreement with the standard deviation estimated from measured data, when the unstirred component is negligible. Also, the repeatability in the chamber is briefly addressed and a correction for an offset in the stirring sequence is performed for one of the chambers.

In addition to the analysis of the chamber performance, the thesis addresses a comparison of methods for estimating the Rician K-factor. The results from simulations and measurements show that a method developed by P.-S. Kildal and the Antenna Group at Chalmers based on the complex mean of the field distribution gives the best estimate of the K-factor close to the real value for the case with a K-factor below 0 dB. The other approaches only give a qualitative analysis for these K values and show a large deviation from the true value. For higher K-factors, all the methods give similar results close to the true value. For measurements with variable antenna positions, the methods based on the distribution of field amplitudes give the best results.

Keywords: accuracy, independent samples, K-factor, repeatability, reverberation chamber, standard deviation, system validation procedure, uncertainty

Table of Contents

1 Introduction

In the recent years a wide range of applications for wireless devices have emerged. Also new wireless technology, like SIMO and MIMO systems, are under development. Consequently, the demand from the industry for an accurate, repeatable and efficient test facility for such devices has increased significantly during the latest years. The reverberation chamber, originally designed for electromagnetic compatibility measurements, has gone through a significant development in order to meet these requirements [1], [2].

Wireless devices, such as cellular phones, in a fading channel will experience a certain distribution of the field amplitudes. The same field distributions are achieved in the reverberation chamber, which thus provides a repeatable test facility for such devices. Due to the increased demand of reverberation chambers it is important to have standardized procedures for evaluating their performance. The accuracy and the characterizing parameters should easily be estimated from acquired data. It is also of interest to be able to estimate these parameters in advance, in order to facilitate the design of new and efficient reverberation chambers.

One important parameter for characterization of a fading channel is the Rician K-factor. This parameter is a measure of the distribution of the electromagnetic energy in components resulting from different interactions with the surrounding environment. It is a characteristic parameter of the environment in which a wireless device is operating in. This information is important, for example in order to accurately simulate a specific real-world fading channel in the reverberation chamber. Another example is given in [3], where the K-factor is related to rain fading effects of broadband fixed wireless access systems. This is said to be an important knowledge for design engineers. Also, the accuracy in measurements of a fading channel is dependent on the magnitude of the K-factor [4]. One part of this thesis addresses different methods for estimating the K-factor from measurements in a fading channel with and without variable antenna positions. The ordinary approach for reverberation chamber data, developed by P.-S. Kildal and the Antenna Group at Chalmers, to estimate the parameter from the complex transfer function will be emphasized and the limitations of this approach discussed. The measurements are performed by utilizing a reverberation chamber at the National Institute of Standards and Technology (NIST) in Boulder, Colorado, USA. Also, data from measurements in an urban setting in downtown Denver is used for the study.

The other main purpose of this thesis is to characterize and evaluate the performance of two reverberation chambers at NIST. These chambers are used for standard measurements and characterization of various wireless devices, which sets high expectations on the performance of the chambers. The focus will be on determining the maximum number of independent samples that can be achieved by different stirring techniques (the way the electric modes in the chamber are perturbed) and determining the accuracy in terms of the standard deviation of the mean field

in different positions in the chamber. The standard deviation is estimated by means of a system validation procedure for measuring the field uniformity in the chamber described in [4] and [5]. The discussion about the maximum number of independent samples and the chamber accuracy will also be extended to a more general analysis, where theoretical formulas for estimating these parameters from chamber characteristics are discussed. In particular, Professor P.-S. Kildal's new physical model for the uncertainty will be evaluated and derived in detail. Finally, the chamber repeatability will also briefly be addressed, which is important in order to repeat an exact measurement. This is also important when designing stirring sequences for achieving certain accuracy.

In addition to the K-factor, the number of independent samples and the standard deviation, there are also other important characteristic parameters for a reverberation chamber. The power delay profile is one example, which describes the time domain behavior of a signal [5]. Due to time limitations, other parameters than the above mentioned will not be evaluated. Furthermore, concerning the number of independent samples, the literature also proposes frequency stirring as a way to increase the number of independent samples in the chamber [5]. This will not be addressed in here.

The thesis is divided into chapters that separately describe the different characterizing parameters. Chapter 2 gives a brief theoretical background to reverberation chambers, its operation, the field distribution in the chamber and the characteristic parameters evaluated in later chapters. Chapter 3 gives an overview of the reverberation chambers at NIST, the additional equipment employed in the measurements and the measurement procedure in general. The following chapters 4, 5, 6 and 7 are the main part of the thesis, where the measurements are described in detail and the measurement results are presented and discussed. The thesis will be closed with conclusions about the K-factor estimation procedures and the performance of the NIST chambers. Some future work in the subject will also be proposed.

2 Theory

This chapter gives a brief background to reverberation chambers, its operation and the field distribution in the chamber. Also, the Rician K-factor is defined and the accuracy in the chamber is introduced.

2.1 Background to reverberation chambers

A reverberation chamber is a metallic enclosure with electromagnetic reflective walls, originally designed and used for electromagnetic compatibility (EMC) measurements. A radiating antenna in the chamber excites the cavity modes with resonances near the frequency of radiation. Due to the highly reflective walls the modes will interfere with each other, which results in constructive and destructive interference of the electric field and thus spatial distribution of maxima and minima of the field amplitudes. By changing the environment in the chamber, e.g. by rotating a metallic paddle, the maxima and minima of the field amplitudes in one point in the chamber will vary in the same way as they vary throughout the chamber. The induced voltage at the port of an antenna located in one position in the chamber will thus be arbitrary and will have a statistical variation similar to if the antenna would be moved to different locations in a fading environment [6], [7], [8], [9], [10].

The movement of objects inside the chamber is referred to as mode stirring. If the chamber is electrically large (that is, large compared to the wavelength of the excited electromagnetic waves) and the mode stirring is sufficient to interact with and perturb a large number of modes, then the real and imaginary parts of the electric and magnetic fields are independently Gaussian distributed. This implies that the real and imaginary parts of the induced voltage at the receiving antenna port are independent Gaussian distributed. The magnitude of the induced voltage will thus be Rayleigh distributed. If there is a line-of-sight component in the received field or if the mode stirring is insufficient, the field distribution will instead be Rician [7], [11], [12], [13].

Wireless devices in a typical radio environment will experience Rayleigh or Rician distributed field amplitudes. Thus the reverberation chamber can provide a repeatable test facility for such devices. In the recent years, as a wide range of applications for wireless devices have emerged, the chamber has gone through a significant development to become an efficient and accurate instrument for measuring characteristics of antennas and antenna systems, including radiation efficiency, diversity gain, capacity of SIMO and MIMO systems, total radiated power, total isotropic sensitivity and average fading sensitivity. As opposed to the anechoic chamber, the reverberation chamber is a more compact and less expensive facility [1], [2].

2.2 **Mode stirring**

The mode stirring mentioned above is crucial in order to make the reverberation chamber an efficient and accurate test facility. By mechanically moving electromagnetic objects in the chamber the boundary conditions will change and different modes will be perturbed. This results in varying field amplitudes in every position in the chamber. Everything that changes the environment in the chamber can be regarded as more or less effective mode stirring. The more non-uniform environment that is achieved by the moving objects and the larger the stirred volume, the more effective the mode stirring [10].

There are many ways to realize the mechanical mode stirring. One way is to use one or more rotating metallic paddles, with a non-uniform shape. This is used in e.g. the NIST reverberation chamber and in [14]. Another example is to move metallic plates to different locations in the chamber, which is employed in [5]. The mechanical stirring can be stepped or continuous, that is the stirrers can be moved continuous or in a stepwise manner.

The second way of stirring is performed by moving the receiving and/or transmitting antenna to different locations in the chamber. In [5] this is referred to as platform stirring, since the receiving antenna is placed on a rotating platform. If the antenna is moved manually, the terminology position stirring is used [5].

It is also possible to use multiple transmitting antennas with different polarizations. This polarization stirring can be used to give polarization balance in the chamber (see section 2.3.3). For a large chamber with a high Q the polarization stirring is not as important as in a small chamber [15].

All the stirring techniques described so far are performed during the actual measurement. There are also ways to achieve some stirring in the post-processing of the data. If the measurements are performed over a frequency band it is possible to average over adjacent frequency points, spaced by at least one coherence bandwidth. This will of course not perturb the actual modes in the chamber, only increase the number of independent samples (see chapter 5). Still it is referred to as frequency stirring [5].

2.3 Field distribution in the reverberation chamber

In this section the field distribution in the reverberation chamber is briefly addressed. Statistical models are used for describing the electromagnetic characteristics of the chamber. The first subsection will also give arguments supporting the statistical approach, as opposed to a deterministic analysis. Only the electric field component is being considered, but the same result would be obtained if analyzing the magnetic component [10].

2.3.1 Motivation for a statistical approach

As discussed in [10], for simple environments where the physical characteristics are fully known it is possible to accurately determine the expected electromagnetic behavior. For example, in an electrical circuit it is possible to determine the exact voltage over a certain load, if the current is known. For a more complex environment with many parameters affecting the final result, it is neither possible nor desirable to determine everything in detail. The wireless communication channel in urban settings is a good example, since it is constantly changing when cars drive by and people move around etc. For practical applications it is more of interest to predict the most expected performance. Due to lack of detailed information of e.g. cables, absorbers and the exact geometry of the stirrers, deterministic approaches are thus not suitable for describing the received field at the port of an antenna in a reverberation chamber. Instead, statistical models have been developed for this purpose [10], [16], [17], [18]. It is however important to ensure that the associated electromagnetic theory underlying the statistics is consistent with the traditional physics, that is Maxwell's equations. This is firmly discussed in [10]. The following subsection briefly addresses this statistic theory.

2.3.2 Field distribution in a fading environment

The real and imaginary parts of the electric field are both Gaussian distributed in fading environments such as urban settings, indoor environments and a well-stirred reverberation chamber, thus making the magnitude of the electric field Rician or Rayleigh distributed. The Rayleigh distribution is a special case of the Rician distribution when all modes are interacting with the stirrers in the chamber [7], [11], [12], [13].

The Rician probability density function (PDF) for the electric field in the reverberation chamber is given by [16], [17], [18]

$$f(|E|) = \frac{|E|}{\sigma^2} e^{-\frac{|E|^2+|E_{unstirred}|^2}{2\sigma^2}} I_0\left(\frac{|E||E_{unstirred}|}{\sigma^2}\right) U(|E|) \tag{2.1}$$

where $|E| = |E_{stirred}| + |E_{unstirred}|$ is the amplitude of the total electric field. $|E_{stirred}|$ is the amplitude of the electric field from the modes that interact with the changing environment and $|E_{unstirred}|$ is the amplitude of the field component from the line-of-sight component and reflections from the unchanging environment. σ^2 is the variance of the magnitude of the real or imaginary parts of the stirred electric field, I_0 is the zeroth order modified Bessel function of the first kind and U is the unit step function

$$U(|E|) = \begin{cases} 1, & |E| > 0 \\ 0, & |E| < 0 \end{cases} \tag{2.2}$$

Equation (2.1) was originally derived for shot noise in electrical circuits [16], but the equation can also be used for describing the distribution of electric fields in a fading environment when there are invariant as well as random components caused by scattering in a moving environment.

The subscript *stirred* in (2.1) is used to emphasize that this component corresponds to the field in the chamber that interacts with the stirrers. In the same way, the subscript *unstirred* in $|E_{unstirred}|$ is used to emphasize that this is the component of the electrical field from the composition of all electromagnetic waves that are not interacting with and perturbed by the stirrers in the chamber, thus constant over time. In the real field this corresponds the line-of-sight component and e.g. some ground reflections, which will be constant over time and have high amplitude compared to the random components. Ideally, it is only the field from the direct line-of-sight between the transmitter and the receiver. However, all the modes that are unchanging over time or between samples will contribute to this component. The distribution of the amplitude values of the transfer function will be Rician independently of what the unstirred part consists of. If the unstirred component consists of the line-of-sight and e.g. a ground reflection that give constructive interference, the Rician PDF will be shifted towards higher amplitudes compared to if only the line-of-sight component is present. When there is no unstirred component, that is $|E_{unstirred}| = 0$, (2.1) simplifies to the Rayleigh PDF. This is true as long as $|E_{unstirred}| \ll 2\sigma^2$. Also, in [19] it is shown that the square of a Rayleigh distributed random variable obtains an exponential distribution. Thus the power transfer function in the reverberation chamber will be exponentially distributed, as long as there is no unstirred field present. If the unstirred component has a significant contribution to the total field and the magnitude of the field is Rician distributed according to (2.1), then the power transfer function will instead have a non-central chi-square distribution.

Figure 2.1 shows the general complex plot of Gaussian distributed data measured from a fading channel with an unstirred component present. The samples (blue dots) are centered around a mean value, which corresponds to the unstirred component. If no unstirred component is present, the samples would instead have been centered around the origin. The random spread of samples around this mean value corresponds to the stirred field.

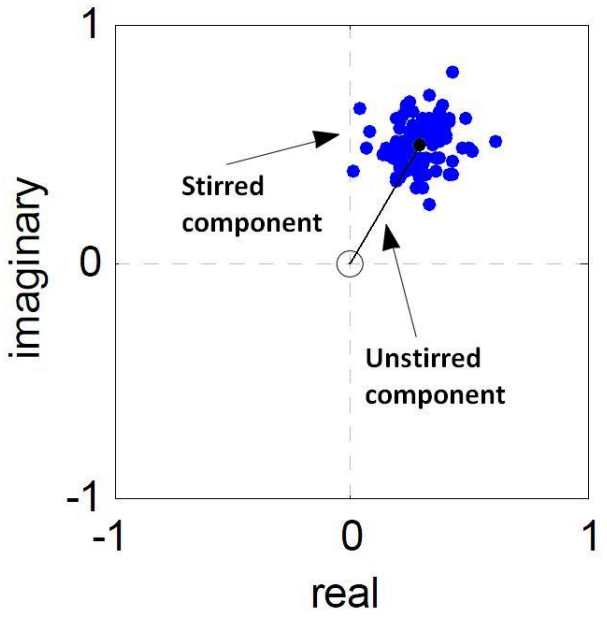

Figure 2.1 The general distribution of the measured data (blue dots) from a fading channel, showing the stirred and the unstirred component. The random spread around the mean value corresponds to the stirred field. If no unstirred component is present, the samples would be centered around the origin.

2.3.3 Polarization balance

Different stirrer positions will give different boundary conditions, thus exciting both TE and TM modes. If the stirring is not sufficient, e.g. since the stirrers are too regularly shaped, the TE and TM mode will not mix and there will be a polarization imbalance. This will imply that the received field is dependent on the orientation of the antennas. In particular, when there is a large amount of unstirred energy present in the chamber, the polarization imbalance will be high. Employing polarization stirring will mitigate this error and increase the field uniformity [5].

2.4 Chamber loading and the average mode bandwidth

When objects that absorb electromagnetic energy are present in the reverberation chamber the electromagnetic modes will be perturbed. This will affect the power received by an antenna. In order to fully replicate a real-field measurement in the chamber, it is important to have a measure of this loading. One common way is to use the chamber Q. By increasing the loading the Q factor in decreased. In [5] it is proposed that the average mode bandwidth, Δf, instead should be used as the measure of the chamber loading. The mode bandwidth is defined as the bandwidth over which the excited power in a particular cavity mode is larger than half the power at the center frequency. The average mode bandwidth is then the mean of the mode bandwidths over all the modes excited at a certain center frequency. The average mode bandwidth is related to the chamber Q according to

$$\Delta f = \frac{f}{Q} \tag{2.3}$$

where f is the frequency.

There are several arguments supporting the use of Δf instead of Q. In [5] it is argued that the average mode bandwidth is more or less invariant with frequency and that this makes it a more practical measure for the loading over a frequency band, compared to the chamber Q. Also, the different contributions to the average mode bandwidth, like the chamber walls, the absorbers and the antennas, are additive, as opposed to the contributions to Q.

2.5 The S-parameter terminology

For reverberation chamber applications it is common to employ a network analyzer that measures the complex scattering parameters (S-parameters) for the transmitting and receiving antenna. In [13] and [18] it is shown that the statistics of the S-parameter S_{21} (the voltage transfer function between the transmitting and receiving antenna) is equivalent to the statistics of the electromagnetic field in the chamber, if the antennas and the connecting cables are well matched to the impedance of the equipment employed for the measurement. Throughout this report the S-parameter terminology will thus be used.

Using the S-parameter approach, the total received field at the antenna port can be expressed as

$$S_{21} = S_{21,unstirred} + S_{21,stirred} \tag{2.4}$$

where $S_{21,stirred}$ is the stirred component of the transfer function and $S_{21,unstirred}$ is the unstirred component, analogous to the electric field components in equation (2.1).

2.6 **The Rician K-factor**

From (2.4) it is obvious that there are two contributions to the receive field, the stirred and the unstirred components. Typically it is desirable to decrease the contribution from the unstirred component as much as possible in order to increase the accuracy in the measurements (see subsection 2.7). This can be achieved by cross-polarizing the antennas and point them away from each other. In some applications it is however desirable to have an unstirred component present, for resemblance between measurements and real field applications. The K-factor can be varied by choosing suitable antenna, antenna positions and orientations, but also by loading the chamber. By loading the chamber with objects that absorbs electromagnetic energy (i.e. lossy objects), the stirred energy in the chamber will be absorbed, while the unstirred energy will be approximately the same. This is true as long as the lossy objects are not placed so that the unstirred field is perturbed (for example between the antennas) [20].

A measure of the amount of unstirred component is the Rician K-factor. In [5], [21], [22] and [23] it is defined in the following way,

$$K = \frac{|E_{unstirred}|^2}{2\sigma^2} \tag{2.5}$$

where the variance σ^2 and the unstirred component $|E_{unstirred}|^2$ is the same as in (2.1). The variable v is normally used for the magnitude of the unstirred field component $|E_{unstirred}|^2$ in order to emphasize that this is the absolute value of the complex mean of the distribution (see chapter 4), which gives

$$K = \frac{v^2}{2\sigma^2} \tag{2.6}$$

When $v^2 = 0$, that is, when there is no unstirred component, the K-factor is zero. When there is no dynamic multipath, the variance of the measured data will be close to zero (only a contribution from the unstirred component) and K approaches infinity.

2.7 Accuracy in reverberation chamber measurements and the number of independent samples

Measurements in the reverberation chamber are normally performed by averaging the power transfer function over a larger number of different stirrer positions. The chamber should provide a repeatable test facility for such measurements of wireless devices in a fading environment. It is thus of great importance to have a uniform field distribution throughout the chamber so that the results obtained from the measurements are independent of the position and orientation of the device under test. According to [24] the typical figure of merit for the accuracy is the standard deviation (STD) of the mean power transfer function for different antenna positions in the chamber. The smaller the STD, the smaller the variations in the mean field throughout the chamber, which results in an increased accuracy.

The STD of an estimate of a mean value decreases when the number of independent samples used for the estimate increases. When the number of independent samples is large, the estimate of the mean power transfer function will thus be very similar in every point in the chamber and very close to the real mean value. This means that a uniform field distribution has been obtained and the accuracy is good [25].

3 The reverberation chambers at NIST

In this thesis the performance of two different reverberation chambers at NIST is analyzed. The chambers have similar volume and shape, but they employ one and two stirrers, respectively. In this chapter the two chambers and their stirring techniques are described. The different loading configurations are defined and the corresponding average mode bandwidths are presented. Also the additional equipment employed for the data acquisition is described and the general measurement procedure is outlined.

3.1 Chamber 1 characteristics

The NIST reverberation chamber that employs two stirrers has the dimensions 2.8 m x 3.1 m x 4.4 m, which gives a total volume of 38.2 m^3. This chamber, which throughout the thesis is referred to as chamber 1, is shown in Figure 3.1. A schematic picture of an empty chamber is shown in Figure 3.2. The stirring is performed by rotating two large metal paddles. The vertical stirrer, which in the following will be referred to as stirrer 1, has an effective volume of 2.34 m^3. The horizontal stirrer, which will be referred to as stirrer 2, has an effective volume of 3.24 m^3. The effective volume is defined as the smallest cylinder in which the stirrer would fit. The stirrers are shown in Figure 3.3 and Figure 3.4.

Figure 3.1 NIST reverberation chamber 1.

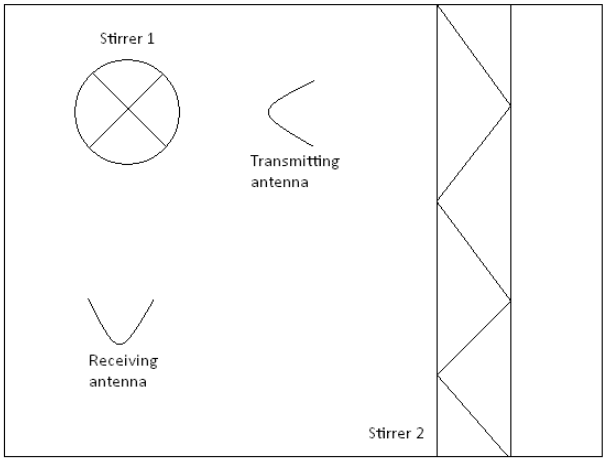

Figure 3.2 Chamber 1 schematics (seen from above).

Figure 3.3 Stirrer 1 in chamber 1.

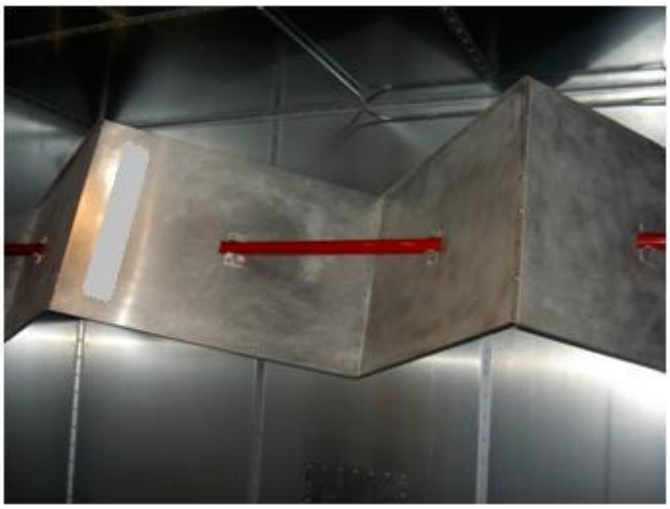

Figure 3.4 Stirrer 2 in chamber 1.

3.1.1 Loading configurations

The loading used in this study is referred to as load 0, 3 and 5. It corresponds to an empty chamber, 3 and 5 absorbers present in the chamber, respectively. The absorbers consist of carbon loaded foam with a height of 61 cm (see Figure 3.6).

As is shown in [26] the position of the absorbers in the chamber significantly affects the loading. It is thus important to clarify the positions of the absorbers. The first three absorbers (load 3) are placed in the corners of the chamber on the chamber floor. The next two absorbers (load 5) are placed approximately 30 cm and 50 cm from the chamber floor. The positions of the absorbers are shown in Figure 3.5. Also, the average mode bandwidths are given as a function of frequency for the different loading configurations in Figure 3.7.

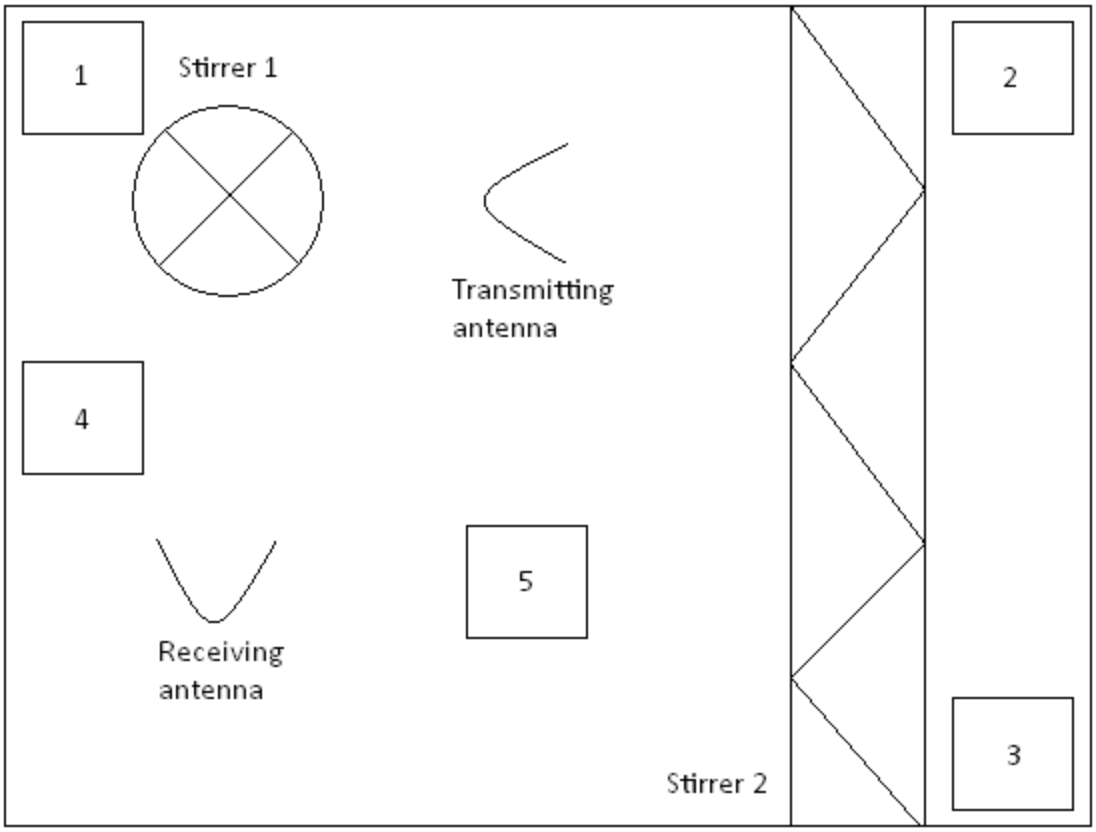

Figure 3.5 Location of the absorbers in chamber 1. The numbers corresponds to the order they are placed in the chamber.

Figure 3.6 The absorber consisting of carbon loaded foam used in the measurements.

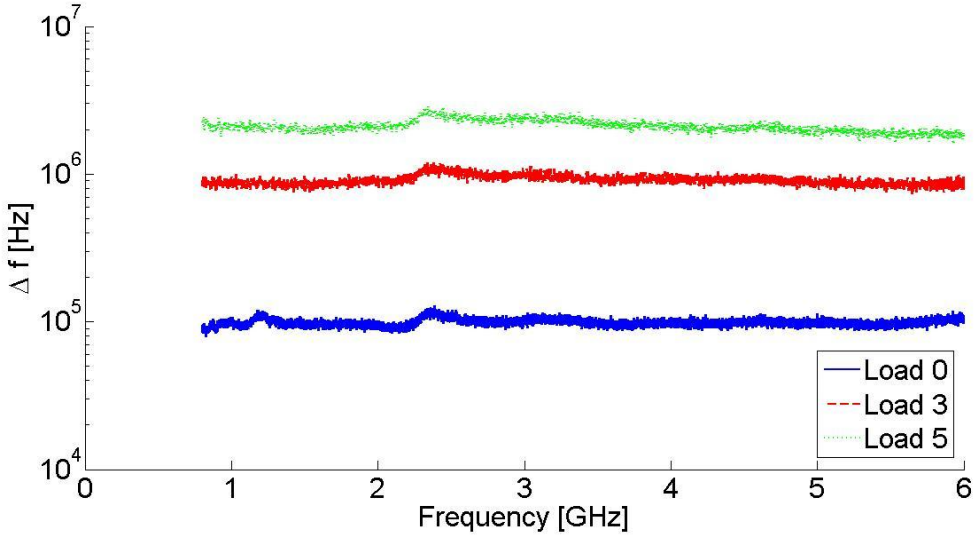

Figure 3.7 The average mode bandwidth for chamber 1 as a function of frequency for different loading cases. The mean over frequency is 0.0970 MHz, 0.820 MHz and 1.77 MHz for load 0, 3 and 5, respectivly.

3.2 Chamber 2 characteristics

The chamber that employs one stirrer, which will be referred to as chamber 2, has the dimensions 2.8 m x 3.1 m x 4.6 m and thus a total volume of 40.0 m^3. A picture of the chamber and the schematics for an empty chamber are given in Figure 3.8 and Figure 3.9, respectively. The stirrer has a variable effective volume, since it consists of metallic plates which can be removed or oriented in different directions. For the measurements in this thesis all the metallic plates is mounted on the stirrer, which then will have the appearance as shown in Figure 3.10. This configuration gives an effective volume of 2.76 m^3.

Figure 3.8 NIST reverberation chamber 2.

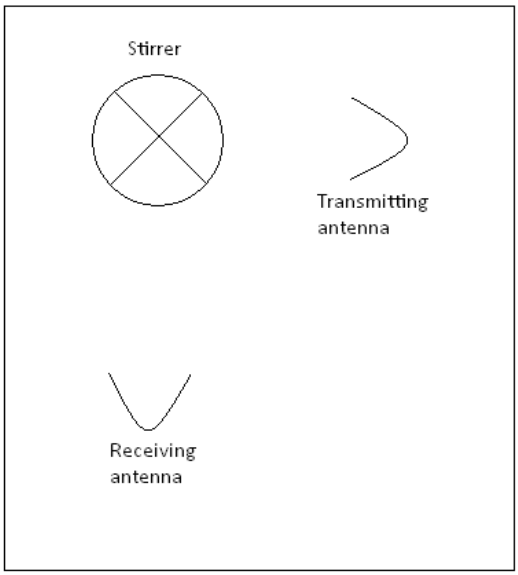

Figure 3.9 Chamber 2 schematics (seen from above).

Figure 3.10 The stirrer in chamber 2.

3.2.1 Loading configurations

In chamber 2, similar loading configurations as for chamber 1 is employed. However, due to the somewhat different volume and the presence of one stirrer only, the average mode bandwidths will be different. This can be seen in Figure 3.12. The same absorbers are used as in chamber 1 and the positioning of these can be studied in Figure 3.11. The three first absorbers (load 3) are placed on the floor and in the corners of the chamber and the two last are placed approximately 30 cm and 50 cm from the chamber floor, respectively.

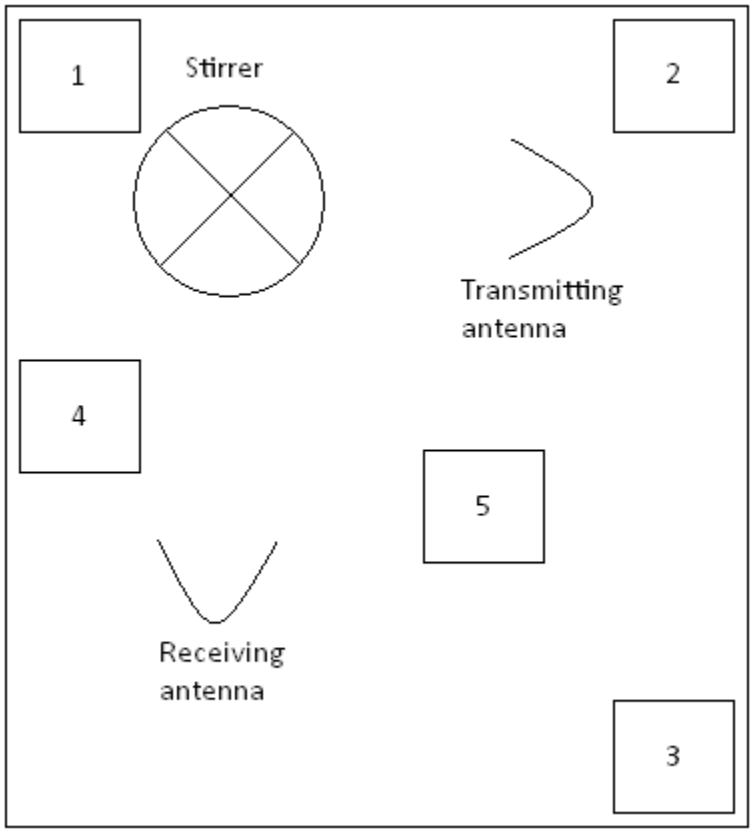

Figure 3.11 Location of the absorbers in chamber 2. The numbers corresponds to the order they are placed in the chamber.

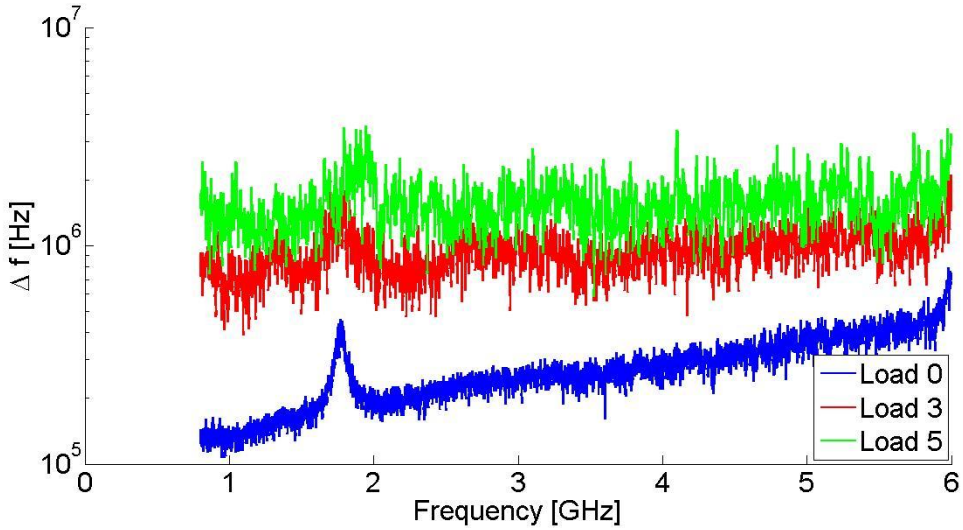

Figure 3.12 The average mode bandwidth for chamber 2 as a function of frequency for different loading cases. The mean over frequency is 0.274 MHz, 0.919 MHz and 1.53 MHz for load 0, 3, and 5, respectively. (The peak at about 1.8 GHz is an antenna effect.)

3.3 Additional equipment

In order to acquire the desired data it is important to choose additional equipment that do not distort the received signal. The choice of antennas that have a good performance in the frequency band of interest is important, just as the choice of network analyzer.

3.3.1 Antennas

For receiving and transmitting antennas both horn and omni-directional antennas are employed (Figure 3.13 and Figure 3.14, respectively). The horn antennas are designed for a frequency band of 800 – 18 GHz and the omni-directional antennas for 1 – 18 GHz. These antennas are used for all the measurements.

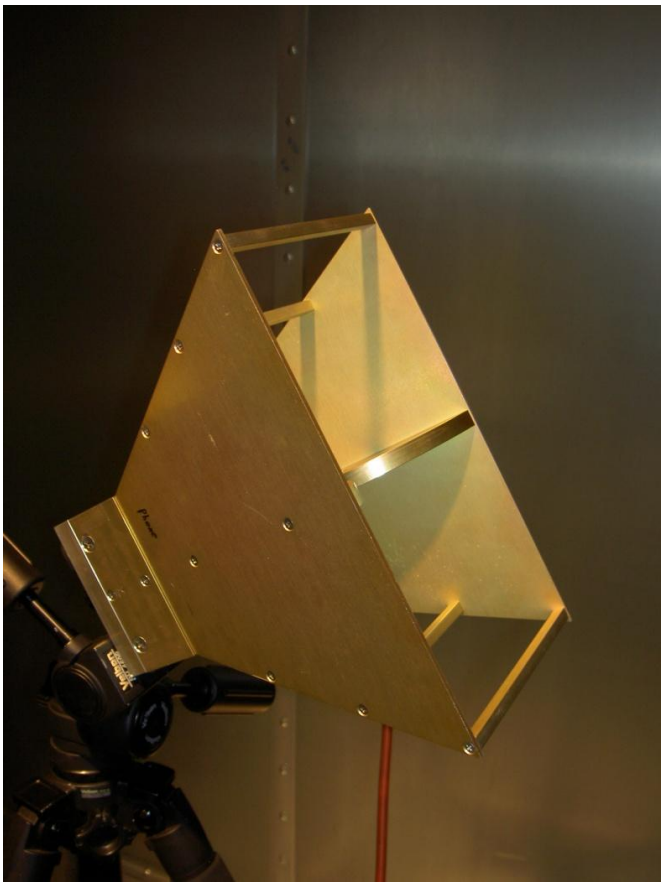

Figure 3.13 The linearly polarized horn antenna used in the measurement.

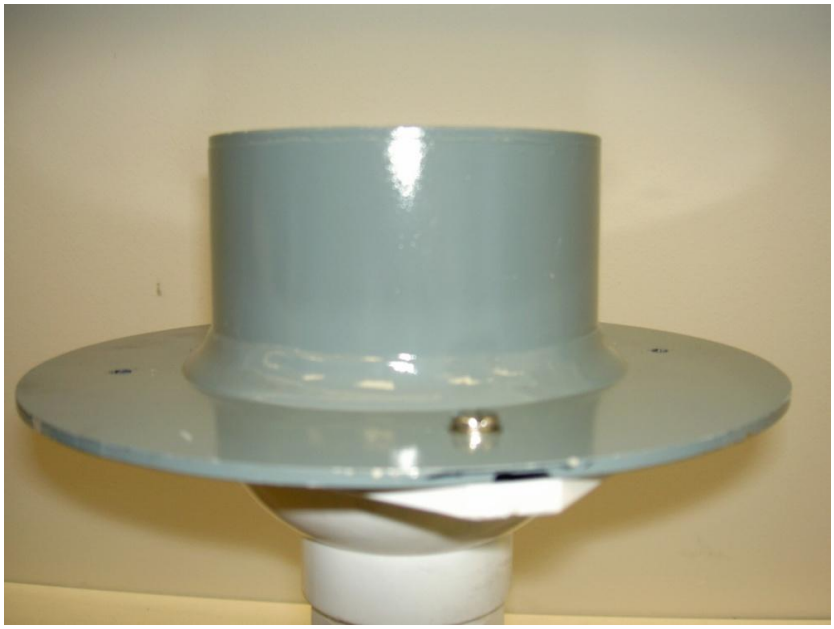

Figure 3.14 The omni-directional antenna used in the measurements.

3.3.2 Performance network analyzer

For some measurements of a received field it is only of interest to measure the field amplitude. For such measurements a spectrum analyzer can be used. For reverberation chamber measurements it is however often desirable to be able to obtain the phase information of the received field. This is important in order to get deeper knowledge of the field distribution etc. Thus in the measurements in this thesis a performance network analyzer (PNA) is used. The PNA N5230C (Figure 3.15) is designed for the frequency band 300 kHz – 20 GHz.

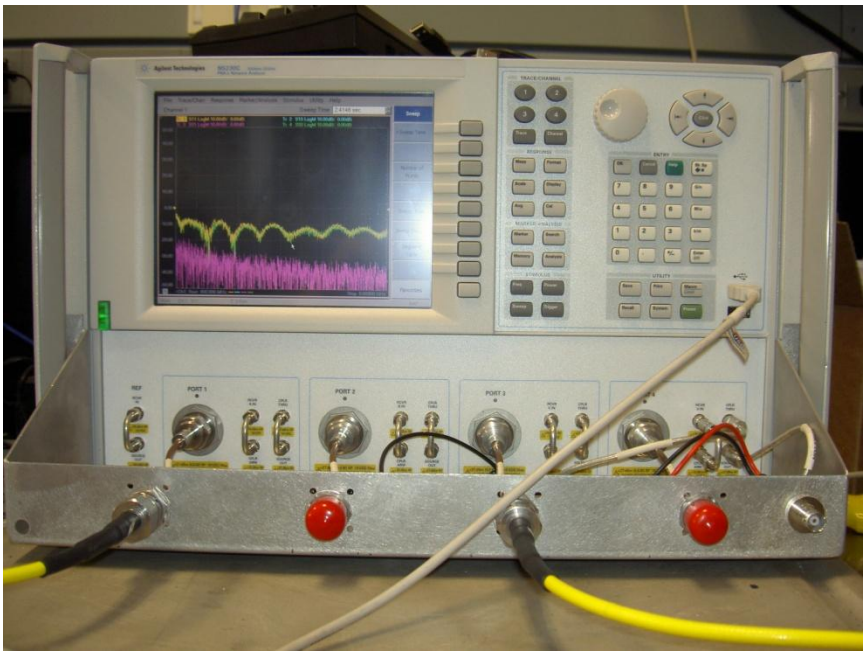

Figure 3.15 The PNA employed in the measurements.

3.4 Measurement procedure in general

The general measurement set-up is shown in Figure 3.16. The computer is connected to the PNA and the stirrers. Two ports of the PNA are further connected to two ports of the reverberation chamber, enabling two separate channels for the transmitted and received signal. The ports of the reverberation chamber are then connected to the antennas inside the chamber.

In the control software (LabVIEW), the step size and the number of stirrer positions are specified by the user. The frequency range and the number of frequency points are specified directly in the PNA software. Before the measurement can start, the losses in the cables etc. must be removed by calibrating the channel. The calibration is performed to the end of the cables that are connected to the antennas inside the chamber.

When the measurement is initialized, a signal is transmitted from the PNA to the transmitting antenna over the specified frequency band. The antenna induces electromagnetic modes in the chamber that interact with the stirrers, the chamber walls and the absorbers. The electric field is then received by the other antenna, measured by the PNA and saved by the software for further

post-processing. The same signal is also transmitted and received by the reverse PNA ports, thus measuring in total four scattering parameters (S_{11}, S_{21}, S_{12}, and S_{22}). After the signal has been received, the stirrers are rotated one step. The measurement procedure is repeated for all the specified stirrer positions. The number of samples for every frequency point will then be the same as the total number of stirrer positions.

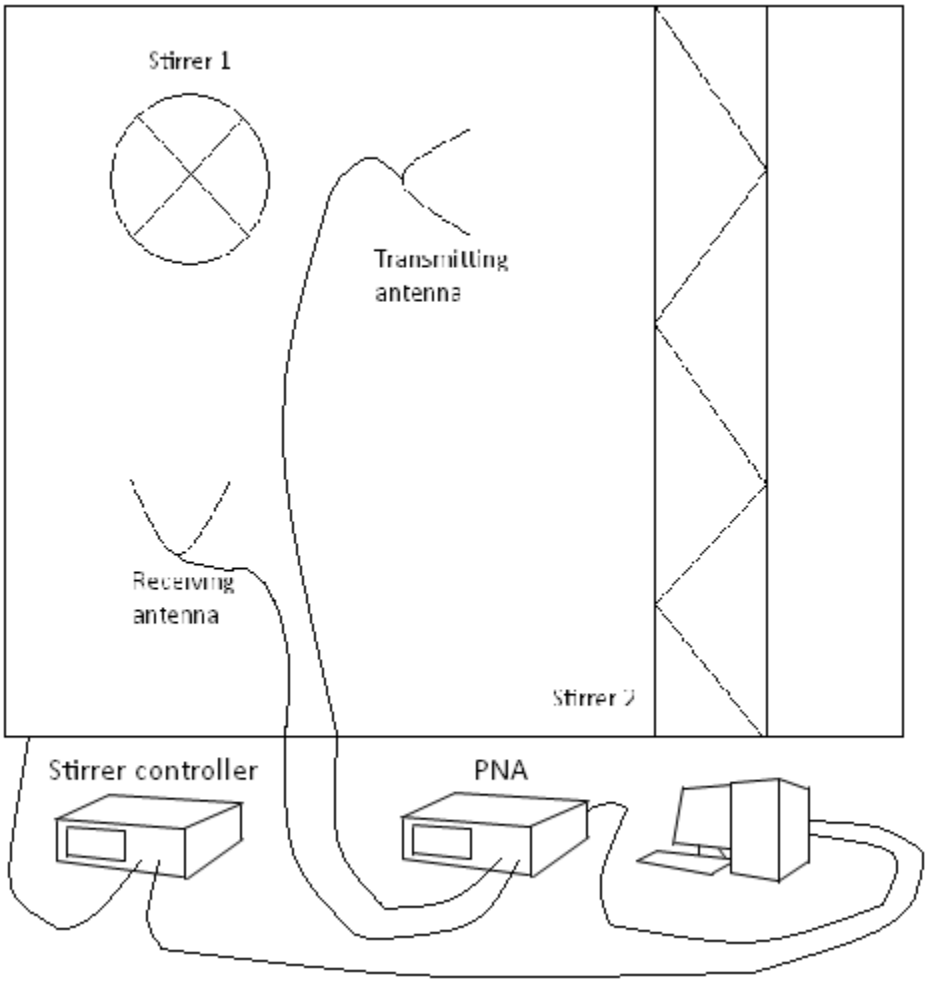

Figure 3.16 The measurement setup in general. The figure shows the schematics for chamber 1, however the same setup is used for chamber 2.

4 Methods for estimating the Rician K-factor in wireless channels

As mentioned in subsection 2.3.2, there are two contributions to the total field in the reverberation chamber, the stirred and the unstirred component. A measure of the amount of power in the different components is the Rician K-factor, which is defined in section 2.6. For the reverberation chamber, this ratio is easily computed from the channel transfer function data for different stirrer positions by using the complex mean of the field distribution, as described below. It is desirable to verify that this method gives the true value of the K-factor by comparing it to other methods and distributions of a known K-factor.

For measurements in a real environment the complex mean approach for finding the K-factor could also be used by measuring the transfer function between the transmitter and the receiver antenna for many different frequency sweeps. This requires that complex data are collected and that the environment is enough dynamic to get uncorrelated samples. However, if the transmitter and receiver are moved between the measurements in order to get different data samples, the phase of the unstirred component is changed and the complex mean approach cannot be used. Thus, there is a need for finding other applicable methods that estimate the K-factor from the field amplitudes only.

In this chapter the complex mean approach is compared to two other methods based on the magnitude of the signal envelope. Estimating the moments of the Rician distribution is one of the approaches that can be used for calculating the K-factor from the field amplitude distribution. By calculating the average of the second and the fourth power of the field amplitudes, the second and the fourth moments can be found. From these, the mean and the variance of the distribution can be computed, which gives the K-factor. Another approach is based on fitting a theoretical Rician probability density function to the measured distribution of amplitude values of the channel transfer function. By using a curve fitting tool, the mean and the variance can be found. The three methods are evaluated by applying them to simulated data with a known K-factor. They are further compared by applying them to data from measurements with and without variable antenna positions. In this way the best method for a certain measurement setup and procedure will be determined.

4.1 Statistical methods for estimating the K-factor

The mean and the variance of the received electric field can be estimated by various statistical methods, thus calculating the Rician K-factor by using (2.6). In this section three different methods for estimating the K-factor are described and the implementation of these methods in a mathematical software package is explained.

4.1.1 The complex mean approach

Complex data for the transfer function of the wireless channel created by the reverberation chamber are often collected using a PNA. The K-factor can then be calculated using a complex mean approach that has been developed by P.-S. Kildal and the Antenna Group at Chalmers.

In [13] it is shown that under ideal conditions (lossless and matched antennas, lossless reverberation chamber and no coupling between walls and antennas etc.), the real and imaginary components of the field in one point are independent and Gaussian distributed in the chamber with zero mean and identical variances. Thus, $S_{21,stirred}$ also has independent and Gaussian distributed real and imaginary components with zero mean and identical variances σ^2, that is [20]

$$\begin{aligned} var\left[Re\{S_{21,stirred}\}\right] = var\left[Im\{S_{21,stirred}\}\right] &= \langle\left[Re\{S_{21,stirred}\}\right]^2\rangle \\ &= \langle[Im\{S_{21,stirred}\}]^2\rangle = \sigma^2 \end{aligned} \tag{4.1}$$

For $S_{21,unstirred}$, on the other hand, the variance is zero and the mean is non-zero. The total mean will thus be given by $\left|\langle S_{21,stirred}\rangle\right|$ and the total variance by

$$var[Re\{S_{21}\}] = var[Im\{S_{21}\}] = \langle[Re\{S_{21}\}]^2\rangle = \langle[Im\{S_{21}\}]^2\rangle = \sigma^2 \tag{4.2}$$

or equivalently

$$2\sigma^2 = \langle|S_{21} - \langle S_{21}\rangle|^2\rangle \tag{4.3}$$

According to [5] and [20] the mean $|\langle S_{21}\rangle|$ is the same as the unstirred component of the electric field. Moreover, the right hand side of (4.3) is the mean of the squared difference between every complex S_{21} measurement and the complex unstirred component, which gives the stirred component. Thus, using (2.6) and (4.3) the K-factor may be given by

$$K = \frac{v^2}{2\sigma^2} = \frac{|\langle S_{21}\rangle|^2}{\langle|S_{21} - \langle S_{21}\rangle|^2\rangle} \tag{4.4}$$

In words, (4.4) is the ratio of the unstirred component and the stirred component.

This approach is often used to find the K-factor from reverberation chamber measurements, since (4.4) is easily evaluated from the measured S-parameters. It will also be suitable for real-world field measurements if complex data have been collected. If no complex data have been collected,

or if variable antenna positions are used, this approach is not suitable. By moving the antenna around in the environment the phase of the signal will be affected. This approach will then be inapplicable, because the measured complex values of the data will be distributed around mean values at different locations in the complex plane (see Figure 2.1). The complex mean will not give the true value of the unstirred component.

4.1.2 Moment method

The first method to be discussed that uses the distribution of the measured signal envelope to estimate the K-factor is the moment method. This approach is based on a relationship between the moments of the Rician PDF and mean values of the measured data.

According to [27] the n:th moment of the Rician distribution function is given by

$$\langle X^n \rangle = \int_0^\infty \frac{X^{n+1}}{\sigma^2} e^{-\frac{M^2+v^2}{2\sigma^2}} I_0\left(\frac{vX}{\sigma^2}\right) dX \tag{4.5}$$

where <…> denotes the expectation value. X is the Rician distributed data (here the magnitude of S_{21}, that is $X = |S_{21}|$), I_0 is the modified Bessel function of zeroth order, σ is the standard deviation of the data and v is the complex mean of the electric field. Evaluating the second and fourth moment gives the following expressions [27].

$$\langle X^2 \rangle = v^2 + 2\sigma^2 \tag{4.6}$$

and

$$\langle X^4 \rangle = v^4 + 8\sigma^2 v^2 + 8\sigma^4 \tag{4.7}$$

Then, by use of some simple algebra, the following relationships can be found.

$$v^2 = \sqrt{2(\langle X^2 \rangle)^2 - \langle X^4 \rangle} \tag{4.8}$$

and

$$\sigma^2 = \frac{\langle X^2 \rangle - v^2}{2} \tag{4.9}$$

Evaluating the left hand side of (4.6) and (4.7) from the measured data set and using (4.8) and (4.9) then gives an estimate of the K-factor according to (2.6).

The advantage with this method is that it does not require phase data and also is simple to evaluate. Due to the lack of phase information, however, this method might be less accurate compared to the complex mean approach.

4.1.3 Rician PDF fitting

If the envelope of the measured data is assumed to be Rician distributed, it is possible to fit a Rician PDF to the measured data set. In this way the stirred and the unstirred components of the measured field can be found from the fitted distribution. The curve fitting procedure may be performed with a mathematical software package, using the following procedure.

It is first necessary to find the distribution of magnitudes of the channel transfer function from the data set. This can be accomplished by creating a histogram of the data. It is important to verify that enough points are created for the Rician PDF to find a good fit and that no empty bins are created. Also, if the bin size (the amplitude interval) is too large, that is if the number of bins is too small, the Rician PDF will be shifted along the x-axis because the amplitude values in a certain interval (the bin size) would be allocated to the center of the bin. This can be mitigated by adding more bins. However, too many bins will result in empty bins and thereby give zeros in the PDF, which will disrupt the fitting.

As discussed in [10], the integral of the PDF must be normalized to equal 1, that is,

$$\int_{-\infty}^{\infty} f_R(x)dx = 1 \tag{4.10}$$

In order to satisfy this condition, some scaling is needed. Because the y-axis is simply the probability that the transfer function has a certain amplitude value, this axis is scaled by the total number of points in the data set. To find a suitable scaling of the x-axis, the following discussion holds.

Equation (4.10) is equivalent to a unity area between the PDF and the x-axis. If the area is considered to consist of infinitely small rectangular pieces, the area before scaling A_o is given by

$$A_o = \sum_i h_{o,i} w_{o,i} \tag{4.11}$$

where $h_{o,i}$ and $w_{o,i}$ are the height and the width of the i:th rectangular piece. If the y-axis (the height of the rectangular piece) is considered to be normalized and the width to be the same for all rectangles, then

$$A_o = w_o \sum_i h_i \tag{4.12}$$

where h_i is the normalized height. Thus

$$\sum_i h_i = \frac{A_o}{w_o} \tag{4.13}$$

Moreover the area after scaling A_n is, using the same reasoning, given by

$$A_n = w_n \sum_i h_i = 1 \tag{4.14}$$

where w_n is the width of one rectangle. This gives

$$w_n = \frac{1}{\sum_i h_i} \tag{4.15}$$

Thus, using (4.13) and (4.15)

$$w_n = \frac{w_o}{A_o} \tag{4.16}$$

Equation (4.15) shows that the scaled x-axis can be found by dividing the un-scaled x-axis by the un-scaled area.

When a suitable scaling has been performed, the parameters v and σ^2 of the Rician PDF can be found by using a mathematical software package with a curve fitting tool. The error in the fit can be minimized by use of a non-linear least squares method, that is choosing the non-linear model parameters that give the smallest sum of squared errors $SSE_{min}(v, \sigma^2)$ between the data and the estimated curve,

$$SSE_{min}(v, \sigma^2) = min\left(\sum_{i=1}^{m} (y_i - prd_i(v, \sigma^2))^2\right) \tag{4.17}$$

where y_i is the i:th data point (the magnitude of the i:th S_{21}) and $prd_i(v, \sigma^2)$ is the i:th prediction based on the parameters v and σ^2. SSE is calculated for every frequency in the frequency band of interest. As starting values for the parameters, the second and fourth moment of the Rician distribution can be used (see subsection 4.1.2). The estimated values of these parameters also need to be scaled with the same factor as discussed above. Once the values for the parameters v and σ^2 have been estimated, the real values of the parameters can then be found by "un-scaling" the values with the inverse of the scaling factor. The K-factor is then found from (2.6).

The Rician PDF fitting is an improvement of the moment method, which should increase the accuracy of the estimates. However, it is more time consuming to calculate the K-factor using this approach than only using the moments.

4.2 Simulations and measurements

In this section the measurements and simulations that are performed in order to test the methods for finding the K-factor are described. First the simulations of data sets with a known K-factor are described, followed by the measurements in the NIST reverberation chamber. Finally, the real-field measurements with variable antenna positions performed in downtown Denver are described.

4.2.1 Simulation of Gaussian distributed random variables

In order to compare the methods for estimating the K-factor with a true value, two different data sets are simulated consisting of Gaussian distributed complex random variables with a known mean and standard deviation (that is, a known K). The first data set has a mean of 0.03 and a standard deviation of 0.02, which corresponds to a K-factor of 3.5 dB. The corresponding values for the second data set are 0.007 and 0.02 and a K-factor of -9.1 dB. Note that only the unstirred components, that is the mean values, are changed. In order to replicate the measurements performed in the reverberation chamber (see below), 16001 data sets of 100 Gaussian distributed variables each are simulated (which corresponds to the number of frequency points and the number of stirrer positions used, respectively).

Moreover, simulations are performed where the difference between the real and the estimated K-factor values can be studied as a function of the K-factor. The K-factor is subsequently decreased from a maximum value of 8.1 dB to a minimum of -25.2 dB. For every K-factor a set of 100, 200, 300, 500 and 1000 Gaussian random variables are simulated as above, but only for one frequency point. The K-factor is estimated with the different methods for each of these data sets.

Finally, in order to study the effect of having a limited number of measured samples when estimating the K-factor, simulations are performed where 1000 Gaussian random variables are simulated as above. The K-factor is then calculated using different numbers of these independent data samples. This simulation is repeated for different values of the K-factor and for the different methods.

4.2.2 Measurements in the reverberation chamber

To compare the different methods for estimating the Rician K-factor, data from measurements in the NIST reverberation chamber 1 are used. Two measurements are performed using horn antennas pointing towards each other and with different orientations. In one measurement the antennas are co-polarized and in the other they are cross-polarized. Besides the orientation of the antennas, no changes are made in the chamber. For each measurement, the values of the channel transfer function (or scattering parameter S_{21}) are collected using the procedure described in chapter 3, with 100 stirrer positions and for load 3. The measurements are performed over the frequency band 800 MHz to 6 GHz, with 16001 frequency points and an IF bandwidth of 100 kHz.

4.2.3 Real field measurements in downtown Denver

For testing the methods on real field data with variable antenna positions, measurements are carried out in urban settings in downtown Denver, Colorado, USA. According to [28], this area contains many high buildings and is a dynamic environment due to pedestrians and traffic etc. The field data taken from these measurements corresponds to a line-of-sight link between a transmitting antenna and a receiver antenna at three different positions (20, 30 and 40 meter from the transmitting antenna). The transmitter is mounted to a positioner, which moves the antenna to nine different positions for each transmitter-receiver configuration. The positions are distributed over a Cartesian coordinate grid with a total range of 0.5 meter by 0.5 meter. At each position two frequency sweeps are made, which is supposed to give different scattering components due to the changing environment, and in total there are 18 different measurement points for each frequency and transmitter-receiver configuration. The channel transfer function is measured using a voltage network analyzer for the frequency band 4900 – 5000 MHz. A discone and a monopole antenna are used for the lower and the higher frequency band respectively, both omni-directional and vertically polarized. For more details about the measurements, see [28].

4.3 Results

In this section results from applying the methods described in section 4.1 to the simulated and the measured data are presented. All plots are smoothed over a 52 MHz frequency window (unless something else is specified). The averaging is carried out in linear scale and then converted into dB values.

4.3.1 Simulations

The results from estimating the K-factor with the different methods from simulated data samples can be studied in Figure 4.1 and Figure 4.2 and the mean values in Table 4-1. As the figures and the table show, the complex mean approach give a value close to the real value. For the case with a high K-factor the other methods give approximately the same result of 3.5 dB, whereas for the case with a low K-factor the envelope approaches give larger values than the known value of -9.1 dB.

Method	Mean over frequency, co-polar antennas [dB]	Mean over frequency, cross-polar antennas [dB]
True value	3.5	-9.1
Complex mean	3.6	-8.7
Moment method	3.8	-1.9
Rician PDF fitting	3.7	-3.2

Table 4-1 The mean K-factor for different estimation methods. The mean is computed over all the frequencies.

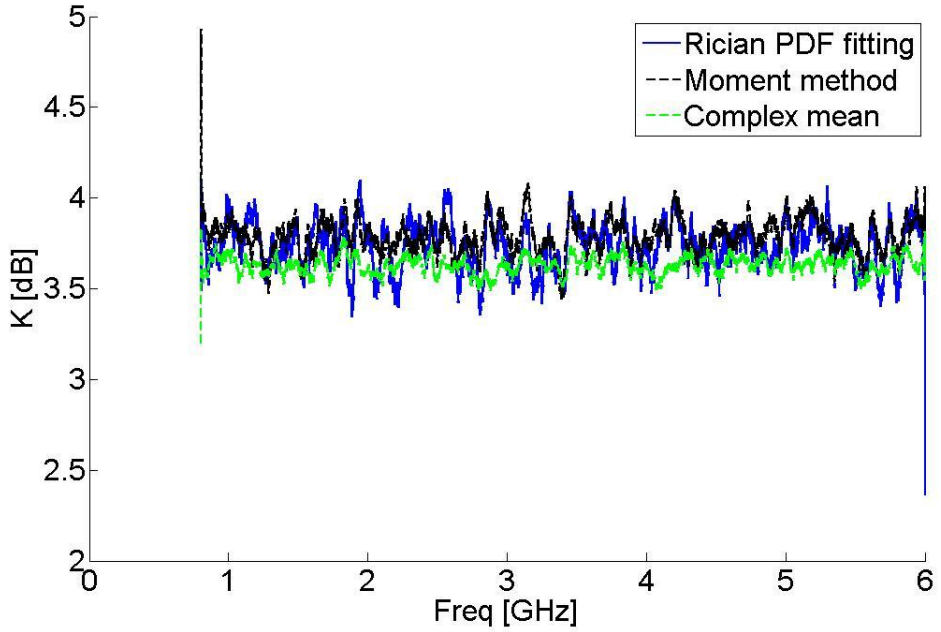

Figure 4.1 The K-factor for simulated Gaussian distributed random data for high K-factor.

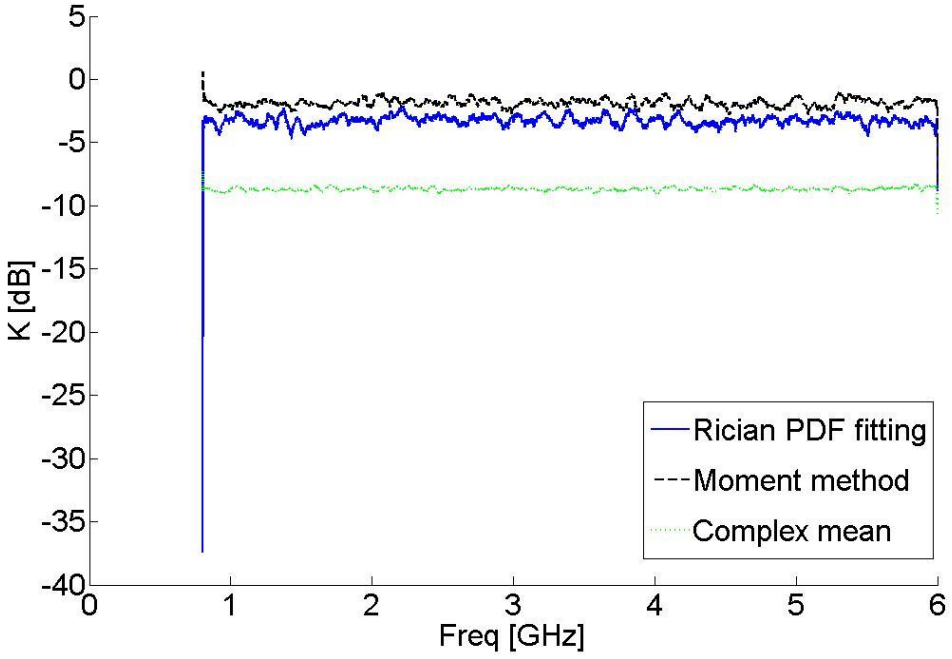

Figure 4.2 The K-factor for simulated Gaussian distributed random data for a low K-factor.

The results from the simulation where K is subsequently given a lower value can be studied in Figure 4.3. As can be seen in the figure, the complex mean approach gives a smaller ratio than the other approaches and even for a K-factor as low as -25 dB, the ratio is below 5 dB. The methods based on the distribution of the envelope give a small ratio for positive K-factor values. However, around 0 dB these methods start to significantly deviate from the real value. The moment method shows larger ratio and more oscillations than the Rician PDF fitting. For a K-factor of -25 dB the ratios are about 20 dB for both methods. Figure 4.3 to Figure 4.5 shows the result for increasing the number of independent samples used for the estimation of the K-factor. Increasing the number of samples seems to affect the envelope approaches by making the ratio smaller, but not the complex mean approach. For the last case with 1000 independent samples the ratio is approximately 10 dB smaller compared to the 100 sample case.

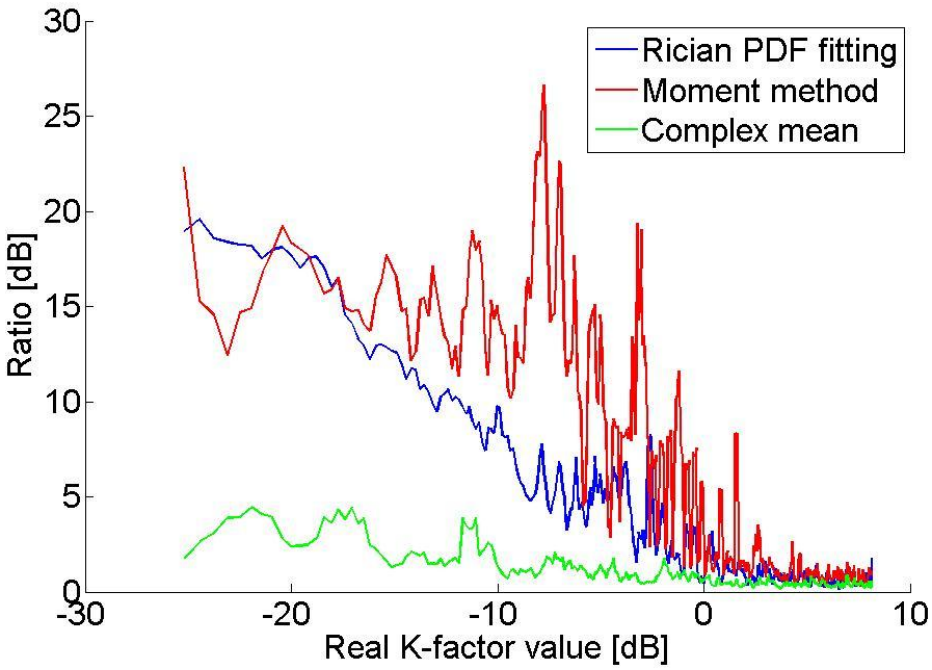

Figure 4.3 The ratio between the estimated K-factor values and the real value using different methods and 100 independent samples.

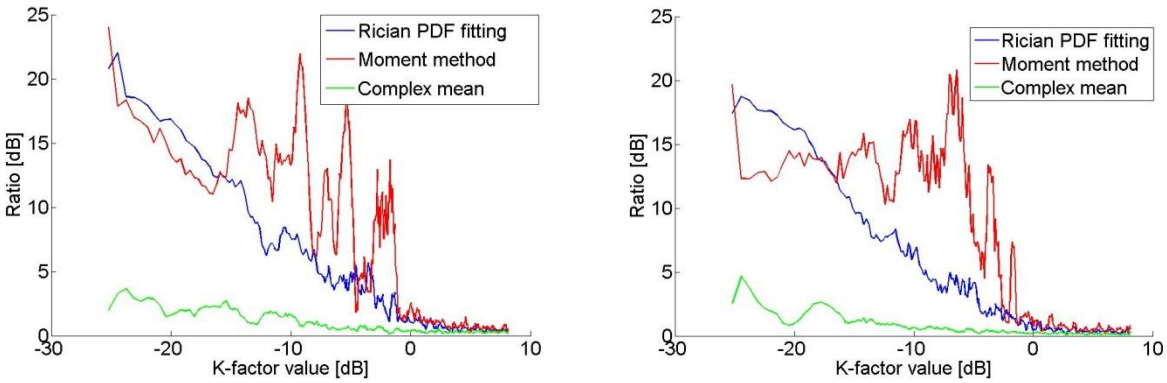

Figure 4.4 The ratio between the estimated K-factor values and the real value using different methods and 200 (left) and 300 (right) independent samples.

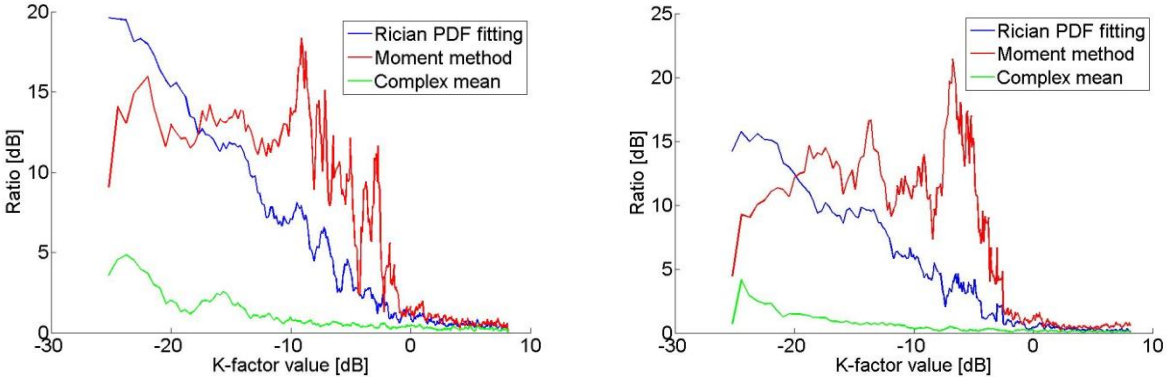

Figure 4.5 The ratio between the estimated K-factor values and the real value using different methods and 500 (left) and 1000 (right) independent samples.

Finally, the results from estimating the K-factor from different number of independent samples (see chapter 5) are presented in Figure 4.6 to Figure 4.11. The plot in Figure 4.6 of the K-factor estimated with the complex mean approach shows that there is a convergence in the K-factor value at approximately 20 independent samples. There are some oscillations around the true value, however the difference is always less than 0.5 dB. Figure 4.7 and Figure 4.8 show the K-factor for lower values estimated with the same method. The figures show that the lower the K-factor, the more independent samples are needed in order for the value to converge. It is clear from Figure 4.9 that it is the unstirred component that is the most difficult parameter to estimate. The convergence in the variance is much faster.

For a high K-factor value the other methods converge at a larger number of samples compared to the complex mean approach, as can be seen in Figure 4.10 and Figure 4.11. The moment method approach is reaching the true value at 50 independent samples, but has large oscillations and gets rather stable at 100 samples. After this there is a deviation from the real value of about 1 dB. The Rician PDF fitting reaches the true value at about 100 samples. However, the K-factor is then rather stable. The case for a low K-factor value is also evaluated for these methods. The simulations showed that there is no convergence at the real K-factor value, which agrees with the results above.

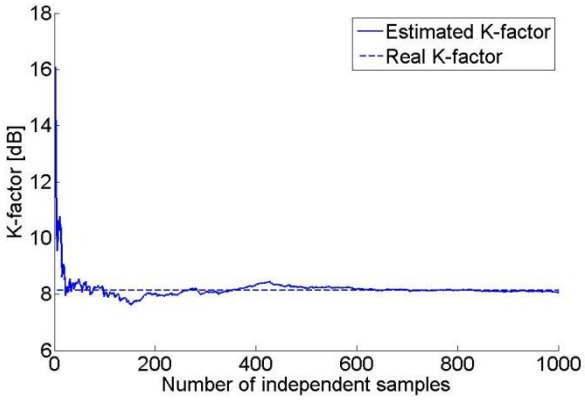

Figure 4.6 K-factor estimated with the complex mean approach from different number of simulated independent samples. The real K-factor value is 8.1 dB.

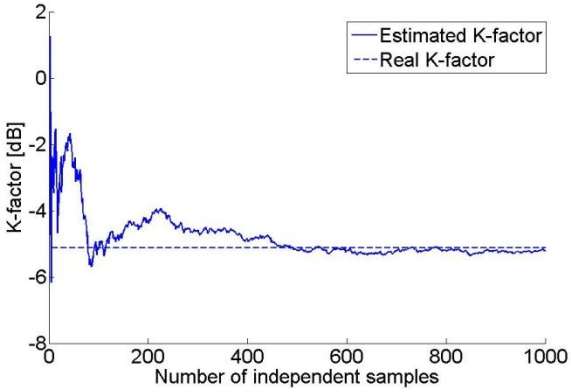

Figure 4.7 K-factor estimated with the complex mean approach from different number of simulated independent samples. The real K-factor value is -5.1 dB.

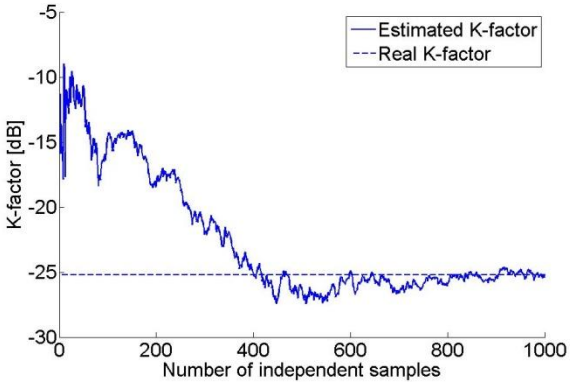

Figure 4.8 K-factor estimated with the complex mean approach from different number of simulated independent samples. The real K-factor value is -26.0 dB.

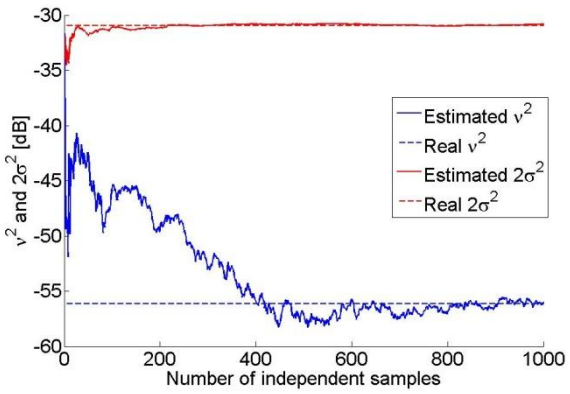

Figure 4.9 v^2 and $2\sigma^2$ estimated estimated with the complex mean approach from different number of simulated independent samples. The real K-factor value is -26.0 dB.

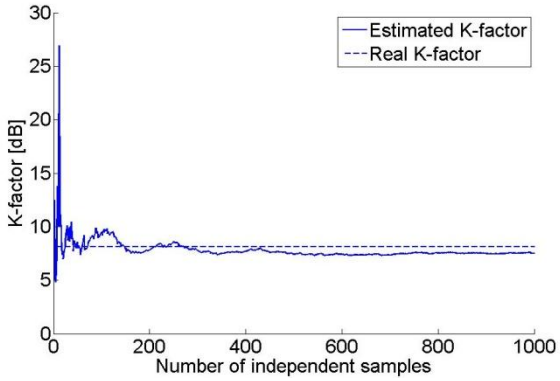

Figure 4.10 K-factor estimated with the moment method approach from different number of simulated independent samples. The real K-factor value is 8.1 dB.

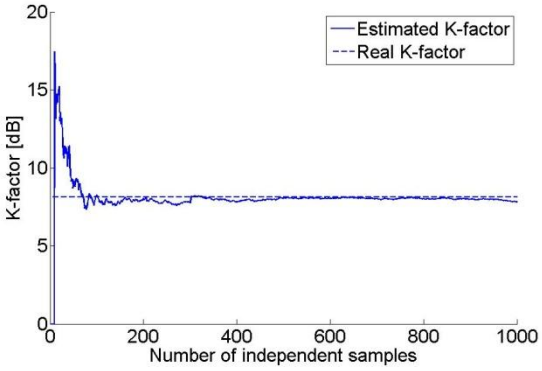

Figure 4.11 K-factor estimated with the Rician PDF fitting approach from different number of simulated independent samples. The real K-factor value is 8.1 dB.

4.3.2 Reverberation chamber measurements

The K-factors estimated with the different methods for measurements with fixed antenna positions in the reverberation chamber are plotted in Figure 4.12 and Figure 4.13 for the co-polar and the cross-polar case, respectively. As can be seen in the figures, the different methods give similar results for the co-polar case, however for the cross-polar case the results deviate significantly. For the cross-polar configuration, the methods based on the distribution of the field amplitude give a higher K-factor than the complex mean approach. The moment method and the Rician PDF fitting give similar results. The means computed in Table 4-2 over the frequency band show the same trend. Also, the mean and the variance are plotted separately in Figure 4.14 to Figure 4.15. As can be seen in the figures, the variances show similar oscillations of about 5 dB when estimated with the different envelope methods, but much smaller oscillations for the complex mean approach. The mean, on the other hand, shows much larger variations.

Method	Mean over frequency, co-polar antennas [dB]	Mean over frequency, cross-polar antennas [dB]
Complex mean	4.3	-9.7
Moment method	4.4	-2.7
Rician PDF fitting	4.3	-3.2
Maximum likelihood estimation	4.4	-4.4

Table 4-2 The mean K-factor for the different methods. The mean is computed over frequency in the frequency interval 800 MHz – 6 GHz.

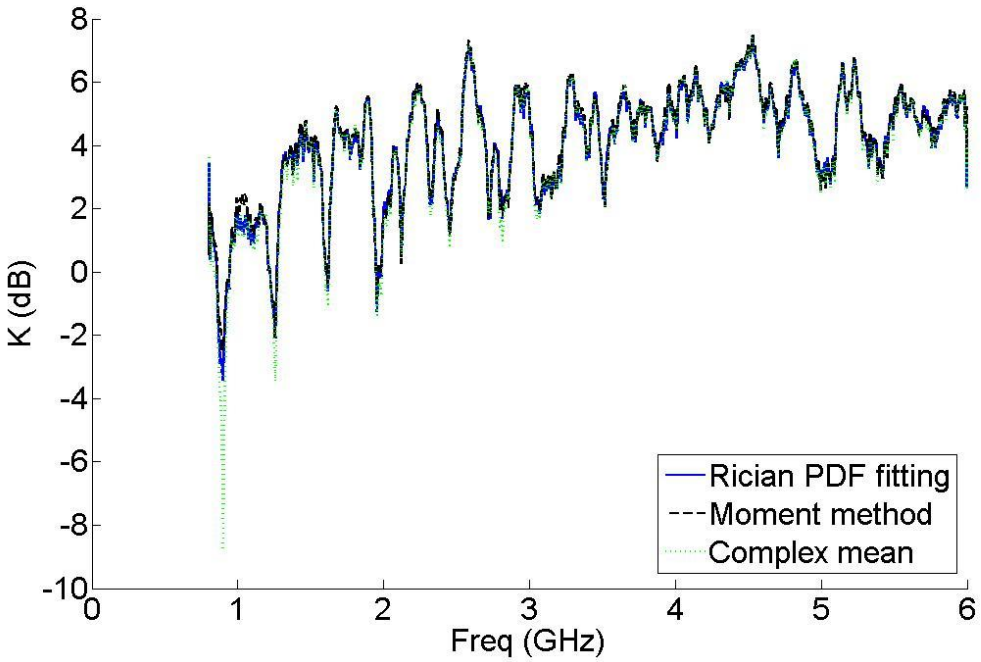

Figure 4.12 The K-factor for co-polar antenna configuration obtained with different methods.

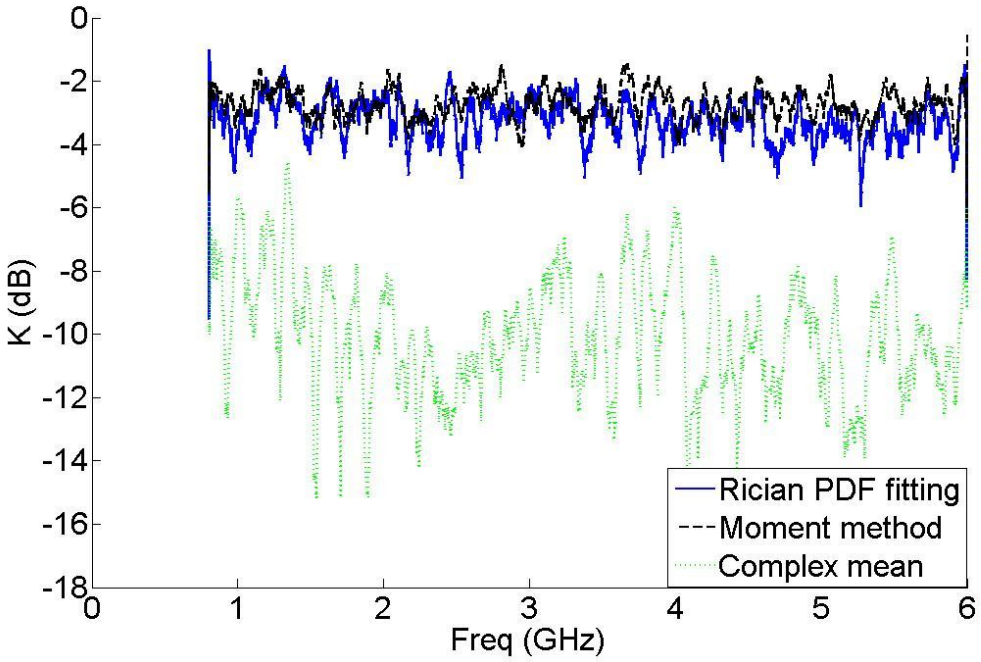

Figure 4.13 The K-factor for cross-polar antenna configuration obtained with different methods.

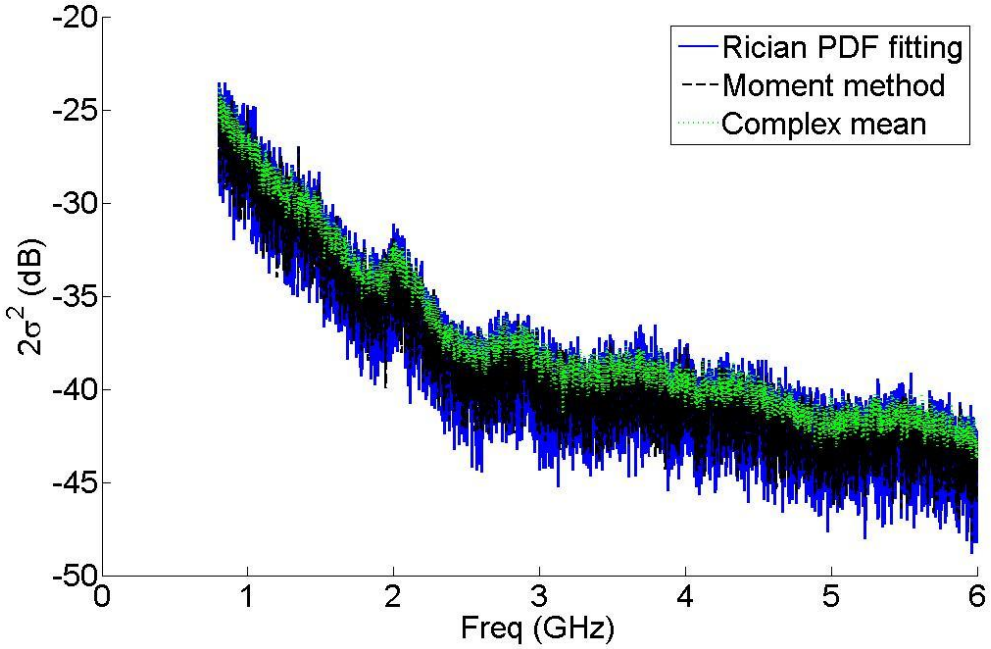

Figure 4.14 $2\sigma^2$ estimated with the different methods for cross-polar antennas. The plots in this figure are not smoothed.

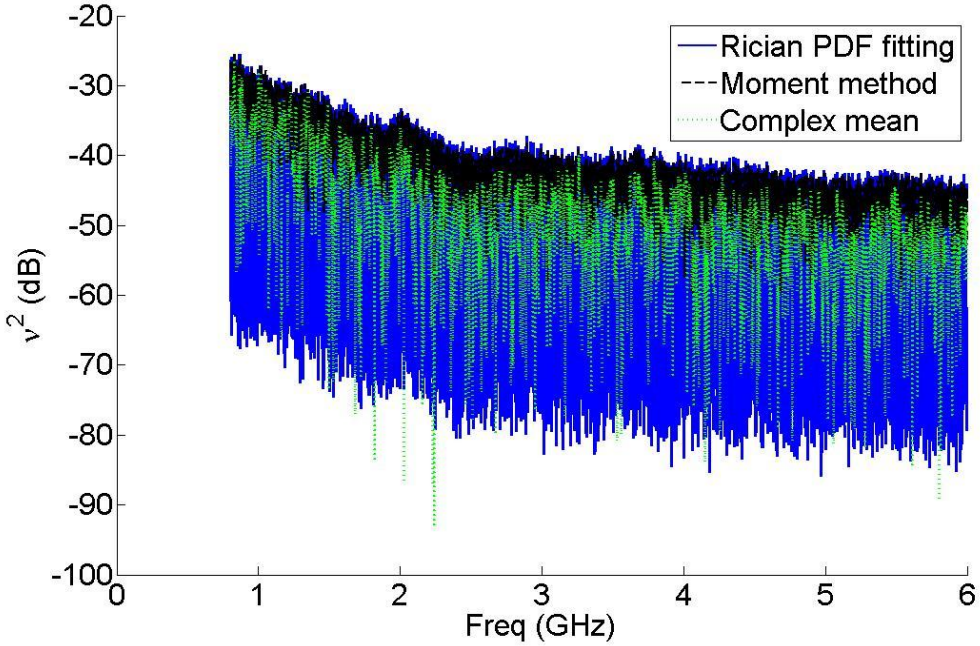

Figure 4.15 v^2 estimated with the different methods for cross-polar antennas. The plots in this figure are not smoothed.

4.3.3 Measurements in downtown Denver

In this section results from the measurements performed in downtown Denver are presented. Figure 4.16 to Figure 4.18 shows the estimates of the K-factor for the different receiver locations obtained by the different methods. The methods based on the amplitude distribution are seen to give similar values of the K-factor. The complex mean approach give a smaller value. The difference between the different methods is about 10 dB. For a larger separation, the K-factors estimated with the moment method and the Rician PDF fitting are decreasing, whereas the values are increasing for the complex mean approach. This is also clearly seen in Table 4-3.

Finally, in Figure 4.19 the K-factor using data from all the positions of the receiver is plotted. This gives a completely different result compared to using data from only one position, with a K-factor below 0 dB for all methods.

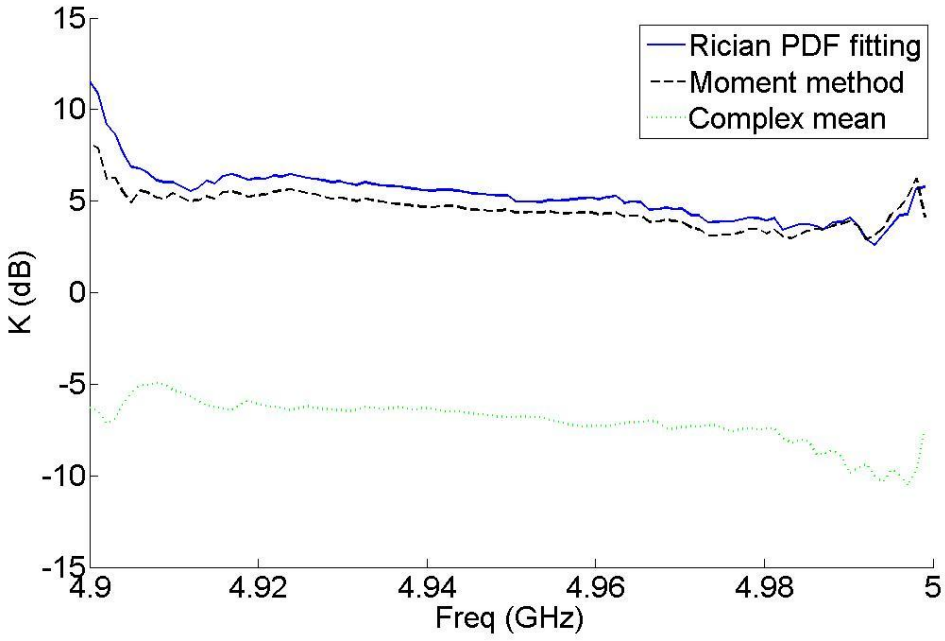

Figure 4.16 K-factor estimated using the different approaches for 20 meter separation between transmitter and receiver.

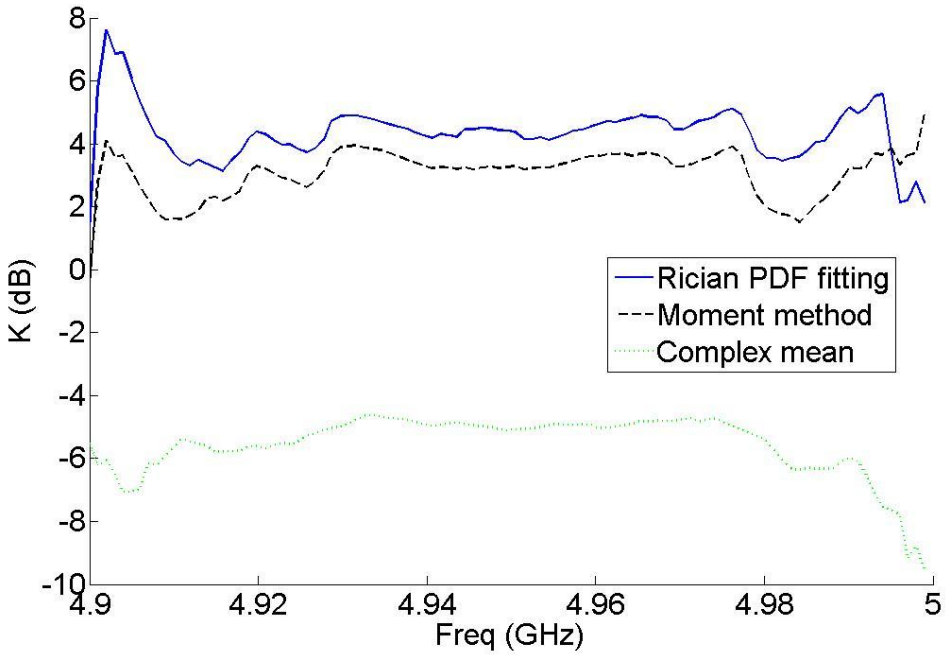

Figure 4.17 K-factor estimated using the different approaches for 30 meter separation between transmitter and receiver.

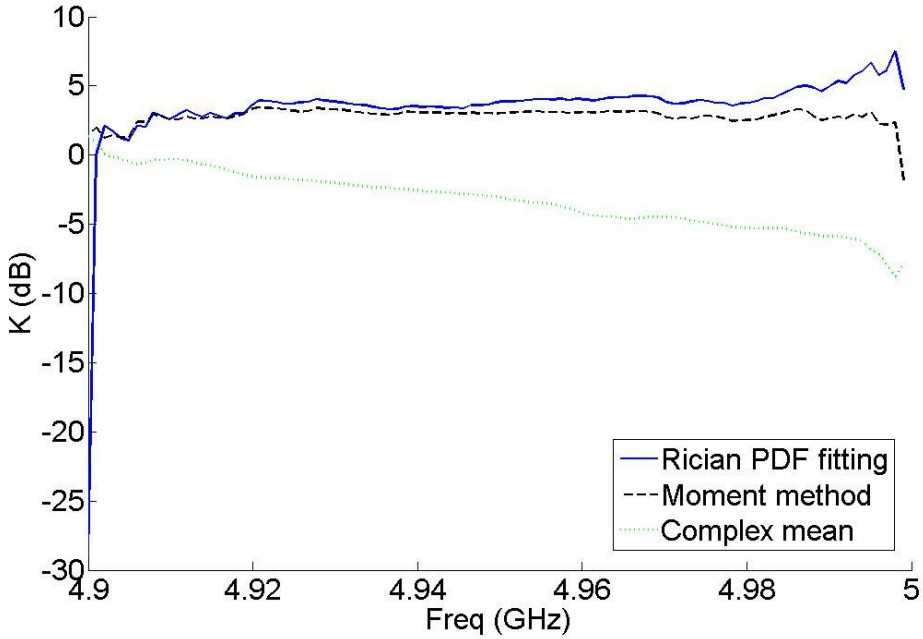

Figure 4.18 K-factor estimated using the different approaches for 40 meter separation between transmitter and receiver.

Method	Mean over frequency, 20 meter separation [dB]	Mean over frequency, 30 meter separation [dB]	Mean over frequency, 40 meter separation [dB]
Complex mean	-6.8	-5.1	-3.0
Moment method	4.5	3.3	3.0
Rician PDF fitting	5.3	4.4	3.8

Table 4-3 The mean K-factor for different estimation methods and receiver locations. The mean is computed over all the frequencies.

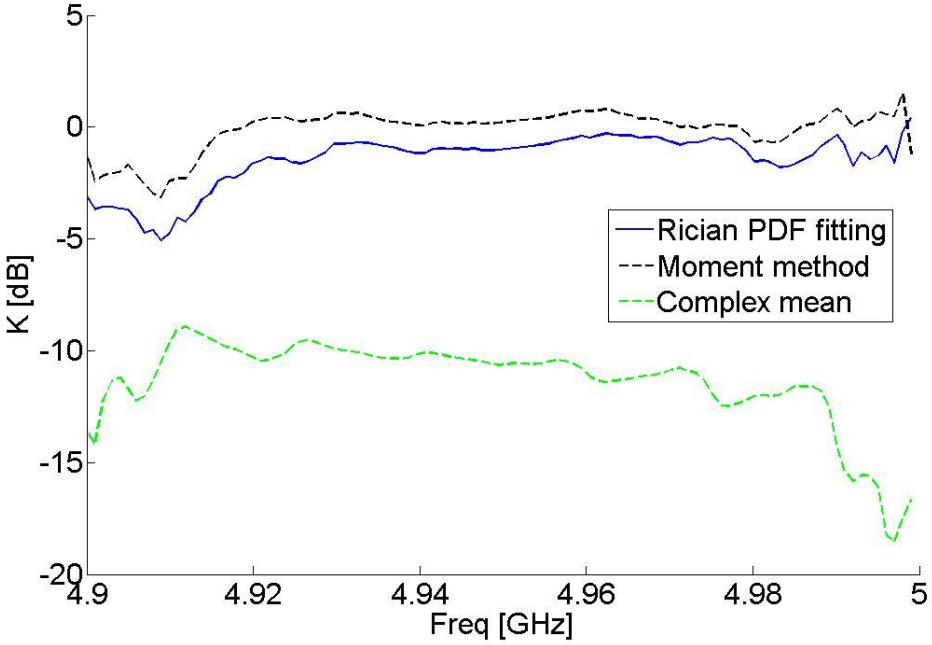

Figure 4.19 K-factor estimated using the different approaches and data from all the different positions of the receiver.

4.4 Discussion

The simulations as well as the measurements show that all the methods for estimating the K-factor give similar results for a high K-factor. The simulations also show that these values are close to the true value. For small K-factors, however, the methods based on the distribution of the field amplitude give an overestimation of the K-factor value, whereas the complex mean approach still gives an accurate estimate. The deviation from the real value for the moment method and the Rician PDF fitting starts to significantly increase for K-factor values below 0 dB, which clearly is seen in Figure 4.3 to Figure 4.5. It is interesting to note that the more samples used for the estimate, the smaller the error.

The less accurate estimation obtained by using the methods based on the field distribution is expected, since these estimations are based on less information due to the lack of phase data. The worse estimate at lower K-factor values can be explained in the following way. When a very weak unstirred component is present, the Rician distribution deviates insufficiently from that of a Rayleigh. The methods try to fit a Rician distribution to a Rayleigh distribution, but the value of the mean is too small to be accurately estimated. This can be concluded from Figure 4.15, where the mean is seen to have much larger oscillations than the variance in Figure 4.14 and thus is estimated poorly. Thus only qualitative conclusions can be drawn when the K-factor is below 0 dB. When there is a strong unstirred component, the mean v has a value large enough to be estimated correctly. This is why the envelope methods work well for the case with a higher value of the K-factor.

Furthermore, when variable antenna positions are used in order to acquire the necessary number of samples, as for the real-field data presented, the complex mean approach cannot be used. This can be concluded when studying Figure 4.16 to Figure 4.18, where the complex mean approach is seen to give a much smaller value than the other methods. Since it is known that the measurement corresponds to a line-of-sight link between the antennas, a mean K-factor of -6.3 dB at 20 m separation is improbable. It is also supported by the fact that the K-factor estimated by the moment method and the PDF fitting is decreasing with increased separation, whereas the K-factor estimated with the complex mean approach is increasing. A larger separation decreases the line-of-sight component and thus the K-factor. In these cases, the estimations from the amplitude distribution methods are necessary. For high K-factors (above 0 dB) the methods will give an accurate value, based on the simulation results. However, for small K-factor values the envelope methods cannot be expected to give the true value.

The reason for not being able to use the complex mean approach for data from measurements with variable antenna positions is that when the transmitters and receivers are moved throughout the measurement, the phase of the transfer function will no longer be distributed around the Gaussian complex mean value (the value of the direct component). The values will instead be spread around complex mean values with the same magnitude but with different orientations in the complex plane. Thus, taking the complex mean of this distribution of data will not give the

true value (it would be close to 0). The methods based on the distribution of amplitude values will not be affected by the altering of the phase when moving the antennas. The data samples at different antenna positions will have the same Rician distribution, as long as the distance between the antennas is not changed too much to affect the amplitude of the signal. The effect of changing the distance too much can be seen in Figure 4.19, where the K-factor is estimated to be below zero dB also by using these methods. The reason for this is that the distribution of amplitude values is not Rician when the amplitude is changing.

Moreover, the results show that there is a small deviation between the moment method and the Rician PDF fitting approach, at least for small K-factors. Based on the simulated data, the PDF fitting method gives the best estimate for small K-factors. It is of interest to mention that also the Maximum Likelihood Estimation (MLE) has briefly been addressed. This method is often used for parameter estimation (see for example [10] and [12]). However, it was seen that the results from the MLE approach did not give any significant difference from the results obtained with the moment method and the Rician PDF fitting. This is probably due to that it also is based on the distribution of the field amplitudes.

Finally, regarding the convergence in the K-factor value, as can be seen in Figure 4.6 to Figure 4.11 the estimated K-factor will deviate from its true value when there is not enough independent samples. This apparent K-factor due to a finite number of independent samples introduces an error in the estimate of the K-factor. To account for this finite sample contribution it is important to verify that the number of independent samples collected in the measurement is enough for having convergence in the K value. From the results in Figure 4.10 and Figure 4.11 it is further concluded that the other methods based on the envelope distribution give convergence at somewhat larger sample numbers. This is reasonable since once again these methods are based on less information (no phase information). The Rician PDF fitting gives convergence at somewhat lower sample numbers as compared to the moment method. This is expected, since the PDF fitting approach is an improvement of the moment method. The graphs in Figure 4.6 to Figure 4.11 can be used to determine the number of samples needed in order to get a desired accuracy in the estimated K-factor, using a specific method.

5 The number of independent samples

As mentioned in section 2.7, the accuracy of an estimated parameter from reverberation chamber data is good when the data consists of a large number of uncorrelated, or independent, samples. The higher the correlation among the samples, the less information is available for the parameter estimation. Measurements in reverberation chambers should be designed to give as many independent samples as possible, in order to increase the accuracy of the estimated parameter. The possibility to generate a large amount of independent samples in a measurement is thus an important characteristic of a reverberation chamber. Both the stirring method employed and the stirring sequence affect the maximum number of independent samples that can be collected.

Moreover, it is of interest to be able to predict the number of independent samples from the chamber characteristic. This would facilitate the design of future chambers and stirring sequences. In the literature various attempts have been made in order to relate physical measures of the chamber as well as characteristics of the field in the chamber to the number of independent samples. The relations are also shown to give good agreement with the estimated number of independent samples from measurements in specific reverberation chambers (see for example [5], [14] and [30]). However, the different relations diverge and show dissimilarities in terms of the constituting parameters and the relation between the parameters. They also include constants that must be determined for a specific chamber and stirring method. No general formula has yet been shown to successfully predict the number of independent samples in an arbitrary chamber.

In this chapter the number of independent samples in the NIST reverberation chambers is studied for different stirring sequences and with a minimized unstirred component. The autocorrelation function is used for determining the degree of correlation between the samples. Since the chambers use rotational stirrers, the minimum angle step required for collecting uncorrelated samples is found. Based on this information, the number of independent samples for one revolution of the stirrers is determined. Also, for chamber 1, other stirring sequences are proposed that give a significant increase in the number of independent samples compared to only rotating the stirrers one revolution. Checking all the possible combinations of the stirrers is of course not possible. Thus some cases are carefully selected. The stirring sequences are designed for rotating stirrers, but can be applied to other stirring techniques as well, with some minor modifications. Finally, two different methods from the literature for estimating the number of independent samples are evaluated for the NIST chambers.

5.1 The maximum number of independent samples in a reverberation chamber

This section presents some theoretical models found in the literature for estimating the number of independent samples. These methods are appropriate for the stirring performed in the NIST reverberation chamber and will be evaluated for measurements in later sections. Also, the method used in the following subsections to determine the number of independent samples from measured data is described and the different stirring sequences employed are presented.

5.1.1 Theoretical models for estimating the number of independent samples

In the literature various expressions for the number of independent samples have been proposed. In [10] Hill derives the correlation function for the total complex electric filed at different points in a reverberation chamber. According to the author, the autocorrelation function $\rho(r)$ at a separation r between two points in the chamber is given by

$$\rho(r) = \frac{\sin(kr)}{kr} \tag{5.1}$$

where k is the wave number. This is a sinc function and decays in an oscillatory manner. The author further defines a correlation length l_c as the distance between the points which corresponds to the first zero in the autocorrelation function.

$$l_c = \frac{\lambda}{2} \tag{5.2}$$

In other words, the smallest required spatial separation between sample points in order to have uncorrelated samples is half a wavelength. This relation can be used to estimate the number of independent samples when samples are to be collected at different antenna locations, for example when platform rotation is employed in the chamber. By separating the sample points by at least half a wavelength, the number of independent samples will simply be the same as the total number of samples. Equation (5.2) is also proposed in [30] to be used to estimate the total number of independent samples when the stirring is performed by spatial displacement of two plates in the chamber. It has been verified from measurements that if the plates are stepped a distance that is equal to or larger than half a wavelength, the samples can be considered to be uncorrelated. However, even much smaller distances than half a wavelength can give uncorrelated samples, depending on the stirrer size in terms of wavelength. The correlation distance is thus also dependent on other factors than the spacing between samples.

There are also other proposed ways of estimating the number of independent samples in the chamber from the chamber characteristics. According to [32] the chamber volume V, the equivalent stirrer volume V_s (the smallest cylinder within which the stirrer fits) and the chamber Q is related to the number of independent samples N_{ind} for one revolution of a rotating stirrer according to the following relation.

$$N_{ind} = C_{mech}\frac{QV_s}{V} \tag{5.3}$$

C_{mech} is a constant and is in [14] found from measurements to be approximately unity. If using the relation between the chamber Q, the average mode bandwidth Δf and the frequency f from [5],

$$Q = \frac{f}{\Delta f} \tag{5.4}$$

(5.3) can be expressed as

$$N_{ind} = C_{mech}\frac{V_s f}{V\Delta f} \tag{5.5}$$

According to this relation the number of independent samples is proportional to the frequency and decreases with increased loading (increasing Δf). Neither in [14] nor in [32] there is a physical explanation for (5.3), however in section 5.4.4 the validity of this expression will be discussed using physical arguments.

Furthermore, in [5] another relation between the number of independent samples and the chamber characteristics is given. If there is no unstirred component present in the total field, the number of independent samples is related to the number of excited modes in the chamber according to

$$N_{ind} = 8N_{mode} \tag{5.6}$$

This equation is physically explained by that every mode in the chamber can be considered to consist of 8 plane waves and that the number of independent samples equals the number of excited plane waves. The number of modes can further be estimated by the mode density in the chamber $\frac{\partial N_{mode}}{\partial f}$ and the average mode bandwidth Δf according to

$$N_{mode} = \frac{\partial N_{mode}}{\partial f}(B_{mech} + \Delta f) \tag{5.7}$$

where B_{mech} is defined as the mechanical stirring bandwidth. B_{mech} is said to be dependent on the stirring method and sequences etc., but has not yet been studied in detail. Using (5.6), (5.7) can be expressed as

$$N_{ind} = 8\frac{\partial N_{mode}}{\partial f}(B_{mech} + \Delta f) \tag{5.8}$$

Equation (5.8) is the product of the number of modes excited for every frequency and the frequency band (number of frequency points) for the present center frequency. The frequency

band has one contribution from the mode bandwidth and one contribution from the mechanical stirring. Using Weyle's formula [5],

$$\frac{\partial N_{mode}}{\partial f} = \frac{Vf^2 8\pi}{c^3} \tag{5.9}$$

where V is the chamber volume, (5.8) can be expressed as

$$N_{ind} = 64\pi \frac{Vf^2}{c^3}(B_{mech} + \Delta f) \tag{5.10}$$

According to this relation, the number of independent samples is proportional to the square of the frequency, when the unstirred component gives an insignificant contribution. Also, the number of independent samples increases with increased loading (increased Δf).

5.1.2 Estimation of the number of independent samples from measured data

An important consideration when performing measurements in a reverberation chamber is how to accurately estimate of the number of independent samples from the measured data. A commonly employed technique is to calculate the autocorrelation function between the measured samples. Also, in [14] the autocorrelation approach is said to be the most widespread method for reverberation chamber data. A high correlation between the samples means that less information is available from the measured data. Calculating the autocorrelation function would give the true number of independent samples, including the contribution from both the stirred and the unstirred components of the electric field.

In [25] the complex autocorrelation function of a data set is said to be the cross-correlation of the data set with itself. For a time-varying signal $x(t)$ the autocorrelation function $R(\tau)$ at time lag τ is given by

$$R(\tau) = \frac{1}{T}\int_0^T x^*(t)x(t+\tau)dt \tag{5.11}$$

If the data set consists of discrete samples the integration can be replaced with a summation. The unbiased form of (5.11) using a summation is given by

$$R(\tau) = \frac{1}{N-\tau}\sum_{n=0}^{N-\tau-1} x^*(t)x(t+\tau), \quad \tau \geq 0 \tag{5.12}$$

where N is the total number of data points and τ is the sample number. The unbiased form of the autocorrelation function assumes an acyclic data set. The summation period are made smaller when the time lag τ increases, which reduces the reliability of this estimate for the larger sample numbers. In the reverberation chamber the samples are measures of the receive signal S_{21} for

different stirrer positions. This is analogous to different time signals. Thus, by substituting this into (5.12), the autocorrelation function for different stirrer positions is given as

$$R(m) = \frac{1}{N-|m|} \sum_{n=0}^{N-m-1} S_{21}^{*}(n) S_{21}(n+m), \quad m \geq 0 \tag{5.13}$$

where m is the sample number at which the autocorrelation function is evaluated ($S_{21}(0)$ corresponds to the first sample). The unbiased form is needed for the samples collected in the reverberation chamber.

The autocorrelation function is according to the above discussion thus a measure of the degree of similarity between samples in a data set. It is evaluated over all the collected samples, comparing them with the previous sample. The sample number Δ at which the normalized autocorrelation function has dropped to a certain threshold is then found and the number of independent samples can be calculated from the relation [14]

$$N_{ind} = \frac{N}{\Delta} \tag{5.14}$$

In the NIST reverberation chamber the sample number Δ can be translated to a stirrer angle offset $\Delta\theta$ and N be replaced by 360°. In this way the total number of independent samples can be found.

Furthermore, (5.13) only accounts for adjacent sample correlation. This might be enough if only one rotation of the stirrers is used and if the stirrers are non-uniform, so that every stirrer position is unique. However, if a stirring sequence is used that includes more than one revolution of the stirrers, there might be additional correlation due to similar stirrer configurations. This will show up as peaks in the autocorrelation function and must be accounted for separately.

Due to the characteristics of the field in the reverberation chamber, the correlation between the samples will never be zero. Thus a threshold is needed at which the samples can be said to be uncorrelated. The 3 dB level is often used in microwave communications in order find unique signals (see for example [22]). This means that when the normalized autocorrelation function is below 0.5 the samples are assumed to be uncorrelated. However, as can be seen in e.g. [14], for reverberation chamber applications a level of 1/e is commonly applied. Thus, this threshold will also be used in this report.

5.1.3 The number of independent samples in the NIST reverberation chamber 1

According to the above discussion, the separation between the sample positions determines the degree of correlation between the samples. As described in chapter 3 the stirring in the NIST reverberation chamber 1 is performed by rotating two non-uniform metal stirrers. Finding the number of independent samples in this chamber thus means that the minimum required angle

step for collecting uncorrelated samples must be determined. Once this required step has been found, different stepping configurations can be designed.

In the discussion below, plots of a so called angular space will be used in order to graphically depict the stepping pattern. These plots visualize the combined stirrer configuration of stirrer 1 and 2 and are very useful for determining the possible stirrer positions and the separation between the different sample points. This gives a starting point for qualitatively determine the degree of correlation between the samples in a chosen stepping pattern.

5.1.3.1 Adjacent sample correlation

The stirrers in the NIST reverberation chamber 1 are rotated using one specified step size for each stirrer throughout the measurements. When both stirrers are stepped with the same angle, the combined stirrer positions will constitute a line in the angular space. When a step size of 1° is used, the stepping pattern will look as shown in Figure 5.1 and Figure 5.2. After one revolution the stirrer positions starts to repeat, which is shown as the black square in the lower left corner in Figure 5.2. The 361:st sample will thus be perfectly correlated to the first sample (since the first sample corresponds to zero rotation). No more information will thus be gained after the 360:th sample. Also, as can be seen in Figure 5.2 the separation between each stirrer position is very small. There is thus a reason to believe that the correlation between these adjacent samples is high. Having a too small angle step, which results in an adjacent sample correlation above the defined threshold, will add no more information. This emphasizes the importance of studying the minimal step size possible in order to collect as many independent samples as possible.

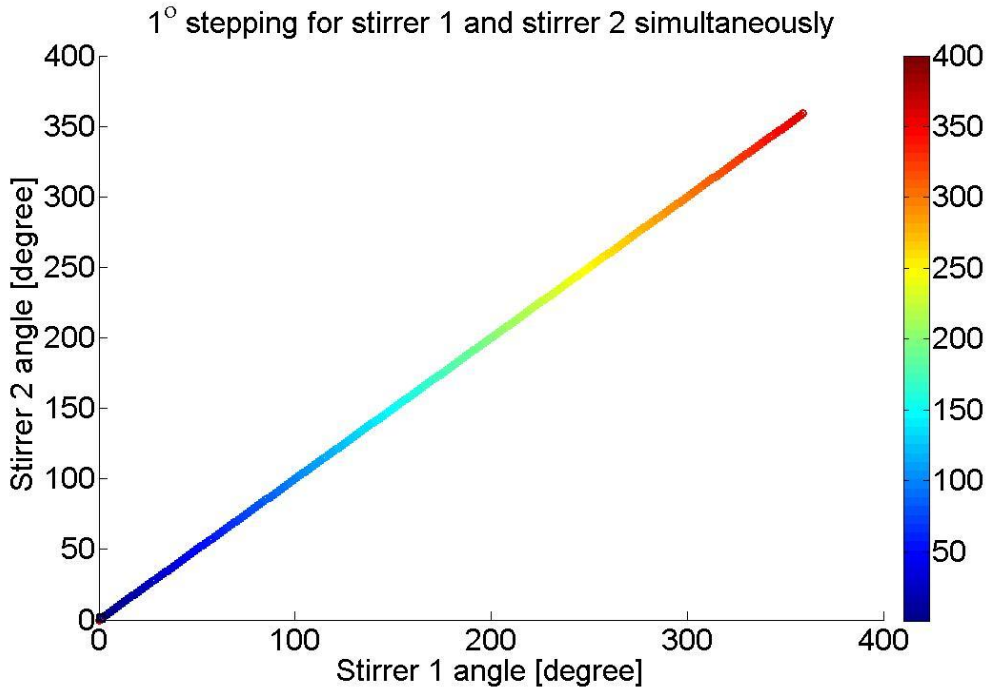

Figure 5.1 The stepping pattern for the 1° stepping for stirrer 1 and 2 simultaneously. The color bar corresponds to the sample number.

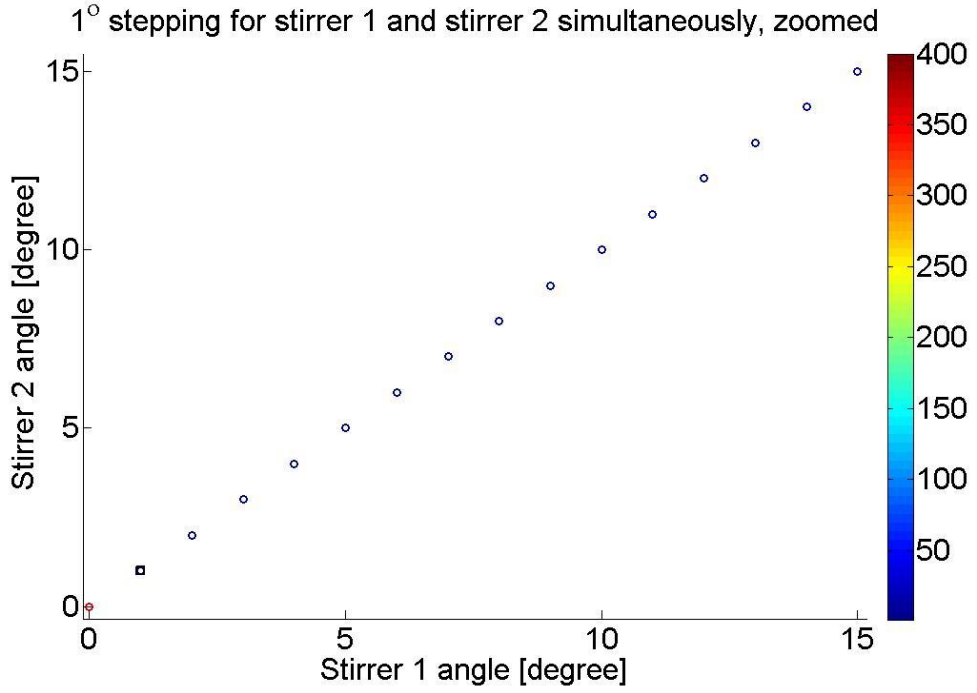

Figure 5.2 The stepping pattern for the 1° stepping for stirrer 1 and 2 simultaneously for the first 15 steps (blue circles) and the last 2 steps (red circle and black square). The color bar corresponds to sample number and the black square in the lower left corner corresponds to repeated stirrer positions (sample number 361).

5.1.3.2 7°/13° stepping configuration

When using the stepping sequence described above where the stirrers are rotated the same angular steps, the stirrer positions are confined to a line in the angular space. This means that only a fraction of the angular space is used. By using angles that are not a factor of 360 the stirrers can be rotated several revolutions without repeating a former position. For example, if one stirrer is rotated in 7° steps it has rotated 364° after 52 steps, which means that it is 4° off from the initial position. All the angle steps that in the same way give an offset from the initial position after one revolution, such as the prime numbers, will spread the combined stirrer positions in different ways. This can mathematically be explained in the following way.

If a stirrer is rotated an angle step α a total of s number of steps, then for the stirrer to return to an identical position the following relation must hold.

$$s\alpha = N \cdot 360 \tag{5.15}$$

where N and s are positive integers not equal to zero. Thus, solving for s gives

$$s = \frac{(N \cdot 360)}{\alpha} \tag{5.16}$$

If α is not a factor of 360, then the right hand side equals a positive, nonzero integer when

$$N = \alpha \cdot m \tag{5.17}$$

where m is a positive integer. Thus, for integer numbers of α, the first time this will be true is for $m = 1$ and the total number of unique stirrer positions will be 360.

Instead of using the same angle step for both the stirrers, different combinations of angles satisfying the requirements above can be used, thus spreading the points in Figure 5.1 over a larger portion of the angular space. There will still be 360 unique stirrer positions, but the separation between every point will be larger. If the stirrers are stepped with an angle that is deemed to give no adjacent sample correlation, there could still be additional correlation due to similar stirrer positions later in the stirring sequence. It is thus of great importance to study the angular plot in order to qualitatively determine if there could be a significant contribution from this additional correlation.

One stepping pattern that is commonly used in the NIST reverberation chamber 1 is shown in Figure 5.3, where stirrer 1 is stepped 7° and stirrer 2 is stepped 13° simultaneously. This 7°/13° stepping configuration is seen to give the minimum separation between adjacent measurement points. This indicates that the correlation between the adjacent samples will determine the number of independent samples. Also, the dotted lines in this figure correspond to rotation of one stirrer only. The points close to these dotted lines are thus also assumed to be correlated with the initial position.

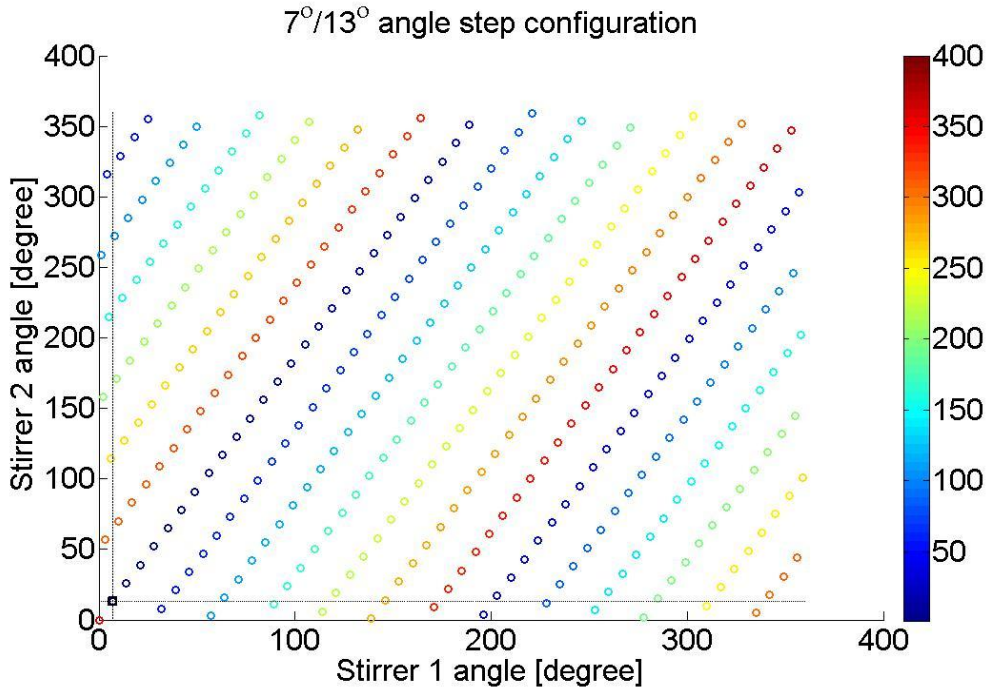

Figure 5.3 The stepping pattern for the 7°/13° angle step configuration. The color bar corresponds to the sample number and the black square in the lower left corner corresponds to repeated stirrer positions (sample number 361). Also, the dotted lines correspond to similar stirrer positions.

5.1.3.3 10° by 10° grid

Another way of spreading the stirrer positions in the angular space is to step one stirrer at a time. When one of the stirrers has completed a full revolution, the other stirrer is rotated one step. By repeating this procedure, a grid of measurement points can be designed. If a sufficiently small angle step is used, the number of unique stirrer positions can be much larger than turning both stirrers simultaneously, as for the 7°/13° stepping configuration. If the angle steps for the stirrers in addition are chosen in order to give no adjacent sample correlation, all the collected samples would be uncorrelated, yielding a large number of independent samples. No additional correlation will be present, since the minimum change in combined stirrer positions for each sample will be the required angle step. An example of such a grid is shown in Figure 5.4 for a 10° step. This grid gives a total of 1296 (36 x 36) unique stirrer positions.

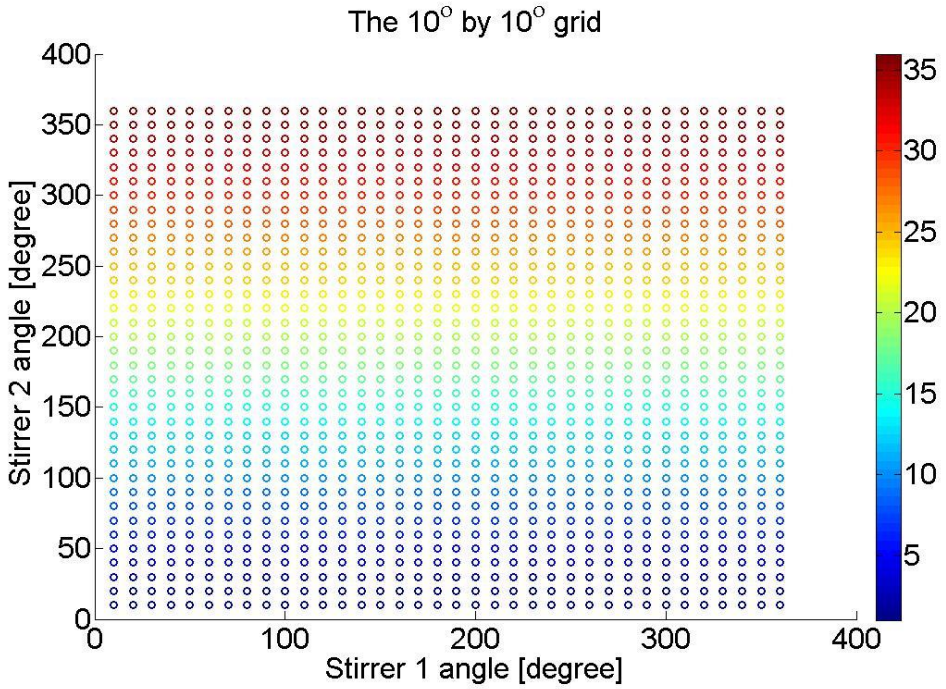

Figure 5.4 The stepping pattern for the 10° by 10° grid. The color bar corresponds to the number of times stirrer 2 is moved.

5.1.4 The number of independent samples in the NIST reverberation chamber 2

For chamber 2 the number of possible stirring sequences is much smaller than for chamber 1, since only one stirrer is employed. The only possibility is to vary the angle step of the stirrer. When the stirrer has been rotated a full revolution, the stirrer positions will start to repeat and the samples will ideally show perfect correlation. If the stirrer is completely non-uniform, there will be no similar stirrer positions during one revolution. In other words, only the adjacent sample correlation must be accounted for. As for the case when stepping the stirrers in chamber 1 one revolution only, finding the number of independent samples thus means that the minimum angle for which the samples are uncorrelated must be found.

5.2 **Measurements**

In this section the measurements for finding the number of independent samples in chamber 1 and chamber 2 are described in detail.

5.2.1 Chamber 1

In order to find the maximum number of independent samples that can be collected in chamber 1 a series of measurements are performed, with different stirrer sequences. The measurements are summarized in Table 5-1 and further described below. In all the measurements the procedure described in chapter 3 is used. The frequency band is 0.8 to 6 GHz using 16001 frequency points, which gives a frequency step of 325 kHz. Cross-polarized horn antennas are employed as transmitting and receiving antennas, thus reducing the unstirred component. The antennas are pointed towards the stirrers, which further minimizes the unstirred energy.

Measurement number	Angle step, stirrer 1 [degree]	Angle step stirrer 2 [degree]	Stepping sequence, stirrer 1/stirrer 2	Number of samples	Loading
1	0.5	0	Step /Hold	720	0
2	0	0.5	Hold/Step	720	0
3	0.5	0.5	Step/Step	720	0
4	0.5	0	Step /Hold	720	3
5	0	0.5	Hold/Step	720	3
6	0.5	0.5	Step/Step	720	3
7	0.5	0	Step /Hold	720	5
8	0	0.5	Hold/Step	720	5
9	0.5	0.5	Step/Step	720	5
10	0.5	0.5	Step/Hold until one revolution of stirrer 1	441	5
11	7	13		400	5
12	10	10	Step/ Hold until one revolution of stirrer 1	1296	5
13	6	6	Step/ Hold until one revolution of stirrer 1	3600	5

Table 5-1 A summary of the measurements performed for studying the number of independent samples in the NIST reverberation chamber 1.

The first nine measurements are designed to test the minimum angle rotation possible without gaining correlated samples. Also the frequency and loading dependence of the number of independent samples are studied. In the first measurement stirrer 1 is rotated a full revolution and stirrer 2 is kept fixed. The stirrers are according to the specifications constrained to 0.1° steps, however this is seen to give an offset in the rotation. In addition, using 0.1° steps would be too time consuming. Instead, a stepping angle of 0.5° is used, which is deemed to give satisfying accuracy and angle resolution. After each step the transfer function is measured, giving a total of 720 samples. In measurement number 2, stirrer 2 is stepped 0.5°, keeping stirrer 1 fixed and in measurement 3 both stirrers are stepped 0.5° simultaneously. These three measurements are performed in an unloaded chamber and repeated for loading 3 and 5, giving a total of nine measurements.

The four last measurements in Table 5-1 are performed in order to study the correlation between samples due to repeated stirrer configurations, in addition to the adjacent sample correlation. In the 10:th measurement an initial test for studying this correlation is carried out, designing a stepping sequence that gives all possible angle combinations for the stirrers up to 10° rotation. Stirrer 1 is moved with 0.5 steps with stirrer 2 in a fixed position. When stirrer 1 has been moved 10° (20 steps) it is turned back to the original position and stirrer 2 is moved 0.5°. This procedure is repeated until stirrer 2 has been rotated 10° (20 steps). Between every step, the transfer function is measured, thereby collecting a total of 441 samples.

In measurement number 11 stirrer 1 is stepped 7° and stirrer 2 is stepped 13° between every sampling, collecting a total of 400 samples. This allows studying the correlation between samples for the 7°/13° configuration.

As a final test, the stepping sequence consisting of a grid of measurement points is used, where only one stirrer is moved between each sampling. Stirrer 1 is moved a complete revolution while stirrer 2 is kept fixed. When a full revolution is completed, stirrer 2 is moved one step. Both stirrers are rotated with the same angle step. For measurement number 12 the angle step is 10° and in measurement 13 the angle step is 6°. A total of 1296 and 3600 samples are collected, respectively.

5.2.2 Chamber 2

The measurement for determining the number of independent samples in chamber 2 is very similar to measurement number 1 – 9 for chamber 1. The stirrer is stepped the minimum angle step 0.1° 4000 times, giving in total a 400° rotation. Cross-polarized horn antennas are used and pointed towards different part of the stirrer, in order to minimize the unstirred component. The same measurement procedure and PNA settings as described above are used.

5.3 Results

The results from the measurements described in section 5.2 are presented here and are further discussed in section 5.4. For all the results presented, the complex mean of the channel transfer function over the stirrer positions is subtracted from every sample, in order to reduce any unstirred component.

5.3.1 Chamber 1

The subsection is devoted to the results from chamber 1. The chamber 2 results will be presented in the next subsection.

5.3.1.1 Autocorrelation between adjacent samples

The autocorrelation functions for different frequencies and stirring configurations are calculated using data collected in measurement number 1, 2 and 3. Interpolation using 10 points between every data sample is applied to the autocorrelation function to get a finer resolution. Figure 5.5 and Figure 5.6 shows an example of the autocorrelation function for a frequency of 1 GHz and 6 GHz when moving stirrer 1 and 2 simultaneously 0.5° steps (measurement number 3). Plotting the similar functions for measurement number 1 to 9 the sample number is found for which the correlation with the first sample has dropped to the threshold 1/e. Thus, the minimum rotation angle required to acquire uncorrelated samples is determined. This angle is also referred to as the correlation angle. The results can be found in Table 5-2 to Table 5-4 for different frequencies and loading. Measurement number 1 is used for finding the minimum angle step for stirrer 1, measurement 2 for stirrer 2 and measurement 3 for stepping stirrer 1 and 2 simultaneously. As can be seen in the table the minimum angle step decreases fast with increasing frequency for all stirrer configurations. Increasing the loading is seen to increase the minimum required angle step. For load 0 and a frequency of 0.8 GHz the minimum angle steps are 4.9°, 4.3° and 3.2° for stirrer 1, stirrer 2 and stirrer 1 + 2, respectively. For a frequency of 6 GHz the corresponding values are 0.9°, 0.7° and 0.6°. Furthermore, for load 5 the minimum angle steps are 61.4°, 17° and 14° and 7.4°, 2.4° and 1.6° for the lowest and the highest frequencies, respectively. Thus the minimum required angle step strongly depends on frequency and loading.

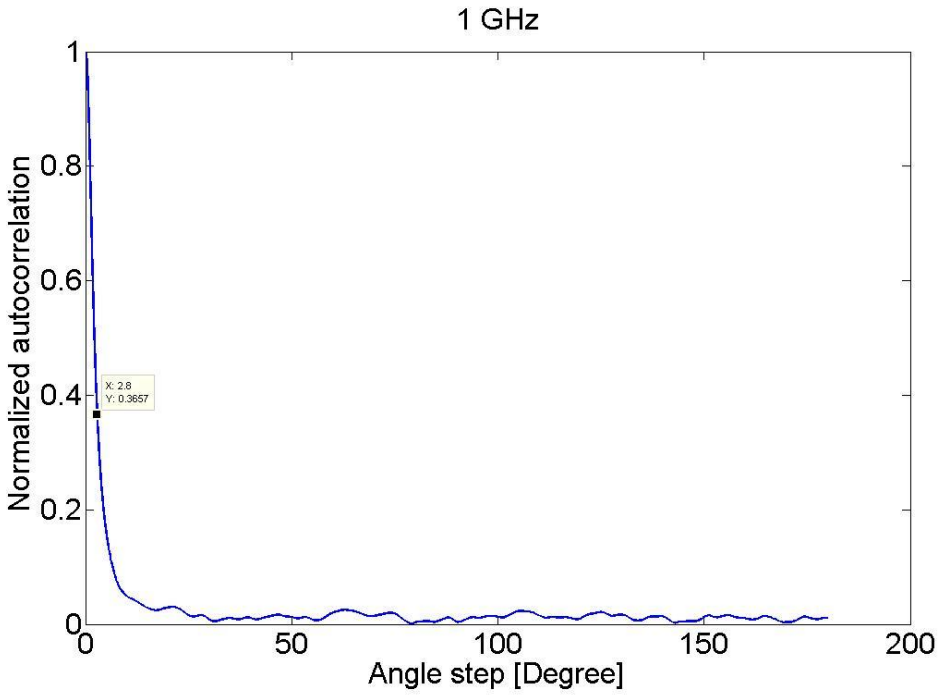

Figure 5.5 The autocorrelation function at 1 GHz between samples collected at different rotation angles when moving stirrer 1 and 2 simultaneously 0.5° steps.

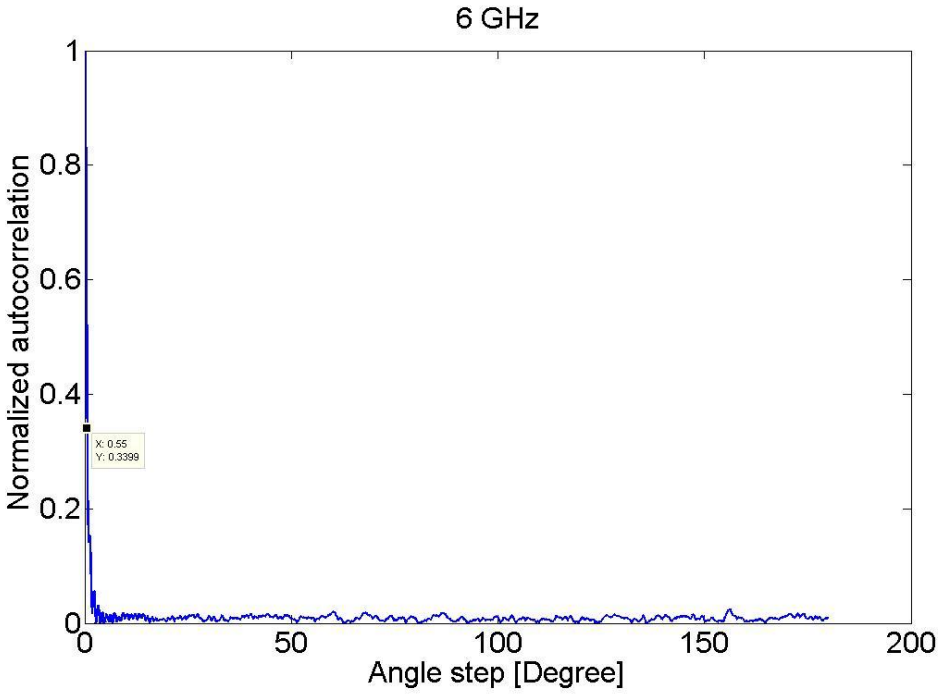

Figure 5.6 The autocorrelation function at 6 GHz between samples collected at different rotation angles when moving stirrer 1 and 2 simultaneously 0.5° steps.

Frequency [GHz]	Q-factor	Minimum angle step, stirrer 1 [degree]	Minimum angle step, stirrer 2 [degree]	Minimum angle step, stirrer 1 + 2 [degree]
0.8	8250	5.0	4.3	3.2
1	10300	4.4	3.8	2.8
1.5	15400	2.9	2.7	2.0
2	20600	2.4	2.0	1.5
2.5	25800	1.8	1.6	1.3
3	30900	1.6	1.4	1.1
3.5	36100	1.4	1.3	0.9
4	41200	1.3	1.1	0.8
4.5	46400	1.1	1.0	0.7
5	51500	1.0	0.9	0.6
5.5	56700	0.9	0.8	0.6
6	61900	0.9	0.7	0.6

Table 5-2 The minimum angle step required for collecting uncorrelated samples in the NIST reverberation chamber for load 0 (average mode bandwidth 0.0970 MHz). The angle step at every frequency is based on a threshold of 1/e.

Frequency [GHz]	Q-factor	Minimum angle step, stirrer 1 [degree]	Minimum angle step, stirrer 2 [degree]	Minimum angle step, stirrer 1 + 2 [degree]
0.8	976	14.6	12.9	9.6
1	1220	13.0	11.2	7.9
1.5	1830	7.2	7.5	5.1
2	2440	7.2	6.2	4.0
2.5	3050	6.5	4.4	3.3
3	3660	4.4	4.1	3.0
3.5	4270	4.1	3.7	2.4
4	4880	3.3	3.0	2.1
4.5	5490	3.3	2.7	1.8
5	6100	3.7	2.3	1.8
5.5	6710	2.5	2.2	1.6
6	7320	2.4	1.9	1.4

Table 5-3 The minimum angle step required for collecting uncorrelated samples in the NIST reverberation chamber for load 3 (average mode bandwidth 0.820 MHz). The angle step at every frequency is based on a threshold of 1/e.

Frequency [GHz]	Q-factor	Minimum angle step, stirrer 1 [degree]	Minimum angle step, stirrer 2 [degree]	Minimum angle step, stirrer 1 + 2 [degree]
0.8	452	61.4	16.9	14.1
1	565	34.9	16.7	11.0
1.5	847	17.6	10.0	6.3
2	1130	14.3	7.7	5.0
2.5	1410	11.2	5.3	4.2
3	1690	11.3	5.3	3.9
3.5	1980	9.9	5.1	3.1
4	2260	9.0	3.9	2.8
4.5	2540	8.3	3.4	2.3
5	2820	9.0	3.0	2.3
5.5	3110	8.1	3.0	1.8
6	3390	7.4	2.4	1.6

Table 5-4 The minimum angle step required for collecting uncorrelated samples in the NIST reverberation chamber for load 5 (average mode bandwidth 1.77 MHz). The angle step at every frequency is based on a threshold of 1/e.

Moreover, using the same set of 9 measurements, the frequency dependence of the number of independent samples for one revolution of the stirrers is shown in Figure 5.7 to Figure 5.9 for different loading. The number of independent samples is calculated at every frequency as described in subsection 5.1.2, that is as the ratio of the number of degrees for a complete revolution (360°) and the minimum angle required for uncorrelated samples, based on a threshold of 1/e. These figures clearly show the frequency and loading dependence of the number of independent samples. Using both stirrers is seen to give the largest number of independent samples. Also stirrer 2 is seen to give more independent samples than stirrer 1. The same trend is seen when increasing the loading.

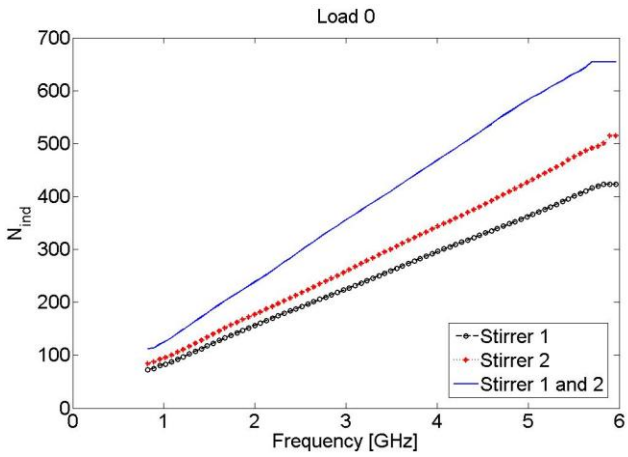

Figure 5.7 The variation over frequency for the number of independent samples for load 0, based on one revolution of the stirrers and a threshold of 1/e.

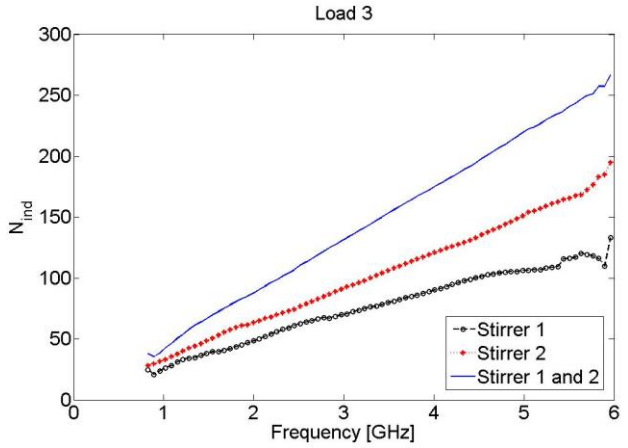

Figure 5.8 The variation over frequency for the number of independent samples for load 3, based on one revolution of the stirrers and a threshold of 1/e.

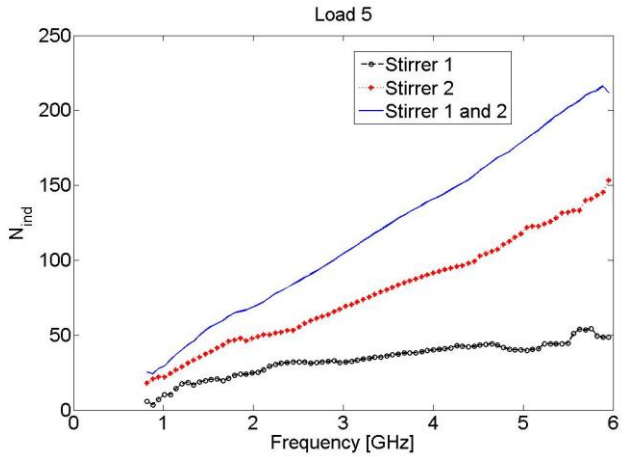

Figure 5.9 The variation over frequency for the number of independent samples for load 5, based on one revolution of the stirrers and a threshold of 1/e.

5.3.1.2 Autocorrelation due to similar stirrer configurations

For a discussion about the additional correlation due to similar stirrer positions the autocorrelation functions for different stirrer sequences are plotted in Figure 5.10 to Figure 5.18. Figure 5.10 corresponds to data from moving the stirrers in the 0.5° grid (measurement 10) for a frequency of 2 GHz. In this figure there are local maxima at every 21:st sample. The maxima are seen to decrease in amplitude for larger sample numbers.

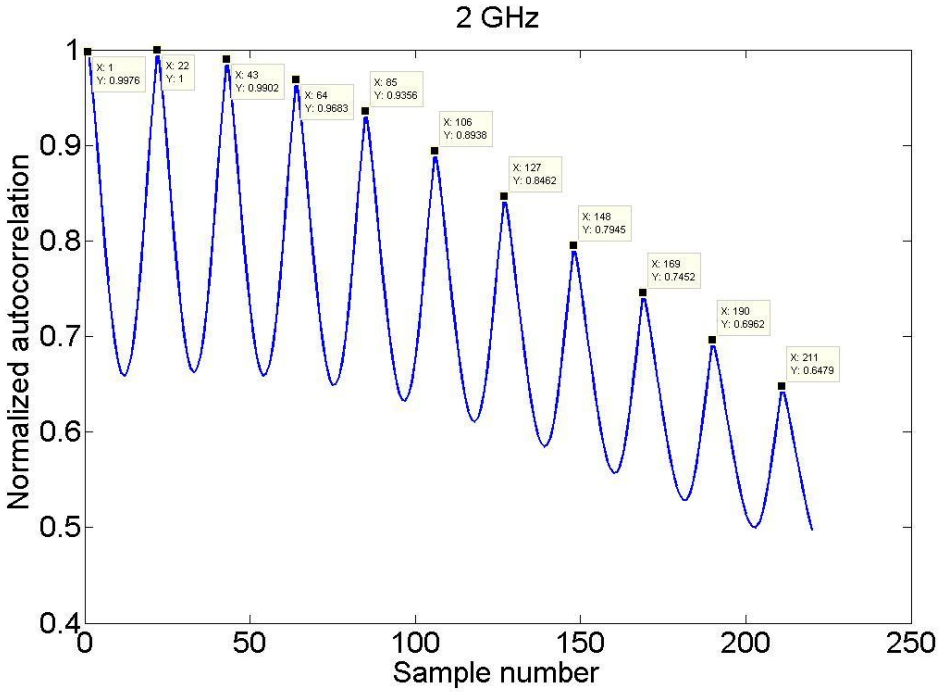

Figure 5.10 The autocorrelation function for stepping 0.5° steps (measurement 1) for 2 GHz. The peaks appear at every 21:st sample.

5.3.1.3 7°/13° stepping configuration

Data from the 7°/13° stepping configuration (measurements 11) is used to find the autocorrelation function in Figure 5.9 for the frequencies 1, 2, 3, 4, 5 and 6 GHz. In this figure there is a distinct peak for sample number 359. (The peak should ideally appear at sample number 361. This deviation is further discussed in chapter 7.) Also, additional peaks appear at various sample numbers. These sample numbers are given in Table 5-5 along with the sample numbers for stirrer positions similar to the initial position, based on Figure 5.3. As can be seen from the table, the sample numbers for the peaks and the similar stirrer positions agree well. In Figure 5.9 the 1/e threshold is also marked. As can be seen, almost all the peaks are below the threshold. Only the peak at sample number 56 for the 1 GHz case is somewhat above. The second sample for the 1 GHz case is also given, which is seen to be above the threshold.

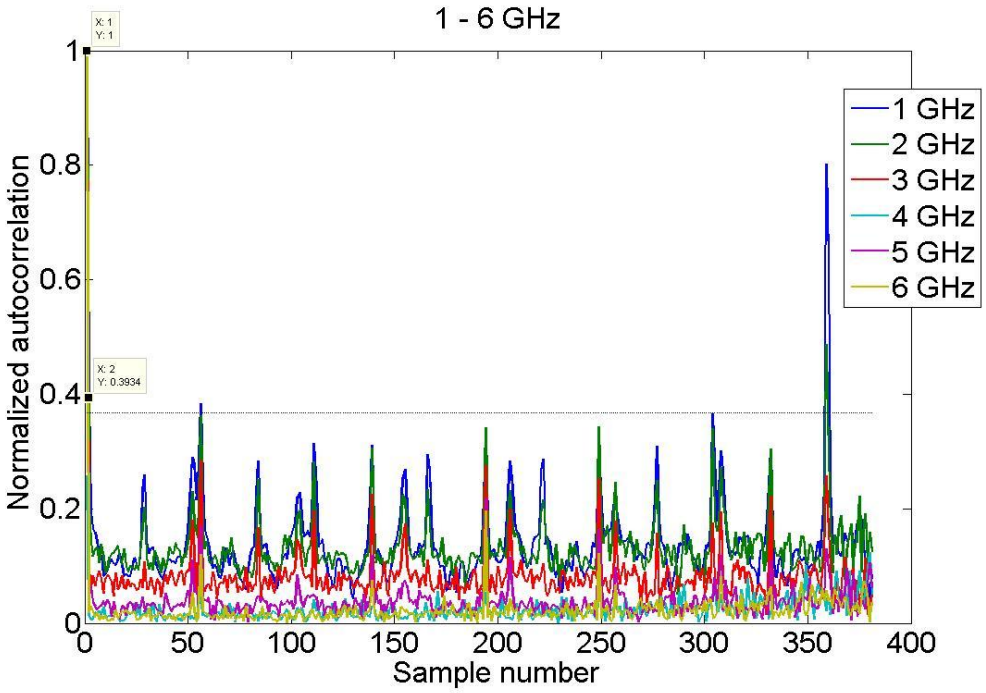

Figure 5.11 The autocorrelation function for the 7°/13° stepping configuration for six different frequencies in the range 1 – 6 GHz. The dotted line is the 1/e threshold.

Sample number for stirrer configurations similar to the initial position	Sample number for the peaks in the autocorrelation
29	29
53	52
57	56
85	84
104	104
111	111
140	139
156	155
168	166
195	194
207	206
223	222
251	249
259	257
278	277
306	304
310	308
334	332
361	359

Table 5-5 Comparison between the sample numbers for stirrer configurations similar to the initial position and the peaks in the autocorrelation function for the 7/13 stirring configuration for 2 GHz.

5.3.1.4 10° by 10° grid

In Figure 5.12 to Figure 5.15 the autocorrelation functions for the grid of 10° steps are plotted for the frequencies 1, 1.5, 2.5 and 6 GHz. These results are based on measurement number 12. The figures show peaks at every 36th sample and the amplitude of these peaks decreases with frequency. At 1 GHz neither the second sample, nor the second peak is below the threshold 1/e. For the 1.5 GHz case, the second peak is below the threshold, but not the second sample. At 2.5 GHz both the second sample and all the additional peaks are below the threshold. Also, the variation over frequency for the number of independent samples for the 10° by 10° grid is plotted in Figure 5.16. The number of independent samples is calculated as the ratio of the total number of samples and the sample number at which the amplitude of the autocorrelation function has dropped to 1/e. To account for the additional correlation, when peaks are present that are above the threshold the total number of samples is replaced by the number of samples before the additional peak in the autocorrelation function. This figure clearly shows that the number of independent samples for this stirrer configuration is reaching the total number of samples at 2.3 GHz. Also, for frequencies between 1.5 GHz and 2.3 GHz there is only correlation between adjacent samples. Finally, for comparison, the autocorrelations for a grid of 6° steps (measurement 13) are plotted in Figure 5.17 to Figure 5.18 for the frequencies 1, 3 and 4 GHz. These figure shows peaks at every 60:th sample. For the 1 GHz case the first peak, as well as the second sample, shows a correlation with the first sample above the threshold. For 3 GHz the amplitude of this peak is below 1/e, however the second sample is still above the threshold. For 4 GHz both the first peak and the second sample is below the threshold.

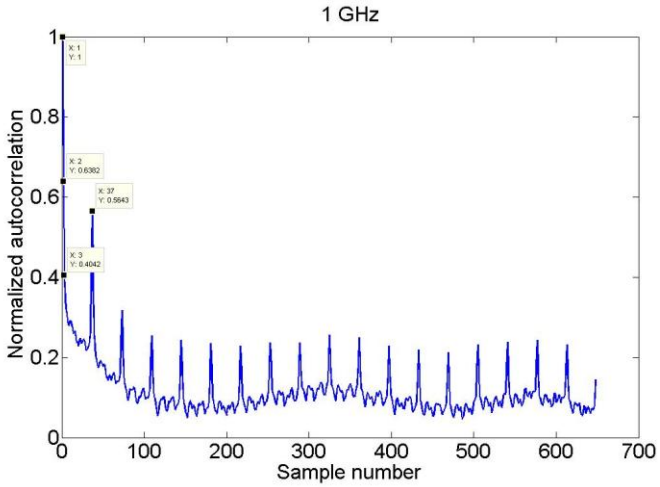

Figure 5.12 The autocorrelation function for the 10° by 10° stepping grid for a frequency of 1 GHz.

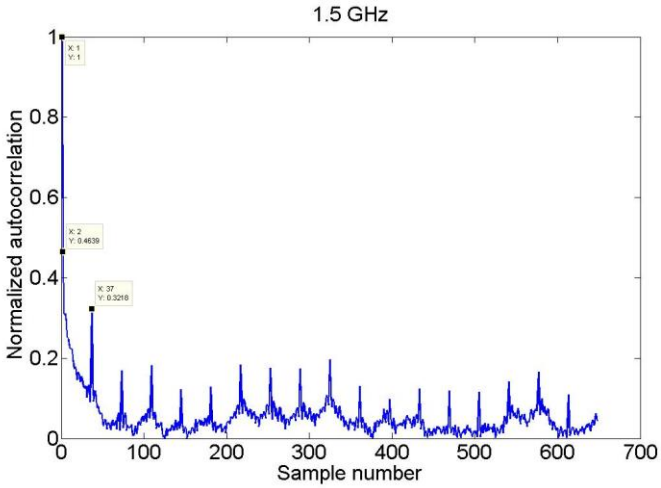

Figure 5.13 The autocorrelation function for the 10° by 10° stepping grid for a frequency of 1.5 GHz.

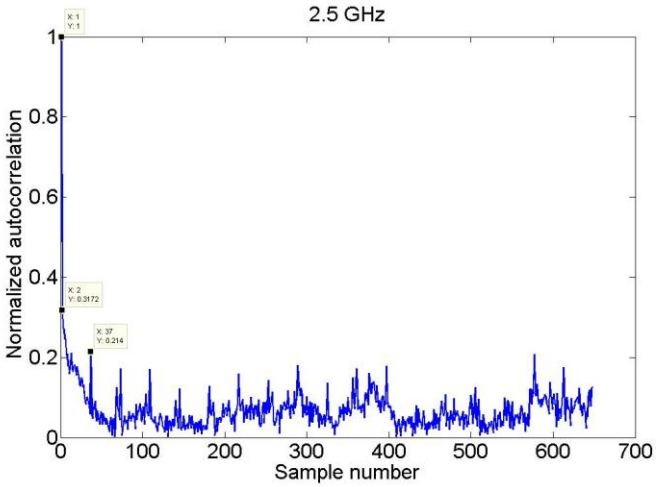

Figure 5.14 The autocorrelation function for the 10° by 10° stepping grid for a frequency of 2.5 GHz.

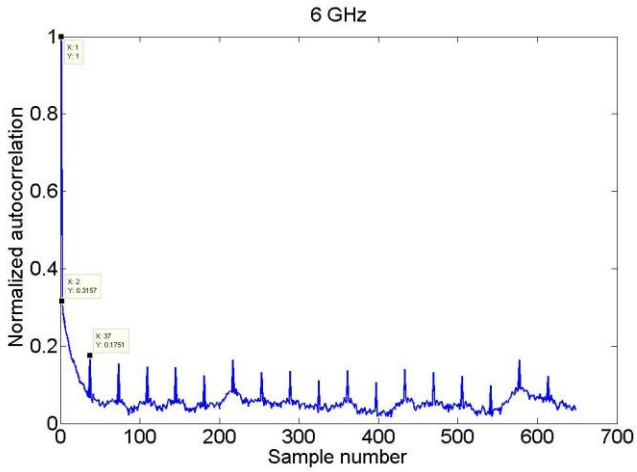

Figure 5.15 The autocorrelation function for the 10° by 10° stepping grid for a frequency of 6 GHz.

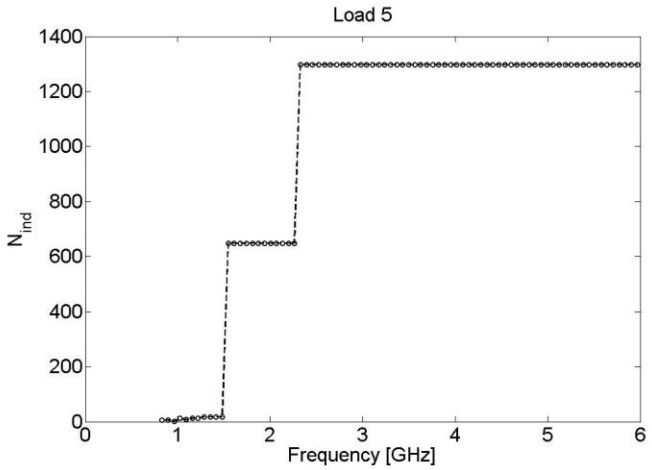

Figure 5.16 The variation over frequency for the number of independent samples for load 5, based on the 10° by 10° stepping grid, using a threshold of 1/e.

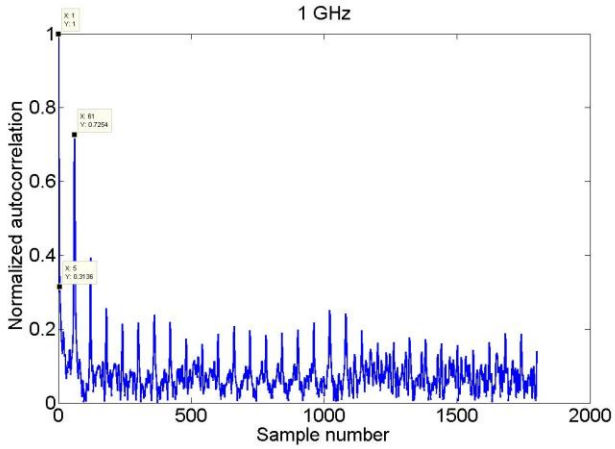

Figure 5.17 The autocorrelation function for the 6° by 6° stepping grid for a frequency of 1 GHz.

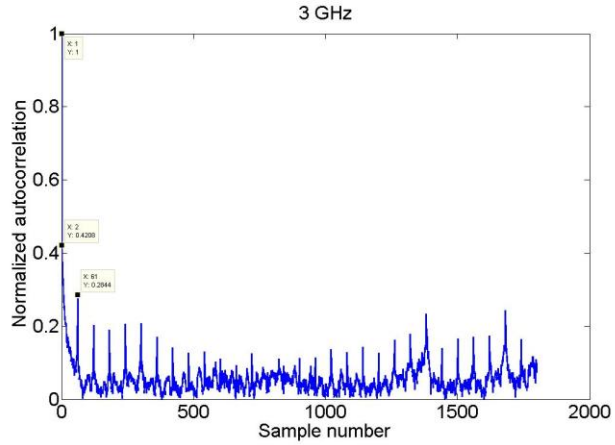

Figure 5.18 The autocorrelation function for the 6° by 6° stepping grid for a frequency of 3 GHz.

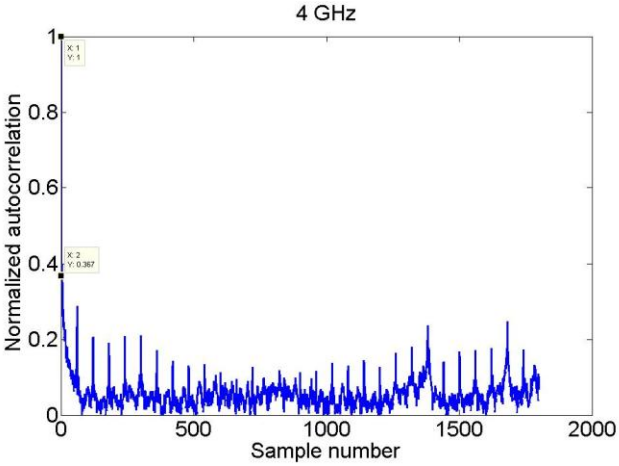

Figure 5.19 The autocorrelation function for the 6° by 6° stepping grid for a frequency of 4 GHz.

5.3.2 Chamber 2

The autocorrelation function calculated from the measurements in chamber 2 is shown in Figure 5.20 for the bandwidth 0.8 – 2 GHz. This plot shows that after the autocorrelation has dropped off below the threshold, no additional peaks above the threshold are present, except at sample number 3677. (The peak should ideally appear at sample number 3600. This deviation is further discussed in chapter 7.) From this figure the minimum angle steps in Table 5-6 is found in the same way as for chamber 1. In accordance to chamber 1, this angle is seen to decrease (the sample number for which the autocorrelation function is below the threshold decreases) with increased frequency. Based on this information the number of independent samples is calculated as a function of frequency using the procedure described in subsection 5.1.2. The result is shown in Figure 5.21.

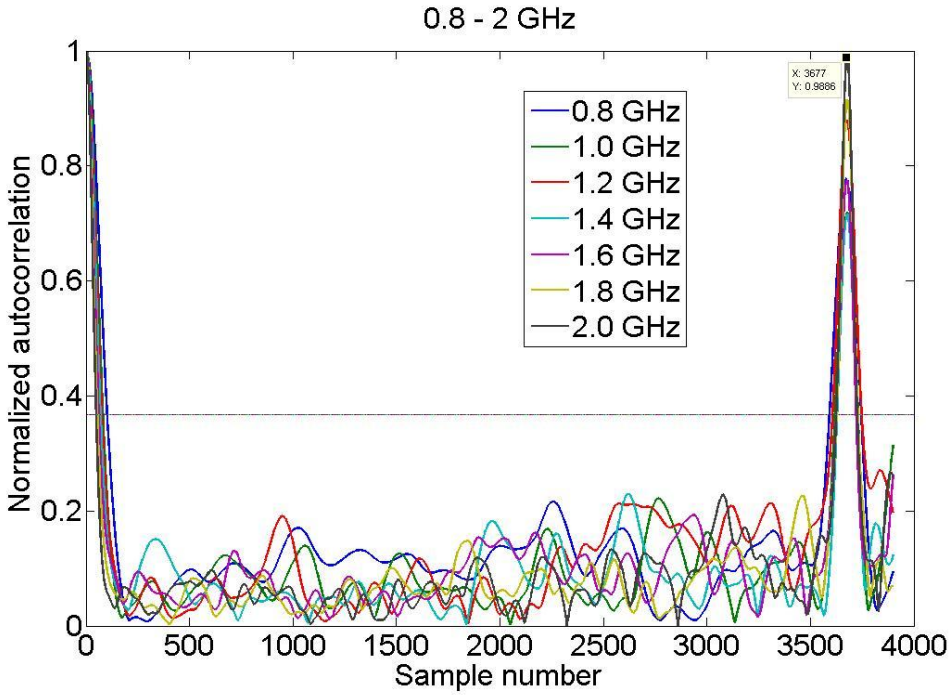

Figure 5.20 The autocorrelation function calculated from the measurements in chamber 2 for six different frequencies in the range 1 – 6 GHz. The dotted line is the 1/e threshold.

Frequency [GHz]	Q-factor	Minimum angle step [degree]
0.8	520	8.7
1	650	6.8
1.5	980	5.9
2	1310	4.0
2.5	1630	3.3
3	1960	2.8
3.5	2290	2.2
4	2610	2.1
4.5	2940	1.8
5	3270	1.6
5.5	3600	1.5
6	3920	1.3

Table 5-6 The minimum angle step required for collecting uncorrelated samples in the NIST reverberation chamber 2 for load 5 (average mode bandwidth 1.53 MHz). The angle step at every frequency is based on a threshold of 1/e.

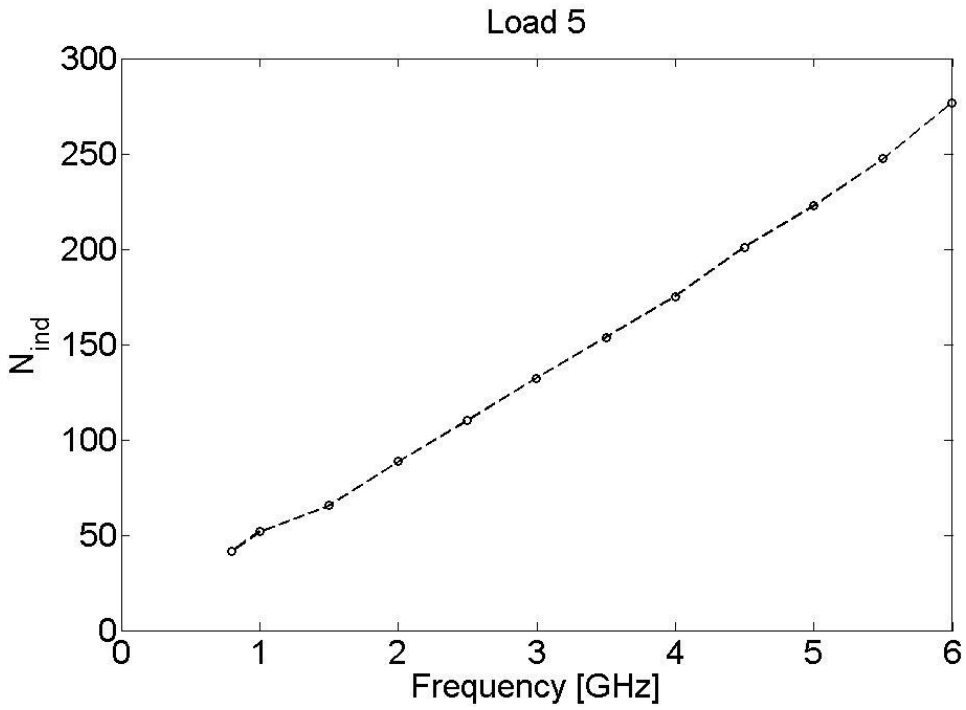

Figure 5.21 The variation over frequency for the number of independent samples for chamber 2 load 5, based on one revolution of the stirrers and a threshold of 1/e.

5.4 Discussion

This section is focused on evaluating the performance of the reverberation chamber and the different stirring sequences in terms of the number of independent samples.

5.4.1 Autocorrelation between adjacent samples

Regarding the adjacent sample correlation, from Table 5-2 it is concluded that for an unloaded chamber the minimum required angle step for gaining uncorrelated samples is small, even for the lowest frequencies. Increasing the loading is seen to increase the required angle step. For a heavily loaded chamber Table 5-4 shows that the required angle step is very large for the lowest frequencies. For higher frequencies this angle decreases fast. A smaller angle means more independent samples for one revolution of the stirrers. In other words, the number of independent samples increases with frequency, which is illustrated in Figure 5.7 to Figure 5.9. This is expected, since the same change in environment will be an electrically larger change for higher frequencies than for lower frequencies. There seems to be a linear dependence between the frequency and the number of independent samples (see subsection 5.4.4 for further discussion about this).

Moreover, Figure 5.7 to Figure 5.9 clearly show the effect of loading on the number of independent samples. As is concluded above, higher loading gives less independent samples. Because of this, load 5 is used to study the additional correlation in order to consider a worst case scenario.

Table 5-2 to Table 5-4 further show that a smaller angle step is sufficient when both stirrers are used. Thus stepping both stirrers simultaneously is more effective than only stepping one, which is expected since a larger volume of the chamber is being stirred when using two stirrers. This is even clearer when studying the plot of the number of independent samples as a function of frequency in Figure 5.7 to Figure 5.9, where the number of independent samples is larger for all frequencies when stepping both stirrers. However, an even more interesting observation from these figures, which is also concluded from Table 5-2, is that stirrer 2 is seen to be more effective than stirrer 1. This is can be explained by recalling the information in chapter 3 that the effective stirring volume of stirrer 2 is larger than the corresponding volume of stirrer 1, thus giving a larger change in the environment when rotated compared to stirrer 1. This means that a smaller angle step is required for having the same change in environment.

For chamber 2 the stirrer is seen from Table 5-6 and Figure 5.21 to be more effective than rotating both stirrers in chamber 1. This might be because the average mode bandwidth, and thus the loading, is somewhat smaller for the 5 absorber case for chamber 2, which gives more independent samples for chamber 2. It is however believed mainly to be due to the more irregular shape of the stirrer in chamber 2. When only the adjacent sample correlation is considered, chamber 2 thus gives the largest number of independent samples.

5.4.2 Autocorrelation due to repeated stirrer configurations

The discussion about the number of independent samples in the NIST reverberation chambers in the former subsection has considered correlation among adjacent samples only. When the stirrers are rotated one revolution, it is reasonable to argue that there is no additional correlation. This is based on that for one revolution every stirrer position is unique, due to the asymmetry of the stirrers, which gives a unique distribution of modes in the chamber for every samples point. This is supported by Figure 5.5 and Figure 5.6, where the correlation is seen to be very low after the first peak.

When a stirring sequence is employed that gives similar positions later in the sequence it is not enough to look at the adjacent sample correlation. The autocorrelation function in Figure 5.10 for the 0.5° stepping grid shows very clearly that there is additional correlation between non-adjacent samples that must be accounted for when determining the number of independent samples. The peaks in the figure appear for every 21:st sample point, which corresponding to the stirrer positions where stirrer 1 is rotated back to its original position and stirrer 2 is rotated one step. These samples are the same as if they had been collected when only rotating stirrer 2.

Concerning chamber 2 the autocorrelation function in Figure 5.20 shows no additional peaks after the first peak, which means that the stirrer is irregular enough for giving unique stirrer positions. Thus, when stepping the stirrer a correlation angle for a full revolution there are no more stirrer positions that give correlation above the threshold. After one revolution there are no more unique positions and there will be perfect correlation.

5.4.2.1 7°/13° stepping configuration

The discussion above emphasizes the importance of choosing a stepping sequence that gives stirrer configurations that are as different as possible. Another way of saying this is that the positions in the angle space discussed in subsection 5.1.3 (see for example Figure 5.1) should be as far as possible from each other. When moving both stirrers simultaneously the same angle step, only a small part of the angle space is used. Using the 7°/13° stepping configuration is seen in Figure 5.3 to spread the points in the entire space. Even if the number of unique positions (360) is the same as moving along the diagonal only, the separation between adjacent points is larger, thus making the autocorrelation functions in Figure 5.11 to drop off to a value below the threshold 1/e at the second sample for frequencies above 3 GHz. Thus, even if the 7° rotation of stirrer 1 according to Table 5-4 is not enough for having uncorrelated samples, the additional rotation of stirrer 2 is sufficient to give uncorrelated adjacent samples at these frequencies.

Moreover, according to subsection 5.1.3 above there will be perfect correlation for repeated stirrer configurations. Thus, for the 7°/13° stepping configuration there should be perfect correlation for sample number 361 (since the first sample corresponds to the original position, that is no rotation). As can be seen in Figure 5.11 there is a peak at the 359:th sample, supporting the discussion above. The fact that the peak is shifted 2 samples and the lack of perfect correlation (the peak does not obtain the value 1) is the effect of an offset in the rotation of the

stirrers, which makes the stirrers turning more than 7 or 13° and makes the stirrer configuration for the 360:th sample deviate somewhat from the original position. This issue of non-repeatable stirrer positions and procedures to account for it will be further discussed in chapter 7.

The autocorrelation function for the 7°/13° stepping configuration further shows peaks at various sample numbers. These peaks appear for sample numbers corresponding to the similar stirrer configurations as described in subsection 5.1.3.2. This can be concluded from Table 5-5, where the sample numbers for similar stirrer positions (from Figure 5.3) and the sample number for the peaks in Figure 5.11 are given. As for the peak at the 361:st sample number, the smaller peaks are shifted somewhat from the expected value. There is also an indication of a small increase in the shift with increased sample number, which also can be explained by the stirring offset. For a threshold of 1/e, it is seen that the samples acquired at 1 GHz with this stirring sequence cannot be assumed to be independent, since neither the second sample nor the first peak, is below the threshold. However, the amplitude of the peak, as well as the second sample, has still a fairly low correlation. It can thus be argued that even at 1 GHz the samples are uncorrelated.

The variation in amplitude of the peaks is due to that some of the different stirrer positions are more close to the initial position than others. In Figure 5.3 this corresponds to points more or less closer to the dotted lines. Some positions of the stirrers might also be more similar than others because of the variation in shape of the stirrers.

According to the above discussion, the 7°/13°stepping configuration can thus be expected to give up to 360 independent samples at frequencies above 1 GHz. After the 360:th sample the stirrer configurations are starting to repeat and no more unique samples can be collected. If a stepping configuration is desired where both stirrers are rotated simultaneously for the lower frequencies, other angle steps might give larger separation between the combined measurement points. Using the angular plot in Figure 5.3 it is concluded that 7° and 13° are the minimum separation between the sample points. If instead a stirring configuration of 17°/13° is used, an angular plot verifies that there are a total of 360 unique positions and further shows that the minimum angular distance is 12° for both stirrers. This might be enough to gain an autocorrelation function below the threshold 1/e for lower frequencies.

5.4.2.2 10° by 10° grid

The stepping grid described in subsection 5.1.3.3 and depicted in Figure 5.4 is using a larger part of the angle space than is possible when rotating both stirrers simultaneously. The spacing between each point however becomes smaller, corresponding to more similar stirrer positions. Figure 5.13 and Figure 5.15 support that for frequencies above 2.5 GHz, this spacing between stirrer positions is enough. First of all, the figures show that there is no adjacent sample correlation for these frequencies, since the second sample is below the threshold. This is expected from the discussion in section 5.4.1. Furthermore, the amplitude of the peaks at every 37:th sample is below 1/e for frequencies higher than 2.5 GHz (the figures have been corrected for the stirrer rotation offset), which shows that there is no additional correlation. Figure 5.16

clearly shows the large increase in the number of independent samples at about 2.5 GHz to 1296, which is equal to the total number of samples. This is an improvement from using the 7°/13° stepping sequence.

For frequencies between 1.5 GHz and 2.3 GHz the number of independent samples is lower, about 650, which is due to that only adjacent sample correlation is present. The additional correlation is below the threshold. Still, this number of independent samples is significantly larger than achieved with the other stirring sequences for the same frequencies and loading. Below 1.5 GHz this stepping sequence does not give satisfying results.

In order to have uncorrelated samples for the lowest frequencies, the angle step must be increased. However, 0.8 GHz would require a 62° angle step, based on Table 5-4, which would give only about 33 unique positions. One way to further increase the number of independent samples when measuring over a frequency band is to use variable angle steps, that is decrease the step for higher frequencies in accordance to Table 5-2, Table 5-3 or Table 5-4, depending on the loading used. This would require more advanced software, which is beyond the scope of this report. Also, if the required step size for the two stirrers would deviate much, different angle step could be used for the different stirrers.

If higher frequencies are to be use in the measurements, even more independent samples can be collected by using smaller angle steps. As an example, a grid of 6° steps is studied which gives a total of 3600 samples. From Figure 5.17 to Figure 5.18 it can be concluded that this stepping configuration gives 3600 independent samples at 4 GHz, since the second sample as well as the first peak is below the threshold for this frequency.

Based on the results regarding the loading dependence in Table 5-2 to Table 5-4 and Figure 5.7 to Figure 5.9 it can be argued that if the chamber loading is decreased, a grid of even smaller angles could be used. Thus the number of independent samples could be increased significantly. For example, for an unloaded chamber an angle step of 5° would be enough, giving a maximum of 5184 independent samples. Due to time limitations, no measurements are performed for decreased loading using this stirring configuration.

Finally, one drawback with the grid stepping sequence configuration is that it is more difficult to reduce the unstirred component in the chamber, since only one stirrer is stepped at the time. Thus it is more difficult to acquire the number of independent samples needed in order to achieve the desired accuracy.

5.4.3 Analogy to other stirring techniques

As discussed in chapter 2, different reverberation chambers employ different stirring techniques. For example, the chamber used in [30] employs moving plates and platform stirring. The new stepping sequences developed in this chapter have only been demonstrated for rotational stirrers. It is however straightforward to translate the grid of angles to other stirring techniques. For example, for the two moving plates used in [30] the angle steps would correspond to spatial

displacement steps. The procedure for designing a similar grid for other stirring methods is outlined below.

- Determine the smallest step size possible for the stirrers due to mechanical constraints
- Use the step size found above to move through a full sequence (corresponds to a full rotation of the stirrers) using one stirrer at a time. For each step, measure the transfer function over the frequency band of interest.
- Calculate the autocorrelation function and find the required step size for different frequencies and the different stirrers in order to have uncorrelated samples, based on the desired threshold.
- Design a grid of measurement points using the step size found above. If possible, use different steps for different frequencies and the different stirrers. An analogy to the plot of the angular space in Figure 5.1 to Figure 5.4 can be used for clarification of the separation between stirrer positions, especially if several cycles are used (corresponds to several revolutions for rotated stirrers).

5.4.4 Analytic expression for the number of independent samples

From the discussion so far some important conclusions about the characteristics of the number of independent samples can be drawn.

- The number of independent samples based on the adjacent sample correlation increases linear with frequency for both chambers.
- The number of independent samples decreases with increasing loading, that is increased average mode bandwidth.
- The larger the volume of the chamber that is stirred, the more independent samples.
- The stirring sequence used effects the number of independent samples.

Of the above mentioned characteristics, the effect of the stirring is probably the most difficult to explain. The stirring methods are very different for different chambers. For example, in [5] and [30] the stirring is performed by moving metal plates and in [14] it is performed by a rotating stirrer. A general expression must account for all these stirring techniques. Equation (5.11) from [5] includes a constant B_{mech} in order to account for this. However, it is not known in detail how this constant is affected by the chamber characteristics. Moreover, (5.11) also indicates that the number of independent samples is proportional to the frequency squared when there is no unstirred component. This is in contradiction to the linear dependence which has been verified from the measurements with a reduced unstirred component in this thesis and also in [14]. Also according to this equation, increased loading (increased average mode bandwidth) increases the number of independent samples, which also is in contradiction with the measurement results. Thus, this equation is not applicable for the results in the present study.

Moreover, separating the stirrer positions by half a wavelength, which is proposed in [30], is an oversimplification. This is concluded from the observations that the minimum required angle

step changes with loading. Also, the different stirrers require different angles for making the received samples at the receiving antenna uncorrelated. This means that the sample points are separated by different spatial distances, since the radius of the stirrers are the same. This spatial separation can be studied in Table 5-7. The correlation spacing l which the stirrers have moved is calculated as

$$l = 2r \sin\frac{\theta}{2} \tag{5.18}$$

where r is the radius of the stirrer and θ the angle which the stirrer has rotated between two consecutive positions. It is interesting to note that the required separation in order to make the samples collected at each position uncorrelated is less than half a wavelength. This shows that the stirrer positions can be separated less than half a wavelength and still give uncorrelated samples. The reason for this is that moving the stirrers are not the same as moving an antenna. Due to the scattering of the modes the received field at an antenna in one point in the chamber will change more than if the antenna is moved around in the chamber. It is also interesting to note that the correlation spacing is very constant over the frequencies for each stirring case.

Frequency [GHz]	Correlation spacing between consecutive sample points, stirrer 1 [λ]	Correlation spacing between consecutive sample points, stirrer 2 [λ]	Correlation spacing between consecutive sample points, stirrer 1 + 2 [λ]
1	0.14	0.12	0.090
1.5	0.14	0.13	0.10
2	0.15	0.13	0.090
2.5	0.14	0.13	0.10
3	0.15	0.13	0.11
3.5	0.15	0.14	0.10
4	0.16	0.14	0.10
4.5	0.17	0.15	0.10
5	0.17	0.14	0.10
5.5	0.16	0.14	0.11
6	0.17	0.13	0.12

Table 5-7 The minimum separation required between adjacent sample points for collecting uncorrelated samples in the NIST reverberation chamber for loading 0. The separation is based on the angles from Table 5-2.

Furthermore, (5.5) from [14] seems to be in better agreement with the observed results stated in the bullet list above. This equation is repeated here for convenience.

$$N_{ind} = C_{mech} \frac{V_s f}{V \Delta f} \tag{5.19}$$

The effect of stirring in this equation is given as a ratio of the effective stirrer volume and the volume of the chamber. Increasing the amount of the total stirred volume would increase the number of independent samples, which agrees with the fourth statement in the list.

Equation (5.19) is applied to the estimated number of independent samples for chamber 1 and the constant C_{mech} is determined. The effective stirrer volume is calculated as the smallest cylinder in which the stirrer would fit. When both stirrers are used, the sum of the two effective stirrer volumes is used. The results can be found in Table 5-8 and in Figure 5.22 to Figure 5.24. As can be seen in the figures, there is a good agreement between the measured data and the theoretical curve for all the stirrer configurations. The results from the stirrer 1 measurements have the largest deviations from the theoretical curve, especially for loading 5. This might be explained by the fact that stirrer 1 alone gives insufficient stirring and thus variation of the field, which would be more noticeable at higher loading. However, as can be seen in the table, the constant is not unity as is found in [14]. If the value for stirrer 1 and loading 5 is rejected, C_{mech} seems to be rather constant for the different stirrer configurations used but be dependent on the loading. This indicates that the factor $\frac{V_s}{V}$ is sufficient to account for the stirring used. Finally, (5.20) is also applied to the estimated number of independent samples for chamber 2. The result is shown in Figure 5.25, from which the linear frequency dependence is clear. In this case, the constant C_{mech} is 0.00043, which is very different from the constants found for chamber 1.

Loading	Stirrer 1	Stirrer 2	Stirrer 1 + 2
0	0.13	0.13	0.10
3	0.34	0.35	0.29
5	0.28	0.59	0.53

Table 5-8 C_{mech} for different loading and stirring configurations.

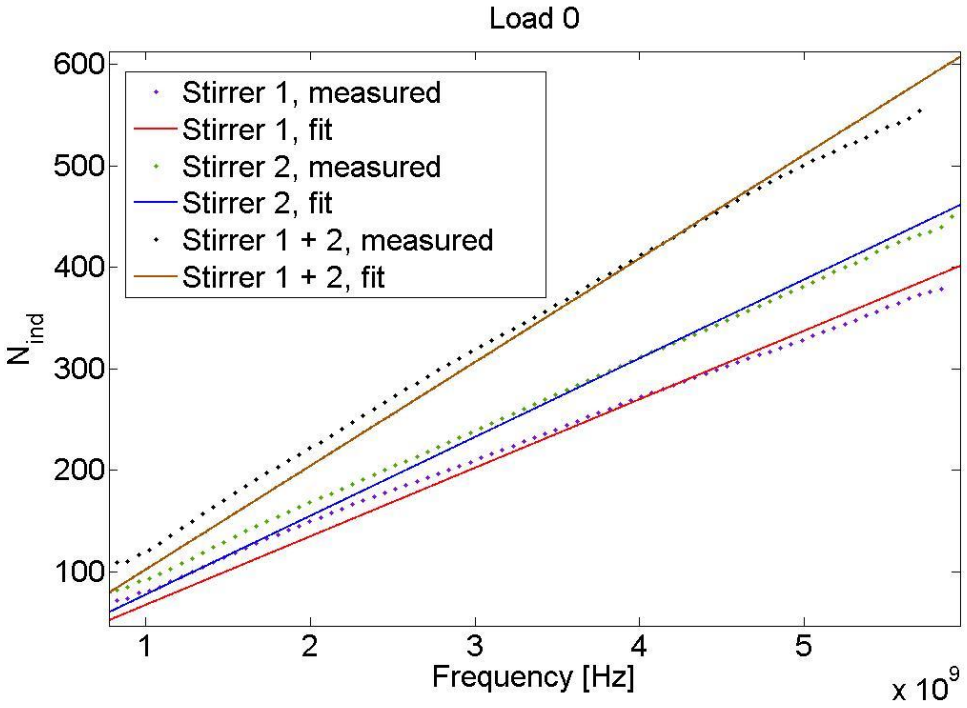

Figure 5.22 Fitting (5.20) to the number of independent samples for load 0.

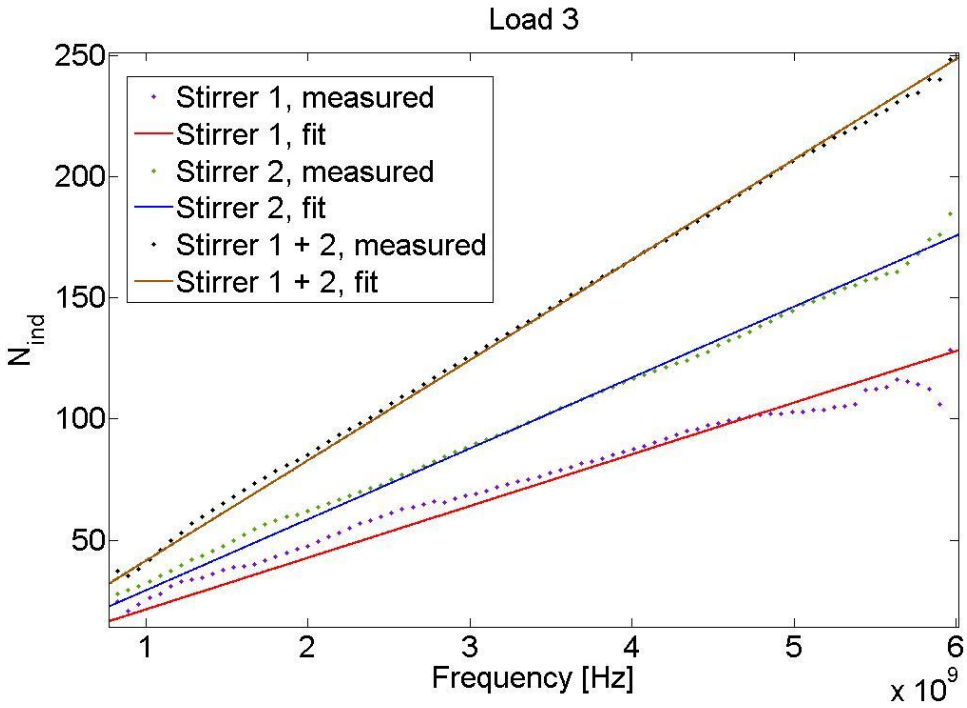

Figure 5.23 Fitting (5.20) to the number of independent samples for load 3.

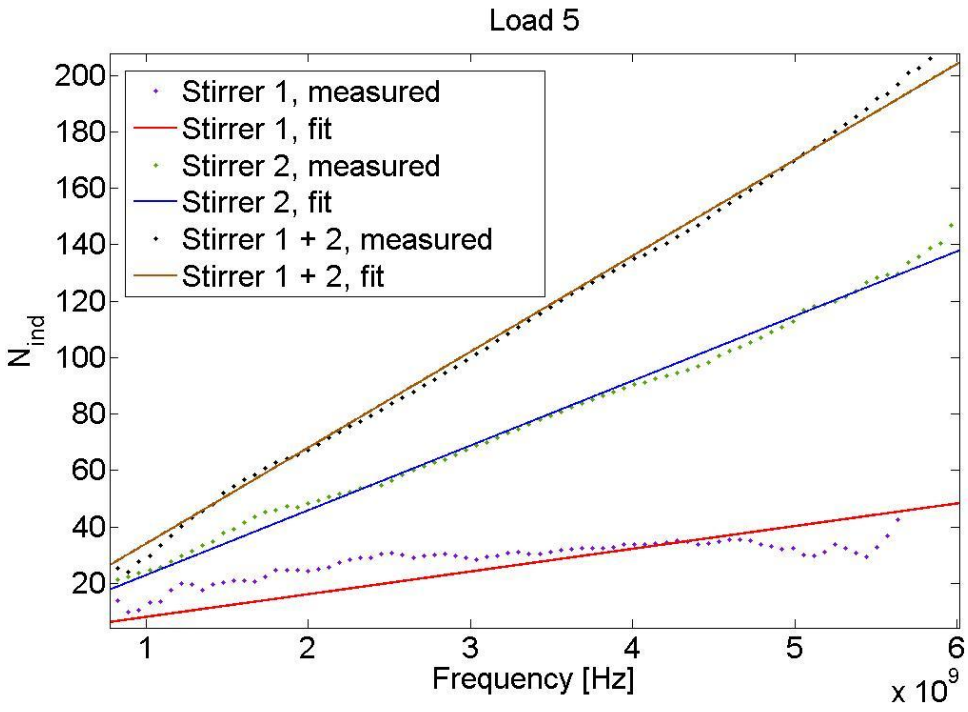

Figure 5.24 Fitting (5.20) to the number of independent samples for load 5.

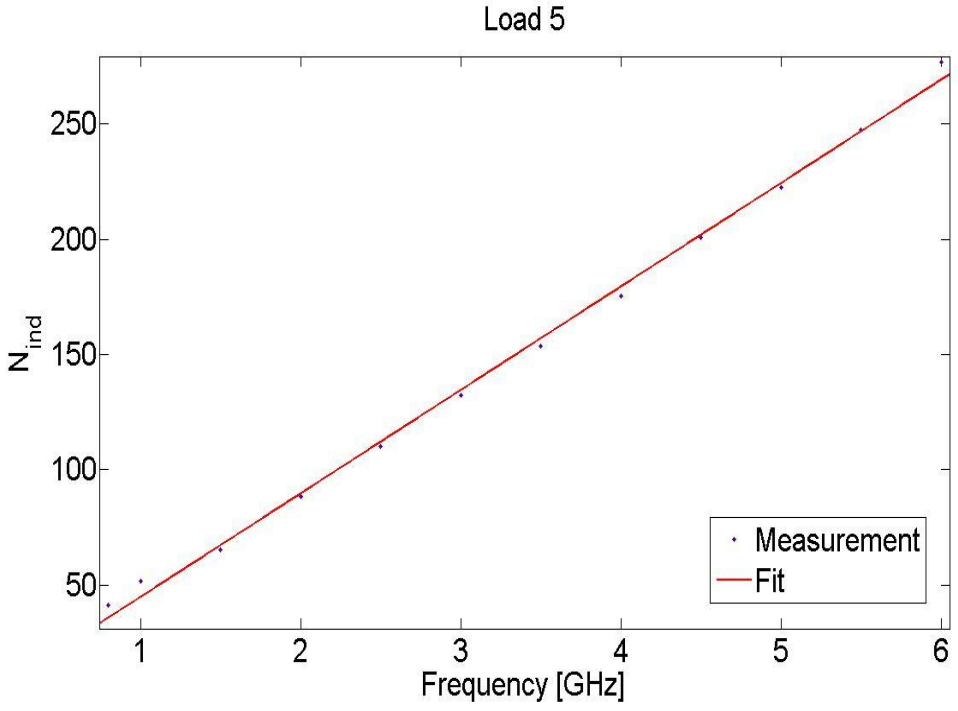

Figure 5.25 Fitting (5.20) to the number of independent samples for chamber 2, load 5.

6 Accuracy of reverberation chamber measurements

As described in chapter 2, the measurements in a well-stirred reverberation chamber should be independent of the locations and orientations of the antennas. In other words, it should be possible to get the same results from measurements with wireless devices regardless of the locations and orientations of the device in the chamber. According to [24] the typical figure of merit is the standard deviation (STD). This gives a measure of the field uniformity and thus the accuracy in the chamber.

The STD is dependent on the number of independent samples acquired in the measurement, which is analyzed in chapter 5. However, this analysis is performed for a minimized unstirred component. When the unstirred component is large relative to the stirred component, that is when the K-factor is large, the correlation between the samples becomes larger and the number of independent samples decreases.

In [4] and [5] an equation for the STD which accounts for this residual error due to the K-factor is proposed. The equation is based on the theoretical expression for the total variance for Gaussian distributed independent samples and on empirical findings. The variables in the equation can be estimated from chamber and antenna characteristics. It is desirable to be able to estimate the STD in advance, for example in order to evaluate chambers without time consuming measurements and to improve the design of future chambers.

Furthermore, in [5] a standardized procedure for calculating the STD in the reverberation chamber from the measured data is proposed. The system validation procedure presented is based on measurements of the mean relative power at different antenna positions in the chamber and has been applied to some chambers with similar sizes and the same stirring techniques (mechanical, platform and polarization stirring). It is shown that the calculated STD from these measurements and the estimation from the theoretical equation mentioned above give similar results.

In this chapter the accuracy in the NIST reverberation chambers is determined by using the system validation procedure proposed in [5]. The validation procedure is also discussed in terms of convergence in the STD value. Moreover, the equation for the STD is explicitly derived from statistical properties and then evaluated by applying it to the measured data from the validation procedure.

6.1 Standard deviation of a Gaussian distributed variable

In order to motivate the system validation procedure and the theoretical equation for estimating the STD, a review of some statistical properties is needed. Thus, in this section the accuracy of an estimated Gaussian distributed variable is first discussed, in terms of the STD. The standard procedure for determining the accuracy in the reverberation chamber proposed in [5] is also presented, along with a standardized way to present it. The expressions for the accuracy from the measured data and the statistical theory are then emerged to give a detailed derivation of Professor P.-S. Kildal's new physical model for the STD in the chamber presented in [4].

6.1.1 Accuracy of an estimated variable

Assume that a data set $X = [x_1, x_2, \dots, x_M]$ with M number of measurements x_i has been collected, with mean μ_X and variance ${\sigma^2}_X$. The estimate $\hat{\mu}_X$ of the mean and the estimate ${\hat{\sigma}^2}_X$ of the variance of the measured data set are then given by [25]

$$\hat{\mu}_X = \frac{1}{M}\sum_{i=1}^{M} x_i \tag{6.1}$$

and

$${\hat{\sigma}^2}_X = \frac{1}{M}\sum_{i=1}^{M} (x_i - \hat{\mu}_X)^2 \tag{6.2}$$

Assume further that there are N number of realizations of X, that is N number of data sets have been collected. It is thus possible to calculate $\hat{\mu}_X$ and ${\hat{\sigma}^2}_X$ for each of these data sets. According to [24] and [25] the variance of the different estimates of μ_X is then given by

$${\sigma^2}_{\hat{\mu}_X} = \frac{\hat{\sigma}_X^2}{N_{ind}} \tag{6.3}$$

where N_{ind} is the number of independent samples in the data. The standard deviation Σ of the estimated mean for the different realizations is thus given by

$$\Sigma_{\hat{\mu}_X} = \sqrt{{\sigma^2}_{\hat{\mu}_X}} = \frac{\hat{\sigma}_X}{\sqrt{N_{ind}}} \tag{6.4}$$

Capital sigma is used to facilitate for the reader to distinguish between the estimated standard deviation of the samples for one measurement ($\hat{\sigma}_X$, which will be seen to correspond to the power over the stirrer positions) and the standard deviation of the estimated mean over the samples for the different measurements ($\sigma_{\hat{\mu}_X} = \Sigma_{\hat{\mu}_X}$, which will be seen to correspond to the mean power over the antenna positions).

For two random variables, X and Y, the sum of their variances is given by [25]

$$Var\{X+Y\} = Var\{X\} + Var\{Y\} + 2Cov\{X,Y\} \tag{6.5}$$

where Cov denotes the covariance between the variables. If the two variables are independent, (6.5) reduces to

$$Var\{X+Y\} = Var\{X\} + Var\{Y\} \tag{6.6}$$

6.1.2 Accuracy estimation in a reverberation chamber

In a reverberation chamber the scattering parameter S_{21} is normally measured for a number of different stirrer positions M. Assume that this measurement is repeated for different receive antenna positions. The standard deviation for these measurements can then be calculated from the measured data. The estimate of the mean power transfer function for the j:th antenna position is according to (6.1) given by

$$\hat{\mu}_{S_{21}j} = G_j = \frac{1}{M}\sum_{i=1}^{M} |(S_{21})_i|^2 \tag{6.7}$$

G_j is the variable used in [4] and [5] for denoting the mean power transfer function over the stirrer positions. Moreover, the estimate of the mean power transfer function for the different antenna positions can be defined as [5]

$$G_{ref} = \frac{1}{N}\sum_{j=1}^{N} G_j \tag{6.8}$$

where N is the total number of receive antenna positions. The estimate of the variance of the power transfer functions over the different receive antenna positions can further be calculated as

$$\hat{\sigma}^2{}_{G_j} = \frac{1}{N}\sum_{j=1}^{N} (G_j - G_{ref})^2 \tag{6.9}$$

If G_{ref}, the estimate of the mean over all receiving antenna positions, is taken as the reference value, then the normalized standard deviation $\bar{\bar{\Sigma}}_{G_j}$ can be expressed as

$$\bar{\bar{\Sigma}}_{G_j} = \frac{\sqrt{\hat{\sigma}^2{}_{G_j}}}{G_{ref}} \tag{6.10}$$

where the bar denotes a normalized variable. The normalization is introduced in order to have comparable measures between different reverberation chambers and between measured and theoretically calculated STD. The relative STD in (6.10) can be translated to a corresponding decibel value according to [30]

$$2\bar{\Sigma}_{G_j}^{dB} = 10log\left\{\frac{1+\bar{\Sigma}_{G_j}}{1-\bar{\Sigma}_{G_j}}\right\} \tag{6.11}$$

or

$$\bar{\Sigma}_{G_j}^{dB} = 5log\left\{\frac{1+\bar{\Sigma}_{G_j}}{1-\bar{\Sigma}_{G_j}}\right\} \tag{6.12}$$

6.1.3 Equation for the standard deviation in a reverberation chamber

According to chapter 2 the average total received power in the reverberation chamber has one contribution from the stirred field and one contribution from the unstirred field. These two contributions are independent and according to (6.6), the total variance Σ_{theory}^2 is then the sum of their variances. Thus

$$\Sigma_{theory}^2 = \Sigma_{stirred}^2 + \Sigma_{unstirred}^2 \tag{6.13}$$

where $\Sigma_{stirred}^2$ is the variance of the mean (over the stirrer positions) power over the different antenna positions. Moreover, $\Sigma_{unstirred}^2$ is the variance of the mean (over platform positions and/or transmitting antennas) power over the different receive antenna positions and is significant whenever platform rotation and/or several transmitting antennas are used. These types of stirring are introduced in order to reduce the contribution from the unstirred component to the standard deviation, which can be explained in the following way. When there is an unstirred component present in the received field, the measured power will be different in different parts of the chamber due to e.g. a varying distance to the transmitting antenna. If platform and polarization stirring is used (see chapter 2), then the direct component can be reduced by averaging the measured power over platform positions and wall antennas. As is discussed [5], the measured power transfer function is proportional to the gain A_{rec} of the receiver antenna.

$$|S_{21d}|^2 \sim A_{rec} \tag{6.14}$$

Since

$$A_{rec} = e_{rec}D_{rec} \tag{6.15}$$

where e_{rec} is the radiation efficiency and D_{rec} is the directivity of the receiver antenna, the average of $|S_{21d}|^2$ over the all orientations of the receiving antenna will be equal to e_{rec} (since the directivity has a mean value of 1). Thus, the unstirred component will be reduced and the measured power for different orientations of the antenna will be more similar, thus reducing the STD. The more platform and wall antennas that are used, the better the estimate of e_{rec}, which decreases the standard deviation of the estimate of the mean power from the direct component.

As is discussed in chapter 2, a well-stirred reverberation chamber gives a Gaussian distributed stirred component. Also, as is further discussed in that chapter, measuring the power at different

positions throughout the chamber is equivalent to measuring the transfer function in one point in the chamber while stirring (this is valid if the line-of-sight component has an insignificant contribution to the unstirred power). The samples measured for different platform positions and/or transmitting antennas will then also be Gaussian distributed, assuming that the samples are uncorrelated. According to equation (6.3), the two terms on the left hand side of (6.13) are then given by

$$\Sigma_{stirred}^2 = \frac{\sigma_{stirred}^2}{N_{stirred}} \tag{6.16}$$

and

$$\Sigma_{unstirred}^2 = \frac{\sigma_{unstirred}^2}{N_{unstirred}} \tag{6.17}$$

where $N_{stirred}$ and $N_{unstirred}$ is the number of independent samples from the different stirring techniques. $\sigma_{stirred}^2$ and $\sigma_{unstirred}^2$ are the variances of the power over the stirrer positions and the platform and/or the different transmitting antennas, respectively. According to chapter 2 the power of the Gaussian distributed field amplitudes is exponential distributed. In [19] it is shown that the mean and the STD for an exponential distributed variable are equal, which evidently implies that the variance and the squared mean are equal. Thus, (6.16) and (6.17) can be expressed as

$$\Sigma_{stirred}^2 = \frac{G_{stirred}^2}{N_{stirred}} \tag{6.18}$$

and

$$\Sigma_{unstirred}^2 = \frac{G_{unstirred}^2}{N_{unstirred}} \tag{6.19}$$

where $G_{stirred}$ is the mean (over the stirrer positions) power from the stirred component and $G_{unstirred}$ is the mean (over the platform positions and/or transmitting antennas) power from the unstirred component, that is

$$G_{stirred} = \frac{1}{N_{stirred}} \sum_{i=1}^{N_{stirred}} |S_{21,stirred}|^2 \tag{6.20}$$

and

$$G_{unstirred} = \frac{1}{N_{unstirred}} \sum_{i=1}^{N_{unstirred}} |S_{21,unstirred}|^2 \tag{6.21}$$

Substituting (6.18) and (6.19) into (6.13) gives

$$\Sigma_{theory}^2 = \frac{G_{stirred}^2}{N_{stirred}} + \frac{G_{unstirred}^2}{N_{unstirred}} \tag{6.22}$$

Equation (6.22) gives the absolute STD. In order to compare it with the relative STD in (6.10) the equation has to be scaled with the mean (over receive antenna positions) total power G_{ref}. Again, the mean for an exponential distributed set of data is equal to the standard deviation of the same data set. Also, the variance of this total power is the same as the sum of the variance of the independent distributions. Thus, the following equation holds.

$$G_{ref}^2 = \sigma_{stirred}^2 + \sigma_{unstirred}^2 = G_{stirred}^2 + G_{unstirred}^2 \tag{6.23}$$

Dividing (6.20) with (6.21) gives

$$\bar{\Sigma}_{theory}^2 = \frac{\frac{G_{stirred}^2}{N_{stirred}} + \frac{G_{unstirred}^2}{N_{unstirred}}}{G_{stirred}^2 + G_{unstirred}^2} = \frac{\frac{1}{N_{stirred}} + \frac{G_{unstirred}^2}{G_{stirred}^2 N_{unstirred}}}{1 + G_{unstirred}^2 / G_{stirred}^2} \tag{6.24}$$

$\frac{G_{unstirred}}{G_{stirred}}$ is the same ratio as is given in (2.6), that is the Rician K-factor K. The relative STD corresponding to (6.10) will thus be given by

$$\bar{\Sigma}_{theory} = \sqrt{\frac{\frac{1}{N_{stirred}} + K^2 \frac{1}{N_{unstirred}}}{1 + K^2}} \tag{6.25}$$

This is the equation proposed by Professor P.-S. Kildal in [4], with a somewhat different notation.

The equations above are only valid if the field amplitudes are Rayleigh distributed. If there is a significant unstirred component present the assumptions will not be valid, since there is no equality between the mean and the variance for the non-central chi-square distribution (the distribution of the power with an unstirred component present).

6.1.4 Reverberation chamber validation procedure

In [5] a systematic way to measure the uniformity of the field in a reverberation chamber is proposed. It is suggested that the mean power over the stirrer positions is measured for at least 9 different receiver antenna positions and orientations. The STD of the mean power should then be calculated using the procedure described in subsection 6.1.2. The 9 measurements should be carried out for the exact same chamber characteristics and stirrer configurations, in order to only study the variation over different positions in the chamber.

In [4] and [5], using moving metallic plates, platform and position stirring, this procedure is shown to give a relative STD (given by (6.12)) below 1 dB, even for a highly loaded chamber. It is proposed that in a well stirred reverberation chamber without any loading a relative STD of about 0.5 dB should be achieved.

6.2 **Measurements**

The system validation procedure described in [5] and briefly outlined in the former section is performed in the NIST reverberation chambers, using different antennas and antenna locations. The purpose is to analyze the field uniformity and the accuracy of the estimate of the STD using (6.25) with the calculated STD from the measured data using (6.12) for different K-factor values. The measurement procedure described in chapter 3 is employed, using the frequency band 800 MHz – 6 GHz and 16001 frequency points.

The system validation procedure is carried out for different loadings, using the horn antennas described in chapter 3. The horn antennas are cross-polarized and pointed away from each other in order to reduce the line-of-sight component. The distance between the two antennas is 2 meters. The receiving antenna is pointed towards stirrer 1 and the transmitting antenna is pointed partly towards stirrer 2 and partly towards the chamber wall. This measurement set-up will give an unstirred component contribution to the total received power. It enables to study the effect of a larger K-factor when the loading is increased, since the unstirred component becomes more significant. If the transmitting antenna would have been pointed towards stirrer 2 completely, the effect of loading would not have been that noticeable, since the field in that case is well stirred and the unstirred component is removed. This would have corresponded to measurement number 11 in chapter 5.

In accordance to [5], the mean power is measured for 9 different antenna positions and orientations. The receiver antenna is moved to 3 heights; 98 cm, 138 cm and 175 cm between the chamber floor and the center point of the antenna. For every height the antenna is oriented horizontally, vertically and in a 45° angle, which in total gives 9 different antennas positions. The transmitting antenna is kept at the same position for all measurements. For every position, the stirrers are stepped simultaneously 100 times, using the 7°/13° stepping configuration described in chapter 5. Between every step, a sample of the complex electric field is collected. This measurement is repeated for loading 0, 3 and 5.

The horn antennas are also used for finding the STD in the chamber when a high K-factor is present. The horn antennas are in this case co-polarized. The transmitting antenna is pointed towards stirrer 1 and the receiving antenna is pointed towards the transmitting antenna. This measurement is performed for load 5. For this setup it is not of interest to change the orientation of the antennas, since that would change the line-of-sight contribution. The mean power from the unstirred component measured in every position would then vary significantly and the STD would increase. Instead, the receiving antenna is moved to 3 different positions in the chamber. The transmitting antenna is also moved in order to have a fixed separation between the two

antennas. In every position, the receiving antenna is moved to three different heights (the same as above), giving a total of 9 positions. The orientation of the receiving antenna relative to the transmitting antenna is kept constant in order to have the same line-of-sight component. The same stepping configuration as above is used.

The system validation procedure is also repeated for omni-directional antennas. As for the co-polarized horn antennas it is not of interest to use different orientations of the antennas, since that would change the line-of-sight contribution. The same procedure and antenna positions as for the co-polarized horn antennas are used. This measurement is also performed for load 5.

Finally, the system validation procedure is also applied to the NIST reverberation chamber 2. For these validation procedures the omni-directional antennas are used. The distance between the two antennas is 1.5 meters. The stirrer is stepped 3.6° to give a total of 100 steps, collecting one sample for each step. The measurement is performed for loading 0, 3 and 5.

6.3 **Results**

In this section the results from the STD measurements described above are presented. The section is divided into two subsections, one for each NIST chamber. All plots are smoothed over a 52 MHz frequency window (unless something else is specified). The averaging is carried out in linear scale and then converted into dB values.

6.3.1 Chamber 1

The STD is calculated with the procedure described in section 6.1.2 for the data from the measurement in chamber 1, where the horn antennas are pointed towards the stirrers (the transmitting antenna is partly pointed towards the stirrer, partly to the chamber wall). Figure 6.1 shows the results for the different loading cases. Also shown in this figure is the theoretically STD computed from (6.25). The K-factors for the different loading cases are also given in Figure 6.2 to Figure 6.4. As can be concluded from the figures, the STD is increased with increased loading (increased K-factor). The mean STD is about 0.5 dB, 0.7 dB and 0.9 dB for load 0, 3 and 5, respectively. The theoretical curves seem to have similar values and characteristic behavior as the STD calculated from the measured data.

In Figure 6.5 the measured and estimated STD is shown for the case when omni-directional antennas are employed in chamber 1. The K-factor is plotted in Figure 6.6. The mean STD is about 1.5 dB for this antenna configuration. The deviation between the theoretically calculated STD and the STD estimated from the measurements is larger than for the previous case.

Finally, Figure 6.7 shows the STD for the case with a strong line-of-sight component. The K-factor is plotted in Figure 6.8. This figure shows an even larger STD and a very large deviation between the calculated and the estimated values.

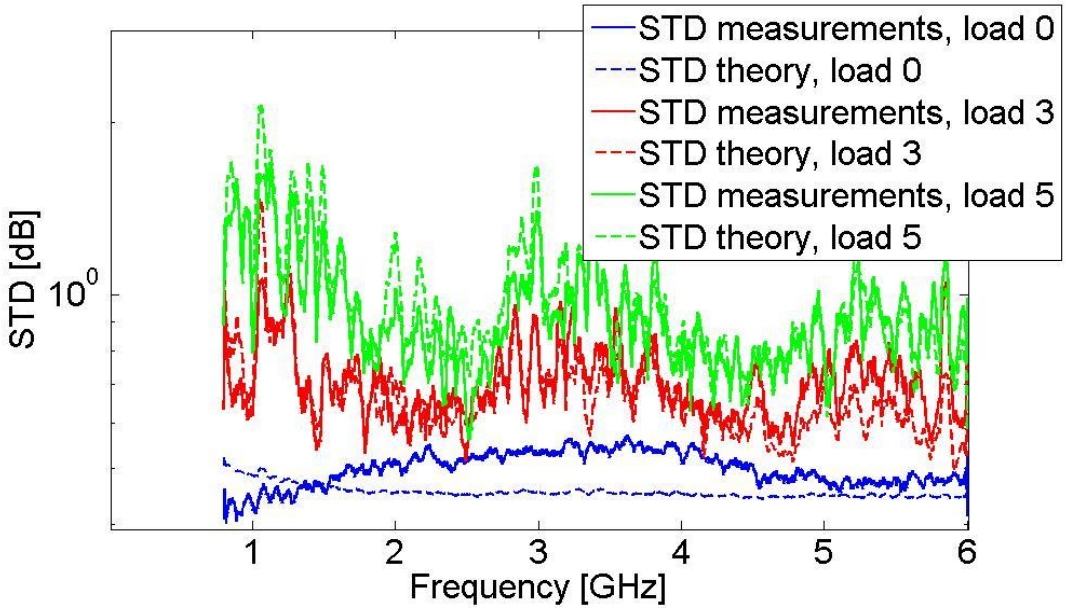

Figure 6.1 The STD calculated from the system validation procedure for load 0, 3 and 5, using the cross-polarized horn antennas. The result is compared to the estimated STD from (6.25).

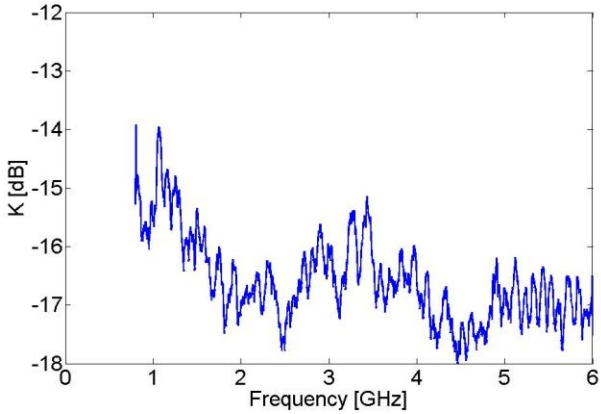

Figure 6.2 The K-factor for the STD measurement in chamber 1 using cross-polarized horn antennas, load 0. The K-factor is averaged over the 9 antenna positions.

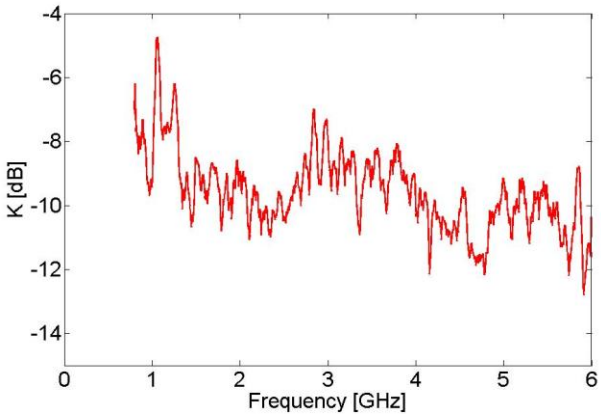

Figure 6.3 The K-factor for the STD measurement in chamber 1 using cross-polarized horn antennas, load 3. The K-factor is averaged over the 9 antenna positions.

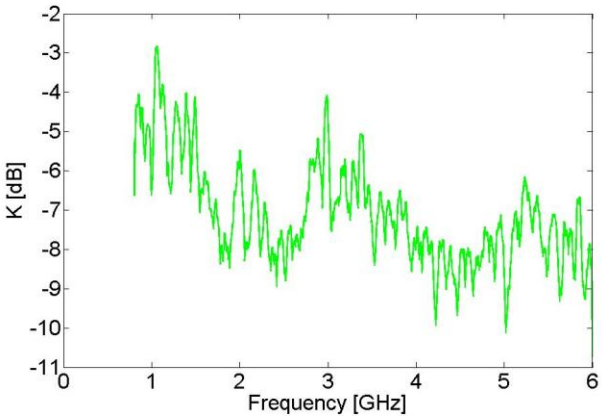

Figure 6.4 The K-factor for the STD measurement in chamber 1 using cross-polarized horn antennas, load 5. The K-factor is averaged over the 9 antenna positions.

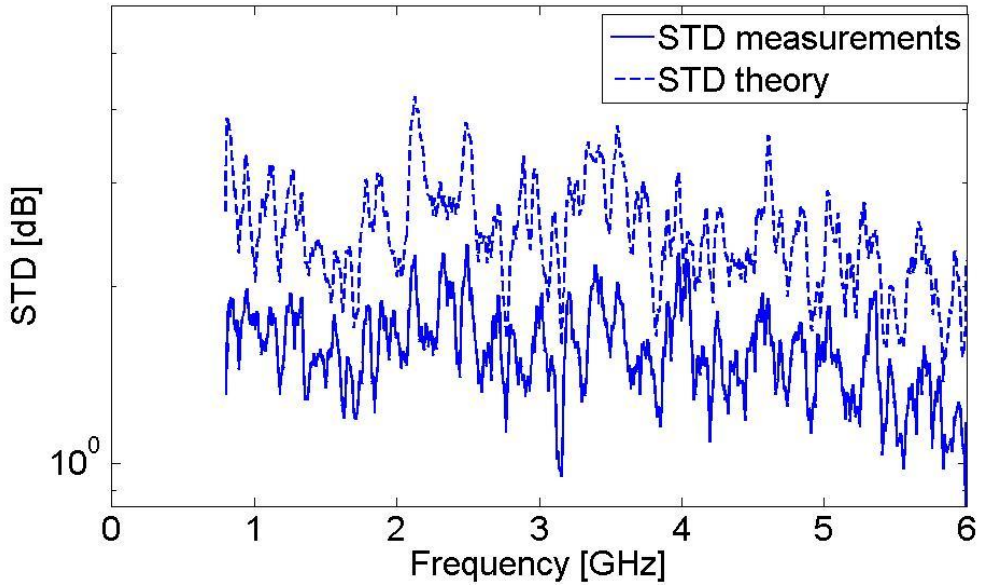

Figure 6.5 The STD calculated from the system validation procedure for load 5 and chamber 1, using the omni-directional antennas. The result is compared to the estimated STD from (6.25).

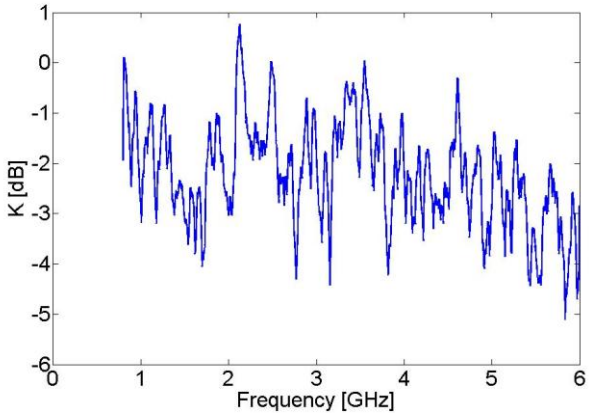

Figure 6.6 The K-factor for the STD measurement using omni-directional antennas, load 5. The K-factor is averaged over the 9 antenna positions.

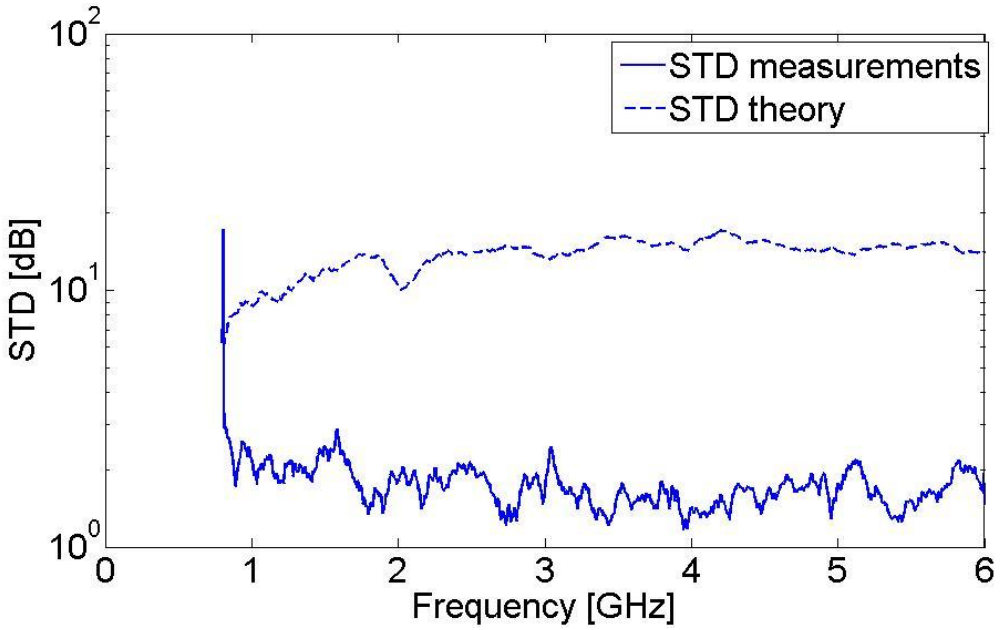

Figure 6.7 The STD calculated from the system validation procedure for load 5 and chamber 1, using co-polarized horn antennas. The result is compared to the estimated STD from (6.25).

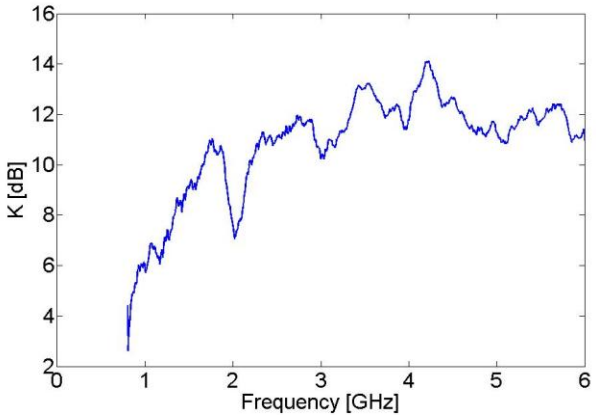

Figure 6.8 The K-factor for the STD measurement using co-polarized horn antennas, load 5. The K-factor is averaged over the 9 antenna positions.

6.3.2 Chamber 2

In Figure 6.9 the results from chamber 2 is shown for the three different loading cases. The K-factors for each of the cases are plotted in Figure 6.10 to Figure 6.12. The STD shows the same dependence on loading as in the chamber 1, that is increased loading give an increased STD. For load 0 the STD is increasing from 0.6 dB at the lower frequencies to 2 dB at higher frequencies. For load 3 and 5 the STD is approximately 2.5 dB and 3 dB, respectively. The difference between the calculated and the measured STD is about 0.5 dB, 2 dB and 3 dB for load 0, 3 and 5, respectively.

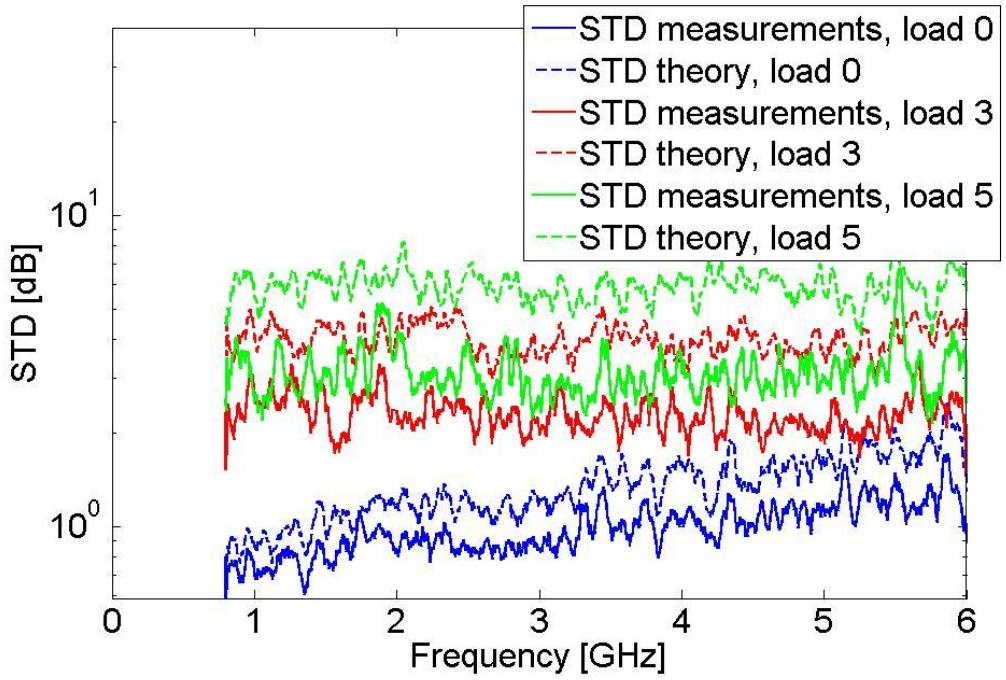

Figure 6.9 The STD calculated from the chamber 2 system validation procedure for load 0, 3 and 5, using the omni-directional antennas. The result is compared to the estimated STD from (6.25).

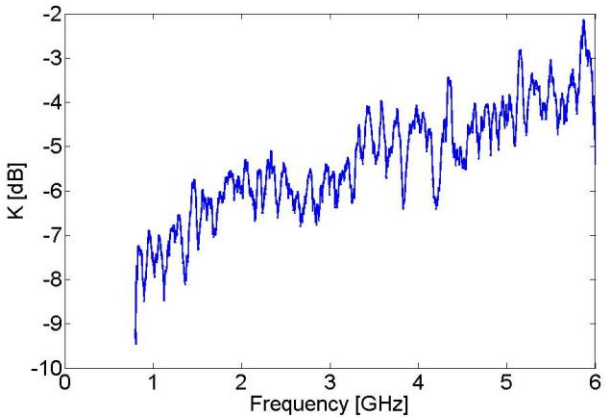

Figure 6.10 The K-factor for the STD measurement in chamber 2 using omni-directional antennas, load 0. The K-factor is averaged over the 9 antenna positions.

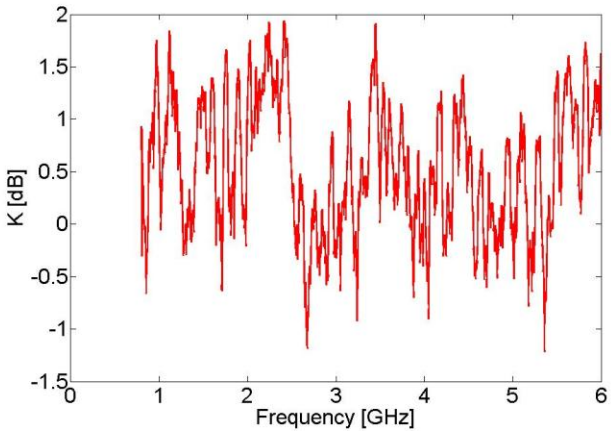

Figure 6.11 The K-factor for the STD measurement in chamber 2 using omni-directional antennas, load 3. The K-factor is averaged over the 9 antenna positions.

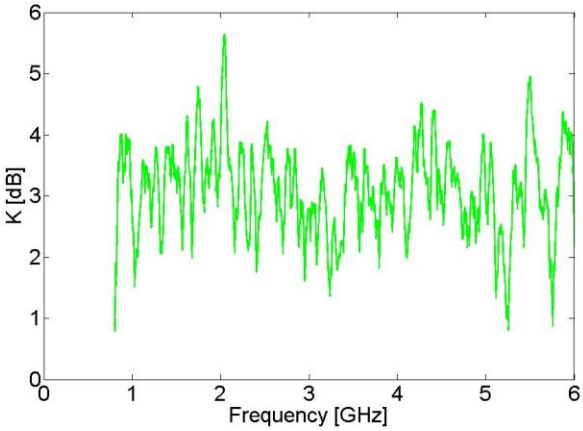

Figure 6.12 The K-factor for the STD measurement in chamber 2 using omni-directional antennas, load 5. The K-factor is averaged over the 9 antenna positions.

6.4 Discussion

In this section the performance of the NIST reverberation chambers is discussed, based on the results from the STD measurements in the former section. Also the theoretical equation (6.25) for estimating the STD is evaluated.

6.4.1 Chamber 1

From the former section it can be concluded that there are two contributions to an increased STD in the reverberation chamber. Increasing the chamber loading gives less of a stirred component and a larger K-factor, which increases the standard deviation when there is an unstirred component present in the total received field. This is seen for the different loading cases in Figure 6.1. Also, when the unstirred component is increased, the STD increases. This is clear from Figure 6.5 and Figure 6.7. These two contributions are both an effect of increasing the relative contribution of the unstirred component to the total field, which will be an invariant component in every sample and increase the correlation between the samples. Thus the number of independent samples will be smaller and the STD will be larger.

For an unloaded chamber and a very small K-factor the STD is seen to be around 0.5 dB, which is close to the ideal value of 0.44 dB for 100 independent samples. For the measurements with higher loading the STD is increasing, which is due to the increased absorption of the stirred electric field but a constant unstirred component. The correlation between the samples is thus higher and the number of independent samples is lower than the total number of samples collected. All measurements with the cross-polarized horn antennas give an STD below 1 dB, except for load 5 and the lowest frequencies. Thus, the deviation between measurements at different positions in the chamber is below 1 dB.

When omni-directional antennas are used, which gives an even larger unstirred component, the STD is increasing even more. The STD for different antenna positions is in this case about 1.5 dB, which is larger than in the measurements in [4] and [5]. Since many wireless devices employ omni-directional antennas, it is proposed that some platform and polarization stirring are used in order to reduce the effect of the unstirred component. This has shown to give good results in other chambers [4], [5]. Further work is needed with modifying the software in order to realize platform and polarization stirring and thus verify the effect in the NIST chambers.

It is of interest to point out that the field uniformity only has been analyzed for part of the chamber. The procedure employed for the system validation has been designed and evaluated for smaller chambers. Thus it can be argued that the 9 number of antenna positions used are not enough to give a true representation of the field uniformity. However, collecting data for more than 9 antenna positions is very time consuming. It also has practical implications, since there is limited space in the chamber. The part of the chamber which has been analyzed is also where most of the wireless devices are located during the measurements, thus motivating the limited number of positions used. Also, the value of the STD as a function of antenna positions seems to

be fairly constant at 9 antenna positions. This can be concluded from Figure 6.13, where the STD is plotted as a function of the number of antenna positions.

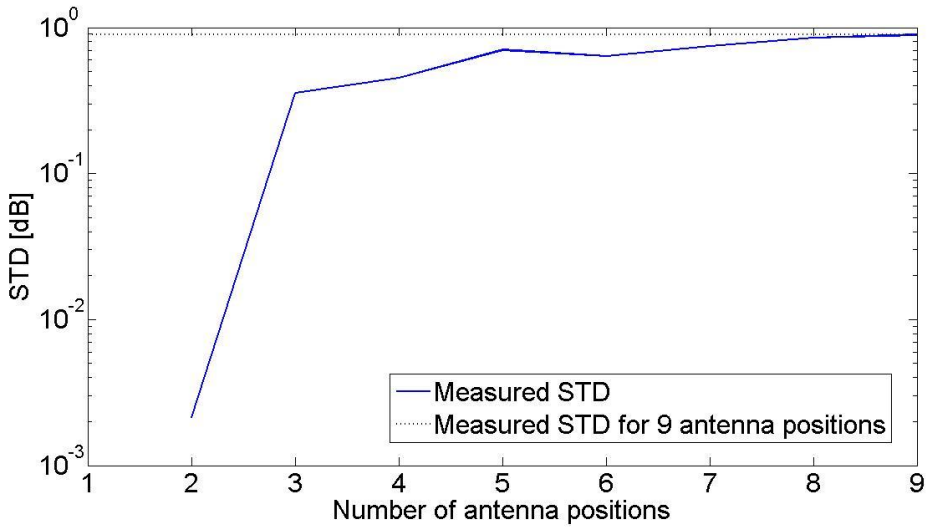

Figure 6.13 STD as a function of the number of antenna positions for chamber 1 at 0.8 GHz.

6.4.2 Chamber 2

As can be concluded from Figure 6.9, the STD for chamber 2 is seen to be large and far from the ideal value of 0.44 dB for 100 independent samples, even for load 0. The same effect as in chamber 1 is observed, that is an increased STD for an increased K-factor. The higher K-factor relative to chamber 1 is partly due to the smaller separation between the antennas, partly because of the less effective stirring. As was seen in chapter 5, not all of the collected samples can be considered to be independent, at least not for load 5 and for frequencies up to 2 GHz. This gives an increase in the STD. The effect of not having enough independent samples can be reduced by introducing frequency stirring (see e.g. [5]). Increasing the number of samples would not decrease the STD, since the stirrer step then would be too small to give uncorrelated samples.

Another reason for the larger STD for chamber 2 compared to chamber 1 might be that the antennas are moved over a larger part of the total volume of the chamber. The non-uniformity of the field for different positions in the chamber is more noticeable when moving over a larger space, especially for an inefficiently stirred chamber. Moving over a larger space will also require more antenna positions to be used for the validation procedure, in order to get convergence of the STD value. This is evident from Figure 6.14, where the STD is plotted as a function of the number of antenna positions. The convergence of the STD value is not as clear as for the chamber 1 measurements. Using more antenna positions would give a more distinct convergence, but would at the same time require more time consuming measurements.

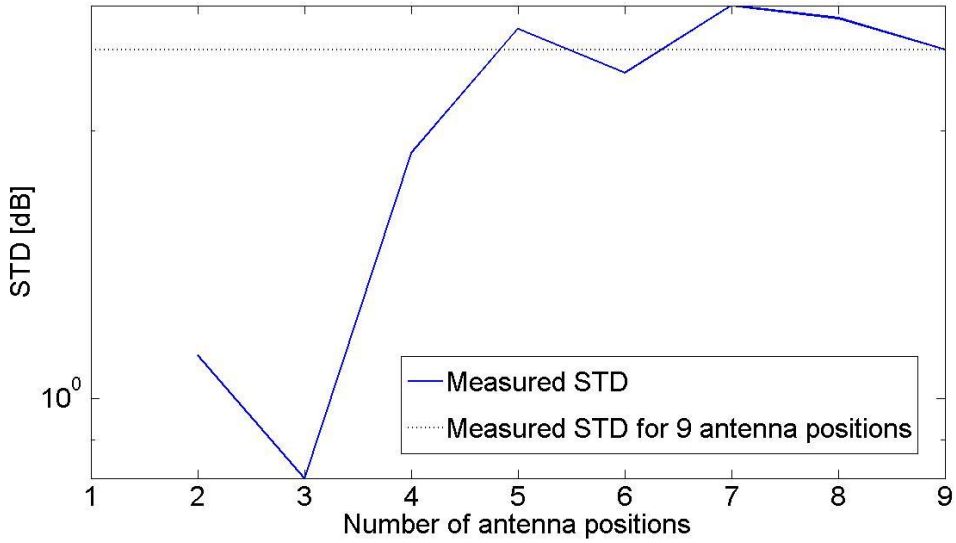

Figure 6.14 STD as a function of the number of antenna positions for chamber 2 at 0.8 GHz.

Finally, it is important to point out that the STD calculated from the measurements is only valid if the omni-directional antennas are kept co-polarized. Throughout the measurements the antennas are kept co-polarized and at a constant separation in order to not affect the line-of-sight component. If the orientation also would be changed, the STD would be even larger, due to a varying line-of-sight component. This is obviously also the case for the measurements with the omni-directional antennas in chamber 1. Using platform and polarization stirring would give polarization balance also for the unstirred component and the field distribution would appear more uniform.

6.4.3 Comparison between chambers

As mentioned in subsection 6.1.4, in [4] and [5] a good accuracy is reported for the chamber employed, in terms of a low STD. The system validation procedure, which is performed by the Antenna Group at Chalmers in the same way as for the NIST chambers, show that for an unloaded chamber (average mode bandwidth of approximately 1.5 MHz) the STD is between 0.2 – 0.6 dB for the bandwidth 0.5 – 3 GHz (the higher the frequency, the smaller the STD). It is of interest to compare the performance of the NIST reverberation chambers to these results. From Table 6-1 it is clear that the NIST chambers have a larger STD and thus a worse performance for similar loading (similar average mode bandwidth). This result is expected, since the chamber at Chalmers has a smaller volume than the NIST chambers. This increases the stirred volume relative to the total volume and should increase the number of independent samples. This also shows that the stirring performed in the chamber at Chalmers is more effective than the stirring in the NIST chambers. Additional improvements are needed in order to obtain satisfying results for low frequencies and high loading. This could include employing position and/or polarization stirring. Also, for chamber 1 the stirring sequences developed in chapter 5 should increase the

number of independent samples and thus the accuracy. Also, frequency stirring would increase the accuracy, at the expense of frequency resolution.

Chamber	Size [m]	Stirring method/Number of stirrer positions	Average mode bandwidth (mean over frequency) [MHz]	Frequency [GHz]	STD, min – max value [dB]
NIST chamber 1	2.8 x 3.1 x 4.4	Mechanical (2 rotating paddles)/100	1.8 (load 5)	0.8 – 6	0.7 – 1.5
NIST chamber 2	2.8 x 3.1 x 4.6	Mechanical (1 rotating paddle)/100	1.5 (load 5)	0.8 – 6	3.0 – 3.1
Chalmers chamber	1.2 × 1.8 × 1.8	Mechanical (2 moving plates), position (rotating platform) and polarization (three orthogonal wall antennas)/100 x 5 x 3	1.5 (empty chamber)	0.5 – 3	0.2 – 0.6

Table 6-1 Comparison of the STD between different chambers.

6.4.4 Evaluation of the equation for estimating the standard deviation

The theoretical equation for estimating the STD for different loading cases plotted in Figure 6.1 shows a good agreement with the calculated STD from the measurements. However, when the unstirred component is increased, the deviation between the measured and the estimated STD becomes larger. This can be concluded from the measurements in both chambers where the omni-directional antennas are used (Figure 6.5 and Figure 6.9) and from the measurement in chamber 1 with the high K-factor (Figure 6.7). The theoretical equation seems to overestimate the STD for all cases. This is the same result as obtained in [5] when no platform or polarization stirring is employed and when the K-factor values is estimated from the measured data. When platform and polarization stirring is used in [5], the estimation becomes better. This is probably due to that the K-factor decreases when employing these stirring techniques, as discussed in section 6.1.3. Thus it is believed that the theoretical equation gives an even better estimation of the STD in the NIST chambers as well, if platform and polarization stirring are used.

The large deviation between the measurements and the theoretical estimation for high K-factors is expected from the discussion in subsection 6.1.3, from which it is clear that the derivation is valid only for Rayleigh distributed field amplitudes, that is for small K-factors. When the field amplitude is Rician distributed, the power will not be exponential distributed and the necessary assumptions will not be valid.

For evaluating (6.25) the K-factor is calculated from the measured data using (4.4). The theoretical equation proposed in [5] for determining the K-factor from antenna characteristics can also be used to find the K-factor value. However, this equation only accounts for the line-of-sight component. When there in addition to the direct component is a large amount of unstirred energy from reflections off the chamber walls, the equation for the K-factor is an underestimation. This is the case for the NIST chamber due to the large volume and motivates the use of a K-factor estimated from the measured data.

Moreover, in [5] a theoretical equation for the number of independent samples estimated from chamber characteristics is also proposed. However, as is shown in chapter 5, this equation overestimates the number of independent samples. Instead, the number of independent samples is set to the total number of samples. It is shown in chapter 5 that this is a reasonable approximation for chamber 1. For chamber 2 it might be an overestimation, at least for load 5. However, when the unstirred component is large this has been verified not to affect the result significantly, since then the K-factor is the dominating factor in (6.25).

7 Chamber repeatability

For measurements in a reverberation chamber, as for all scientific experiments, it should be possible to repeat the exact same procedure in order to show consistency in the results. Also concerning the chamber, if some specific stirrer positions are desired, as for the 7°/13° stepping configuration or the grid of angles discussed in chapter 5, it is important to know that the stirrers really are rotating the angle specified by the user.

In this chapter the repeatability of the stirrers in the NIST chambers is discussed. For the stirrers in chamber 1 a correction for a rotational offset is also performed.

7.1 Chamber 1

When studying the autocorrelation function for determine the number of independent samples an offset was found in the rotation of the stirrers. For chamber 1 this was briefly mentioned in the chapter 5 when the 7°/13° stepping configuration was discussed. Figure 5.11 shows that the last peak is shifted 2 sample numbers from the expected value, which can be explained by a rotational offset. If the stirrers are rotating more than the specified angle the stirrer configuration will start to repeat earlier than expected. For example, if one stirrer is rotated 1° steps, then the 361:st sample should show perfect correlation with the first sample because of the repeated stirrer position. However, if the actual rotation is somewhat larger due to the offset, the rotation of the stirrer will be very close to a complete revolution at earlier sample numbers. This also explains the lack of perfect correlation, since the exact same stirrer configuration is not obtained. The error will accumulate when more revolutions are used.

From the measurement in chapter 5 it is thus concluded that there is an offset in the rotation of the stirrers and that the stirrers are rotating more than the specified angle. This chapter considers the quantification of this error and proposes a way to correct for it, by means of a calibration procedure.

7.1.1 Calibration procedure

According to the specifications the rotation of the stirrers is controlled by a count number. Every 0.1° step of the stirrers should correspond to one count. Due to the verified offset it is reasonable to argue that one count in reality gives a larger rotation than 0.1°.

In order to find the correct degree of rotation corresponding to one count number the transfer function for the original position (the position corresponding to a rotation of 0°) is compared to stirrer positions close to a full revolution (360°). Each stirrer is separately rotated 350° and then further stepped 0.1°, measuring the transfer function between every step with the PNA. In this way the position which makes the channel transfer function coincide with the transfer function for the original position can be found. For stirrer 1 this position is found to correspond to a rotation of 358.7° and for stirrer 2 to a rotation of 358.3°. Assuming that this is an accumulated

offset which has the same magnitude for every step, a correction factor C can be calculated for each stirrer using the following equation.

$$C = \frac{\theta_{offset}}{360}$$

θ_{offset} is the stirrer rotation angle which gives a perfect match between the transfer function in the position corresponding to this angle and the transfer function measured at the initial position. The correction factors for stirrer 1 and stirrer 2 can be found in Table 7-1. In the stirrer control software, each specified angle step is then multiplied with C, which decreases the count number. Since the count number must be an integer the correction factor must be rounded to the closest integer, which will introduce an additional error. For one revolution of the stirrers this error can be considered to be insignificant, however when using more than one revolution it will accumulate. It is found that by rotating the stirrers back after one revolution, as opposed to rotate them forward, the stirrers are returned to the exact same positions as the original position. Using this stepping sequence will thus improve the repeatability of the stirrers further.

Stirrer 1 correction factor	Stirrer 2 correction factor
0.9964	**0.9953**

Table 7-1 The correction factors for the roattional offset for stirrer 1 and stirrer 2.

7.1.2 Validation of the calibration procedure

The autocorrelation function from measurement number 10 in chapter 5 is used to verify the improved repeatability by using the calibration procedure described above. As described previously, in this measurement stirrer 1 is rotated 0.5° steps. After 20 steps stirrer 1 is rotated back to its original position and stirrer 2 is stepped a 0.5° step. This procedure is repeated until stirrer 2 has been rotated 20 steps. The stepping sequence should result in similar stirrer positions at every 21:st sample. In other words, the peaks in the autocorrelation function should appear at every 21:st sample.

Figure 7.1 shows the autocorrelation function for the case without correction for the rotational offset and when rotating stirrer 1 forward to the original position after 20 steps. Every 21:st sample is marked, which clearly shows the accumulated rotational offset. In order to fully understand this plot it is of importance to know how the autocorrelation is calculated. A brief explanation follows below.

The collected data set is a vector with 441 values of the channel transfer function, measured at every stirrer position. The autocorrelation function compares this vector with an identical copy, starting at the current sample position. For example, the correlation between the first and the 21:st sample is found by comparing the data vector with a copy starting at sample number 21.

These vectors will agree well, since they correspond to samples collected at stirrer positions with a small rotational deviation, that is stirrer positions that are close to each other in the angular space (see chapter 5). This gives the second peak in Figure 7.1 (sample number 21). However, comparing the data vector which starts at sample number 20 with the original vector also gives a good agreement, since all but the first sample in the original vector are similar to the elements in the other vector, because these samples are collected at similar stirrer positions. This explains the smooth increase in the autocorrelation function prior to the expected peak at e.g. sample 21. This also explains the shift of the peaks when there is a rotational error present. Since stirrer 1 is rotated forward to its original position every time stirrer 2 is moved one step, the offset will accumulate. After some revolutions the sample at the first position of stirrer 1 for a particular rotation angle of stirrer 2 will be more similar to the second sample in the initial data vector. This will imply a higher correlation for sample numbers prior to the expected samples than for the samples that corresponds to the actual rotation of stirrer 1 to its original position.

Figure 7.1 shows that the first and the second peaks appear at the expected sample number. For these peaks the angular deviation is not large enough to give a significant change in the autocorrelation function. However, when the number of steps increases and stirrer 2 has been stepped several times, the deviation from the initial position becomes larger and the effect of having higher correlation for samples prior to the expected samples is apparent.

In Figure 7.2 the autocorrelation function for the data collected with the same stepping procedure is shown, however with correction for the rotational offset and by moving stirrer 1 backwards after 20 steps. As can be seen in this figure, the peaks appear at every 21:st sample as expected. Also, the amplitudes of the peaks are deceasing uniformly, since the steps are consistent. This verifies that the calibration procedure is successful.

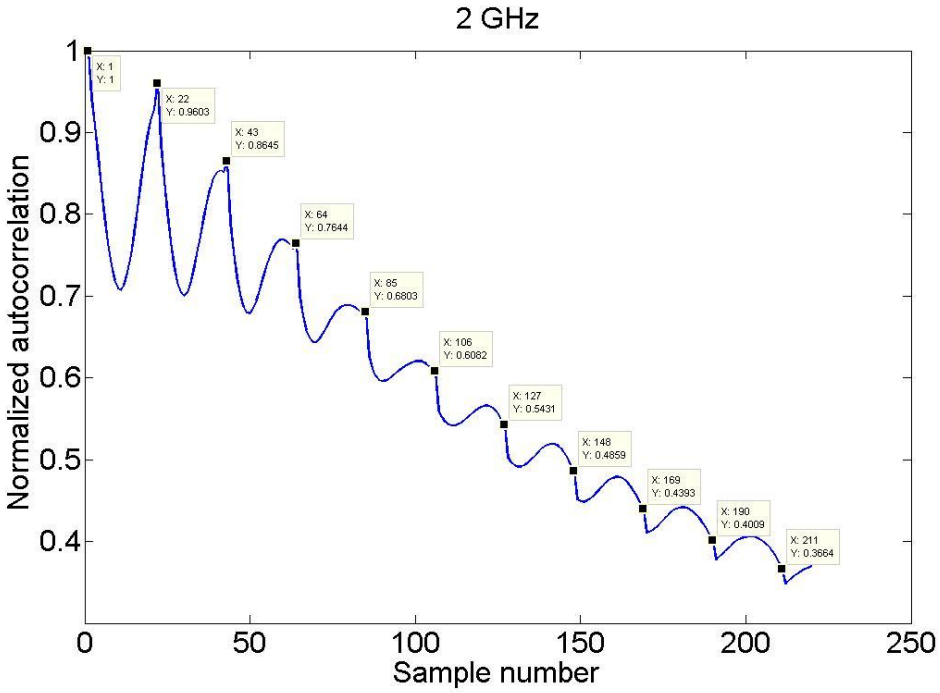

Figure 7.1 The autocorrelation function for stepping the stirrers in the 0.5° grid with a rotational offset.

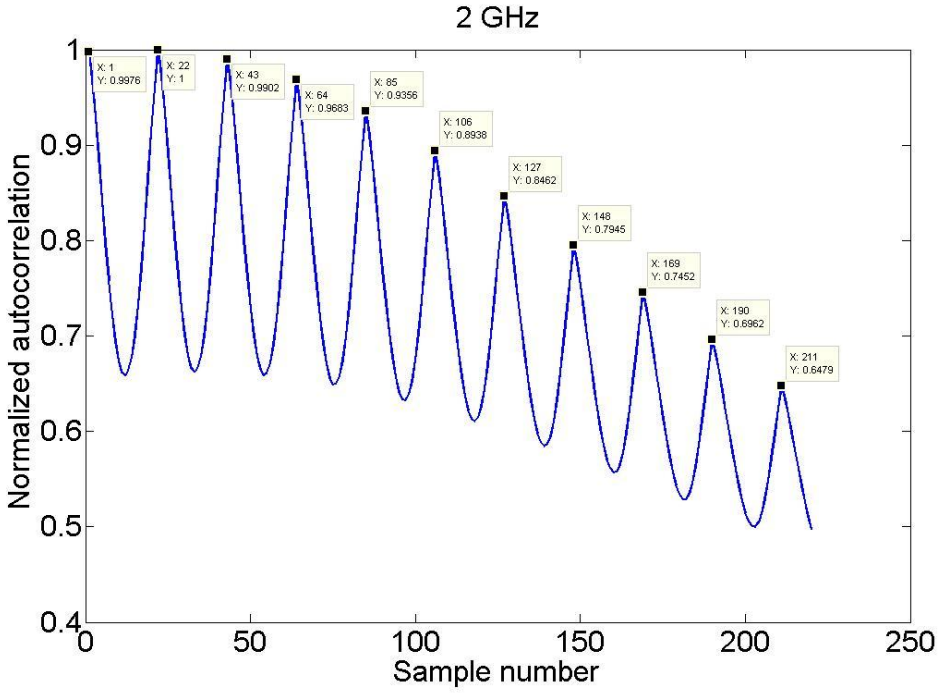

Figure 7.2 The autocorrelation function for stepping the stirrers in the 0.5° grid after the calibration procedure and the correction has been performed for the offset.

7.2 **Chamber 2**

For chamber 2 an offset was found when studying the autocorrelation function from the measurements in chapter 5 where the stirrers are stepped 0.1°. This autocorrelation function is repeated in Figure 7.3 for convenience. Ideally there would be a peak in the autocorrelation function for sample number 3600 when using this stepping sequence. As can be seen in the figure, the peak appears at sample number 3677. Thus there is a rotational offset of 77 samples. In contrast to the stirrers in chamber 1, the chamber 2 stirrer is moving less than the specified angle. The offset is probably due to an accumulated rounding error and if fewer steps are used, the total offset after one revolution will most certainly be smaller.

The offset of 77 samples corresponds to a total angle offset of approximately 7.7°, which is more than for chamber 1. It is proposed that a calibration procedure similar to the one described for chamber 1 is performed in order to have a perfect repeatability. Due to time limitations such a calibration procedure has not been performed.

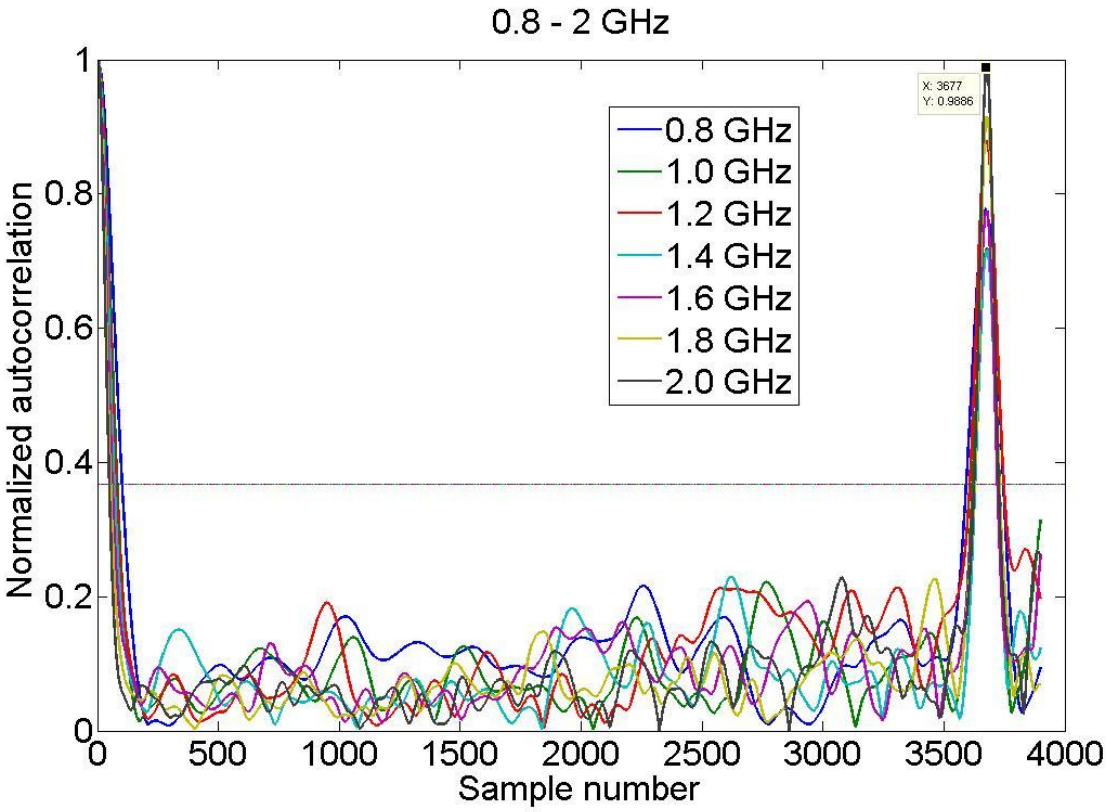

Figure 7.3 The autocorrelation function calculated from the measurements in chamber 2 for six different frequencies in the range 1 – 6 GHz. The dotted line is the 1/e threshold. (Repeated from chapter 5.)

8 Conclusions and future work

The two main topics of this thesis, comparison of methods for estimating the Rician K-factor and evaluation of the performance of the NIST reverberation chambers, have been discussed in detail in the preceding chapters. The present chapter closes the thesis by drawing some conclusions based on the findings and by proposing some further work. The chapter is divided into separate sections for each of the subjects discussed, in order to facilitate for the reader.

8.1 Methods for estimating the Rician K-factor in a fading environment

From the discussion in chapter 4 it is concluded that the complex mean approach developed by P.-S. Kildal and the Antenna Group at Chalmers is the most accurate method for estimating the K-factor from complex data collected in a wireless channel with fixed antenna positions. This method gives the correct value when there is an unstirred component present, as well as without an unstirred component. Thus, the complex mean approach should be used if complex data have been collected and if stationary receive and transmit antennas are used, like in the reverberation chamber.

If the measurement is based on variable antenna positions or if only the amplitude of the signal has been measured, the moment method and the Rician PDF fitting approach give an accurate estimate in the presence of an unstirred component. In absence of an unstirred component, the methods do not give a quantitative measure. A small improvement is obtained when using the Rician PDF fitting, as opposed to using the moment method. Further work on finding models based on amplitude values for a weak unstirred component is needed.

Furthermore, the estimate of a K-factor with a high value is seen to converge to its real value at small sample numbers. For smaller values of the K-factor, more independent samples are needed in order to reduce the deviation from the true value. The poor estimate at smaller K-factor values is seen to be due to the difficulty of estimating the mean. For the methods based on the distribution of the signal envelope, more samples are needed in order to obtain the true value compared to the complex mean approach. Figure 4.6 to Figure 4.11 can be used as a starting point for determining the number of independent samples needed for estimating the K-factor with a certain method, if the approximate value is known.

8.2 The number of independent samples

In chapter 5 some limits for the number of independent samples in the NIST reverberation chambers have been found for different stirring sequences. The limits are valid for the case with a minimized unstirred component. From the adjacent sample correlation it is concluded that the required angle step decreases with increased frequency and decreased chamber loading. The number of independent samples thus increases with frequency. Furthermore, the increase is seen to be linear with frequency. This is in contradiction to the theoretical formula proposed in [5] and

to the results reported in [29], where the number of independent samples increases as frequency squared. Further work is needed in order to explain this difference.

From chamber 1 it is concluded that the larger the volume of the chamber that is stirred, the more independent samples can be collected. By using both stirrers simultaneously it is possible to collect about 100 independent samples at 0.8 GHz and 650 independent samples at 6 GHz for an unloaded chamber. For load 5 the corresponding numbers are 25 at the lowest frequency and 200 at the highest frequency.

For chamber 2 the maximum number of independent samples for load 5 is about 50 at a frequency of 0.8 GHz and increases linearly with frequency to about 280 at 6 GHz. Based on the results from chamber 1 the minimum angle step will decrease, and thus the number of independent samples will increase, with decreased loading. If more independent samples are needed, then frequency stirring must be applied.

Moreover, it is concluded from chamber 1 that using a stirring sequence that spreads the stirrer positions in the angle space is giving more independent samples. It is however important to account for the additional correlation that might appear for similar stirrer positions later in the stirrer sequence due to similar distribution of modes in the chamber. For a threshold of 1/e the 7°/13° stepping configuration is seen to give satisfying results for frequencies above 1 GHz, but gives too high correlation between the samples for lower frequencies. It is believed that a 17°/13° stepping would give more independent samples for lower frequencies. This has not yet been experimentally verified.

Using the new proposed stepping sequence consisting of a grid of 10° steps a maximum of 1296 independent samples can be collected for frequencies above 2.3 GHz and for a threshold of 1/e. For frequencies between 1.5 GHz and 2.3 GHz the corresponding value is about 650. Thus the new stepping sequence outperforms the 7°/13° stepping configuration in terms of number of independent samples for all frequencies above 1.5 GHz. Using the information in Table 5-2 to Table 5-4 it is further possible to design the grid for a specific frequency and loading of interest. Because of the small angle step required for the higher frequencies, a grid can be designed to give even more independent samples than for the 10° by 10° grid. If a large frequency band is to be used in the measurement it is proposed that the angle steps are made variable.

The new stirring sequence proposed is based on rotating stirrers, but it can easily be applied to other stirring techniques with some minor adjustments. Using the procedure described in section 5.4.3, suitable steps for different frequencies and loading cases can be found for different chambers. It is desirable to test a similar sequence in other chambers in order to determine the generality of the results, that is if the grid of sample points always is the optimal way of stirring.

The effect of loading has only briefly been addressed in this report and more input is needed in order to draw any quantitative conclusions. It would for example be of interest to verify that

grids designed from Table 5-2 and Table 5-3 will give the theoretically possible number of independent samples.

Finally, a relation for the number of independent samples in the chambers based on the chamber characteristics is also tried to be found. One equation from the literature is seen to give a fairly good agreement with the number of independent samples calculated from the measurements. Further work is needed in order to draw any final conclusions.

8.3 Accuracy of reverberation chamber measurements

The procedure for measuring the STD in a reverberation chamber proposed in [5] has been employed to the NIST reverberation chambers. The mean STD over frequency for an unloaded chamber 1 and a very low K-factor is about 0.5 dB, which is close to the ideal value for 100 independent samples. When the K-factor increases, the STD also increases. For load 5 the STD is 0.7 – 1.5 dB. When increasing the K-factor even further by employing omni-directional antennas, the STD is increased significantly. For load 5 the STD is approximately 1.5 dB. It is believed that the STD for the measurements with a high K-factor and loading can be reduced by introducing platform and polarization stirring. This has not yet been experimentally verified for the NIST chamber. Due to the high uncertainty and the fact that most wireless devices use omni-directional antennas, it is proposed that the chamber and the software are modified accordingly. Also, the stirring sequences developed in chapter 5 could be used to increase the number of independent samples and thus the accuracy.

For chamber 2 the STD for using omni-directional antennas is seen to be approximately 1 dB for load 0. For load 5 it is about 3 dB. Thus this chamber has a worse accuracy than chamber 1. The larger STD is due to the less effective stirring compared to chamber 1, since only one stirrer is employed. The STD can be improved by installing additional stirrers, which would increase the number of independent samples. Also, frequency stirring would be a way to increase the number of independent samples, at the expense of frequency resolution. Employing platform and polarization stirring would also give a more uniform field distribution.

Concerning the validation procedure, 9 antenna positions are seen to be enough to give convergence in the STD value. When the validation procedure is carried out over a large part of the total volume of the chamber and the chamber employs inefficient stirring, more antenna positions should be used. The drawback is that this would increase the measurement time for the validation procedure.

Finally, a detailed derivation of Professor P.-S. Kildal's new physical model for the STD presented in [4] is given in section 6.1.3. This model, equation (6.25), is seen to give good agreement with the STD calculated with the validation procedure from the measured data, when the unstirred component is small. When the unstirred component increases, there will be a larger deviation between the STD calculated from measurements and estimated with (6.25). This is explained by the fact that the assumptions made for the derivation of the model are only valid for

exponential distributed relative power values. Moreover, as is concluded in chapter 5, further work is needed in order to find a model for the number of independent samples. Also, a better expression for the K-factor, which includes all contributions to the unstirred component, must be derived. These improvements would make it possible to evaluate (6.25) solely from the knowledge of the chamber and the antenna properties.

8.4 **Chamber repeatability**

It is concluded that there is an offset in the rotation of the stirrers in both chambers. For chamber 1 it is shown that the offset corresponds to a larger rotation of each stirrer than specified by the user in the software. One correction factor for each stirrer is found in order to correct for this offset. These factors are given in Table 7-1. Also, if more than one revolution is used the stirrers should be rotated back to a corresponding value after a complete revolution, in order to achieve the best repeatability. Using this new stirring sequence and the correction factors is seen to reduce the offset error significantly. For chamber 2 the offset corresponds to a smaller rotation than specified by the user in the software. Due to time limitations no correction for this error has been performed.

References

[1] P.-S. Kildal and K. Rosengren, “Correlation and capacity of MIMO systems and mutual coupling, radiation efficiency and diversity gain of their antennas: Smulations and measurements in reverberation chamber”, IEEE Communications Magazine, vol. 42, no. 12, pp. 102-112, Dec. 2004.

[2] K. Rosengren and P.-S. Kildal, “Radiation efficiency, correlation, diversity gain, and capacity of a six monopole antenna array for a MIMO system: Theory, simulation and measurement in reverberation chamber”, Proceedings IEE, Microwave Antennas Propagation, vol. 152, no. 1, pp.7-16, Feb. 2005. See also Erratum published in Aug. 2006.

[3] A. D. Panagopoulos and K. P. Liolis, “Rician K-factor distribution in broadband fixed wireless access channels under rain fades”, IEEE Communications letters, vol. 11, no. 4, pp. 301-303, Apr. 2007, 10.1109/LCOMM.2007.061857.

[4] P.-S. Kildal, S.-H. Lai and C. Xiaoming, “Direct coupling as a residual error contribution during OTA measurements of wireless devices in reverberation chamber”, IEEE AP-S International Symposium on Antennas and Propagation, Charleston, SC, USA, Jun. 1-5, 2009.

[5] P.-S. Kildal, and C. Orlenius, “TRP and TIS/AFS measurements of mobile stations in reverberation chambers (RC)”, CTIA Certification Program Working Group Contribution, Mar. 2009, RCSG090401.

[6] P. Corona, G. Latmiral and E. Paolini, “Performance and analysis of a reverberating enclosure with variable geometry”, IEEE Trans. Electromagn. Compat., vol. 22, pp. 2-5, Feb. 1980.

[7] M. L. Crawford and G. H. Koepke, “Design, evaluation, and use of a reverberation chamber for performing electromagnetic susceptibility/vulnerability measurements”, U.S. Nat. Bur. Stand. Tech. Note 1092, Apr. 1986.

[8] H. A. Mendes, “A new approach to electromagnetic field-strength measurements in shielded enclosures”, Wescon Tech. Papers, Western Electronic Show an Convention, Los Angeles, CA, Aug. 20-23 1968.

[9] M. Bäckström, O. Lundén, P.-S. Kildal, “Reverberation chambers for EMC susceptibility and emission analyses”, Review of Radio Science 1999-2002, pp. 429-452.

[10] D. A. Hill, “Electromagnetic fields in cavities”, Piscataway, NJ, USA: IEEE Press, 2009, 978-0-470-46590-5.

[11] J. M. Ladbury, G. Koepke and D. Camell, “Evaluation of the NASA Langley Research Center mode-stirred chamber facility”, Nat. Inst. of Standards and Technology Tech. Note 1508, Boulder, CO, USA, Jan. 1999.

[12] B. H. Liu, D. C. Chang and M. T. Ma, “Eigenmodes and the composite quality factor of a revereration chamber”, Nat. Bureau of Standrds Tech. Note 1066, Boulder, CO, USA, Aug. 1983.

[13] D. A. Hill, “Electromagnetic theory of reverberation chambers”, Boulder, CO, Nat. Inst. of Standards and Technology Tech. Note 1506, Dec. 1998.

[14] K. Madsén, P. Hallbjörner and C. Orlenius, “Models for the number of independent samples in reverberation chamber measurements with mechanical, frequency, and combined stirring”, IEEE Antennas and Wireless Propag. Lett., vol. 3, pp. 48-51, 2004.

[15] P.-S. Kildal and C. Carlsson, “Detection of a polarization inbalance in reverberation chambers and how to remove it by polarization stirring when measuring antenna efficiencies”, Microwave Opt. Technol. Lett., vol. 32, pp. 145-149, Jul. 20, 2002.

[16] S. O. Rice, “Mathematical analysis of random noise”, Bell Syst. Tech. J., vol. 23, pp. 282-332, Jul. 1944.

[17] A. Papoulis, “Probability, random variables and stochastic processes”, New York, NY, USA: McGraw-Hill, 1984, 9780073660110.

[18] P. Corona, G. Ferrara and M. Migliaccio, “Reverberating chamber electromagnetic field in presence of an unstirred component”, IEEE Trans. Electromagn. Compat., vol. 42, no. 2, pp. 111-115, May 2000.

[19] D. Childers and S. C. Miller, “Probability and random processes: With applications to signal processing and communications”, San Diego, CA, USA: Elsevier Academic Press, 2004, 0121726517.

[20] C. L. Holloway, D. A. Hill, J. M. Ladbury, P. Wilson, G. Koepke, J. Coder, “On the use of reverberation chambers to simulate a rician radio environment for the testing of wireless devices”, IEEE Trans. on Ant. and Propag., vol. 54, no. 11, pp. 3167-3177, Nov. 2006.

[21] G. D. Durgin, “Space-time wireless channels”, Upper Saddle River, NJ, USA: Prentice-Hall, 2003, 0076092030072.

[22] W. C. Jakes, “Microwave mobile communications”, New York, NY, USA: IEEE Press, 1974, 9780780310698.

[23] R. Steele, “Mobile radio communications”, New York, NY, USA: IEEE Press, 1995, 9780471978060.

[24] “Electromagnetic compatibility (EMC), Part 4—Testing and measurement techniques, section 21: Reverberation chambers”, Geneva, Switzerland, International Electrotechnical Commission, Aug. 2003, IEC 61000-4-21.

[25] K. G. Beauchamp and C. K. Yuen, “Digital methods for signal analysis”, London, England: George Allen & Unwin LTD, 1979, 0-04-621027-X.

[26] J. B. Coder, J. M. Ladbury, C. L. Holloway and K. A. Remley, “Examining the true effectiveness of loading a reverberation chamber; how to get your chamber consistently loaded”, submitted to Proceedings of the 2010 IEEE EMC Symposium, Apr. 2010.

[27] J. Sijbers, A. J. den Dekker, P. Scheunders and D. Van Dyck, “Maximum likelihood estimation of Rician distribution parameters”, IEEE Trans Med. Imaging, Jun. 1998, 17:357–361.

[28] D. W. Matolak, K. A. Remley, C. Gentile, C. L. Holloway, Q. Wu, Q. Zhang, “Ground-based urban channel characteristics for two public safety frequency bands”, submitted to IEEE Trans. on Ant. and Propag., Aug. 2010.

[29] A. Sorrentino, P.-S. Kildal, U. Carlberg and E. Pucci, “Accuracy in reverberation chamber for wireless testing: Simple formulas for the number of independent samples”, EuCAP 2009, 3rd European Conference on Antennas and Propagation 2009, Berlin, pp. 2673-2677, Mar. 23-27 2009, 978-1-4244-4753-4.

[30] P. Hallbjörner, “A model for the number of independent samples in reverberation chambers”, Microwave Opt. Technol. Lett., vol. 33, no. 1, pp. 25-28, Apr. 2002.

[31] J. G. Kostas and B. Boverie, “Statistical models for a mode-stirred chamber”, IEEE Trans. Electromagn. Compat., vol. 33, no. 4, pp. 366-370, Nov. 1991.

[32] L. Lauwers, K. Barbe, W. Van Moer, R. Pintelon, “Estimating the parameters of a Rice distribution: A Bayesian approach”, Instrumentation and Measurement Technology Conference 2009, I2MTC '09 IEEE, Singapore, May 5-7 2009, pp. 114-117, 1091-5281.

[33] I. J. Myung, “Tutorial on maximum likelihood estimation”, Journal of Mathematical Psychology, vol. 47, no. 1, pp. 90-100, Nov. 2003.